MEASUREMENT OF HYDRODYNAMIC FORCES ON GRAVEL PARTICLES IN THE EROSION FUNCTION APPARATUS

A Thesis

by

ZIHAN ZHANG

Submitted to the Office of Graduate and Professional Studies of
Texas A&M University
in partial fulfillment of the requirements for the degree of

MASTER OF SCIENCE

Chair of Committee,	Jean-Louis Briaud
Committee Members,	Charles Aubeny
	Cristine Morgan
Head of Department,	Robin Autenrieth

December 2018

Major Subject: Civil Engineering

ABSTRACT

Many theoretical methods in the literature have been introduced that require the knowledge of the normal stress and shear stress acting at the contact between the soil particles in the river bed and the fluid (mostly water). However, there are not many practical methods to measure the normal stress and the shear stress. In this study, the goal is to find a way to directly measure and calculate the normal force and drag force that acts on the surface of soil particles during the erosion phenomenon before departure in the Erosion Function Apparatus (EFA). If these stresses caused by hydrodynamic forces can be quantified, this will help improve the current erosion model.

During the erosion process, drag forces and the resulting shear stresses develop on the surface at the interface between the soil particles and the eroding fluid. Also the eroding fluid causes a decrease in the normal stress induced on the surface of the soil particle, and due to the turbulence in the water, the induced normal stress and shear stress fluctuate. The erosion phenomenon is proposed to be analyzed using an image analysis technique where the movement of the particles is recorded by a camera. Through derivative calculations, the velocity and then the acceleration of each particle are obtained. Then the forces are obtained by using the mass times the acceleration. One major goal of this study is to find out what roles the hydrodynamic shear and normal forces play in the detachment of the particle from the river bed. The answer to this question can also help to obtain the most practical erosion model.

It is concluded that shear stresses tend to be larger for rougher particles, while normal stresses are larger in samples with a bigger mean particle size (D_{50}). Also, it was observed that when the particles are more uniform in size, the displacement of the particles prior to detachment

tends to be smaller. The vibration frequency of particle movement also tends to be smaller when the soil is composed of smaller particles.

Both normal and shear stresses were observed to be proportionally correlated with the erosion rate. The effect of normal stresses tends to be more prevalent on smaller gravel particles, while the effect of shear stresses seems to play a more prominent role in the erosion of larger gravel particles.

ACKNOWLEDGMENTS

I would like to thank the chair of my committee, Dr. Briaud, and my committee members. Dr. Aubeny, Dr. Morgan, for their guidance and support throughout the course of this research.

Thanks also go to my friends and colleagues and the department faculty and staff for making my time during graduate studies at Texas A&M University a great experience. Finally, thanks to my mother and father for their love, patience, and encouragement.

CONTRIBUTORS AND FUNDING SOURCES

Contributors

This work was supervised by the chair of the dissertation committee Dr. Briaud of the Zachry Department of Civil Engineering.

The experimental data collected in the Erosion Function Apparatus and also some of the movies used in the image analysis of this study were obtained under the help of Dr. Iman Shafii of the Zachry Department of Civil Engineering.

All other work conducted for the thesis was completed by the student

Funding Sources

There are no funding contributions to acknowledge related to the research and compilation of this document.

TABLE OF CONTENTS

Page

LIST OF FIGURES

LIST OF TABLES

1. INTRODUCTION

The goal of this study is to measure the hydrodynamic forces acting on gravel particles during the erosion phenomenon in the Erosion Function Apparatus (EFA). There are many theoretical approaches in the literature which help calculate the shear stress induced on the surface of a riverbed by the eroding fluid. However, there are not so many practical methods to directly measure the hydrodynamic forces acting on the soil particles on the contact surface between the soil and eroding fluid. There is a remarkable gap in appropriate measuring techniques to calibrate the findings of the theoretical approaches. The objective of this study is to bring up a new method to precisely monitor the erosion phenomenon using image analysis techniques, and consequently obtain the hydrodynamic forces acting on each particle before detachment. If this objective is achieved, then the roles that shear and normal forces play in the erosion process can be explored and the current erosion model can be improved by considering all influencing forces.

There are three main components involved in the phenomenon of erosion: the erodible material, the eroding fluid and the geometry of the obstacle impacting the flow. In this process, the fluid generates the "load", the erodible material provides the resistance while the obstacle induces the disturbance. Erodibility can be characterized as the behavior of the eroding material when subjected to the flow of the eroding fluid. The eroding water is quantified by its velocity, and the obstacle geometry is characterized by its dimensions.

Examples of surface erosion include bridge scour at the bottom of a river and overtopping of a levee or an embankment. Surface erosion happens according to three main phenomena: 1) a drag force and the resulting shear stress are develops at the interface between the soil particles/ rock block and the eroding fluid. 2) the eroding fluid causes a decrease in the normal stress induced

on the surface of the soil particle/ rock block. Indeed as the velocity of the eroding fluid increases in the space surrounding the soil particles, the normal pressure induced by the eroding fluid decreases to maintain conservation of energy and Bernoulli's principle. 3) due to the turbulence in the water, the normal stress and the induced shear stress on the hydraulic interface between the eroding fluid and soil fluctuate. At high velocities, these fluctuations create cyclic loading of the soil particle which makes erosion easier to occur (Croad 1981; Hofland et al. 2005).

The combination of the drag shear force, the uplift normal force, and their fluctuations act together to remove the soil particle/rock block and initiate the surface erosion process. In this study, this process is monitored by a camera and then analyzed using image analysis techniques. Then through derivative calculation, the horizontal and vertical velocity and acceleration of each of soil particles selected before detachment are obtained. These measurements help in formulating a better erosion model for soils partciles.

2. BACKGROUND

2.1 Literature Review

Many researchers have tried to measure the hydrodynamic force by using different methods. Shan et al. (2011) used an innovative direct force gauge in an ex-situ scour testing device (ESTD) to study forces acting on cohesive soil samples and to analyze the incipient erosion of cohesive soils. They used a direct force gauge and a sensor disk to measure the acting horizontal and vertical forces on the surface of the soil during the erosion process. The direct force gauge is separated into wet and dry parts by a rubber membrane, and on top of the core platform sits the sensor disk so that the normal and shear force acting on the soil specimen from the flow are directly measured (Figure 1).

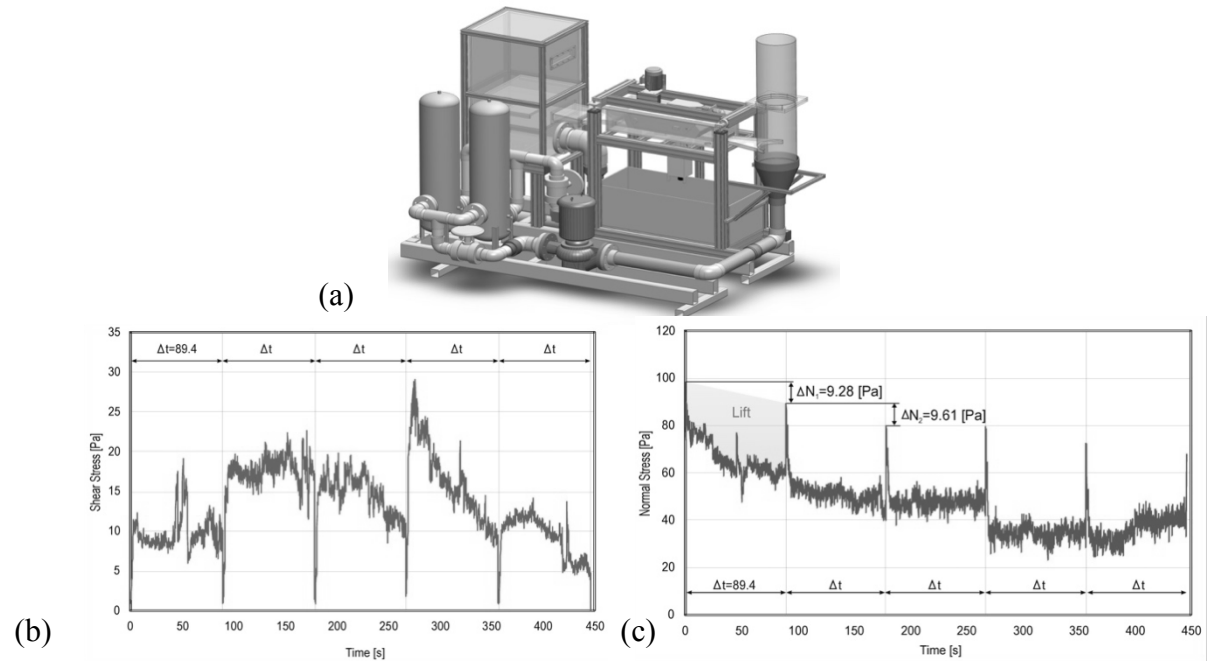

Figure 1. (a) The ESTD; (b) The shear stress recorded in one erosion test; (c) The normal stress recorded in one erosion test (Reprinted from Shan et al., 2011)

The soil was an artificial Kaolin clay. The test was perfomed 5 times at 90 seconds intervals. The shear stress reached 28Pa, then the shear stress decreased as erosion took place. The vertical stress was 80 Pa and decreased to 40 Pa as erosion took place. This force is hard to predict because it depends on the weight loss of the sample and the attenuation of the lift force (Shan et al. 2011).

Dwivedi et al. (2011) carried out a fixed ball experiment to measure the hydrodynamic forces and velocity on the particle at the entrainment condition. This experiment (Figure 2) was performed using a force sensor in a flume and aimed to replicate conditions similar to a flow condition. The target spherical particle is fixed to a hollow rod which is attached to the force sensor so that the sensor will measure the forces that acted on the target particle. As shown in Figure 2, both the drag force and lift force fluctuatre during the test, the specific values are not given.

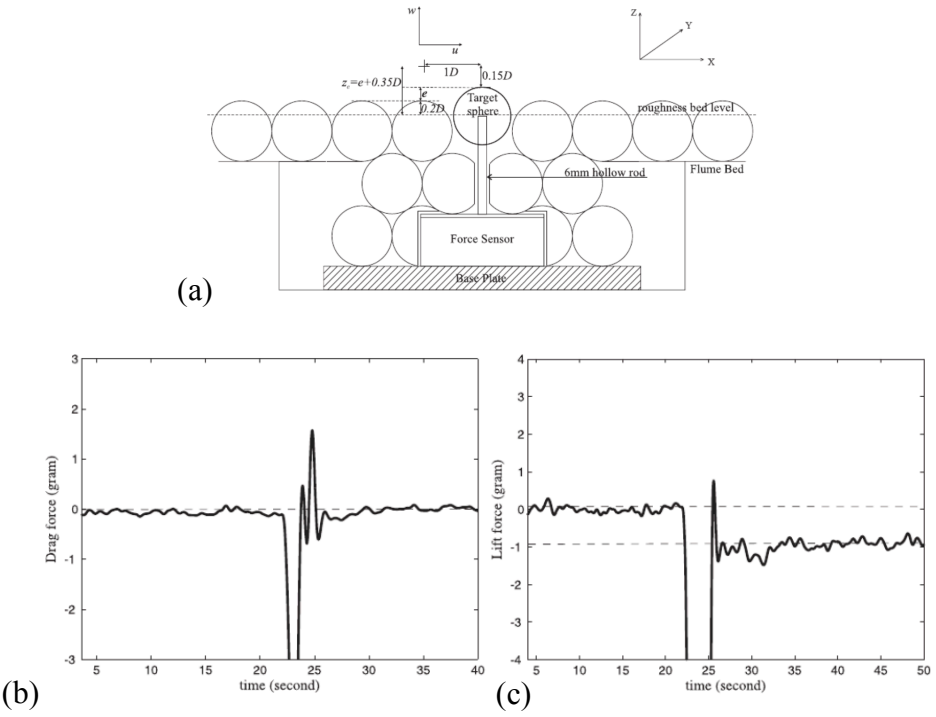

Figure 2. (a) Schematic of force sensor in the flume; (b) Response of the installed force sensor in x direction due to loading and unloading of a gram mass in the negative z direction; (c) Response of the installed force sensor in z direction due to loading and unloading of a gram mass in the negative z direction (Reprinted from Dwivedi et al., 2011)

Maali et al. (2012) used a colloidal probe Atomic Force Microscopy (AFM) to quantify the slip length and drag-force on microstructured surfaces in a drainage experiment. The AFM is in contact mode during this test, and the hydrodynamic drag force is given by the deflection of the cantilever when the particle is subjected to a constant velocity flow. The particle used in this test is a spherical borosilicate particle with a 52.5 μm diameter. Figure 3 below shows the measured hydrodynamic drag force divided by the velocity as a function of the separation distance for different surfaces, when the velocity is 56 μm/s.

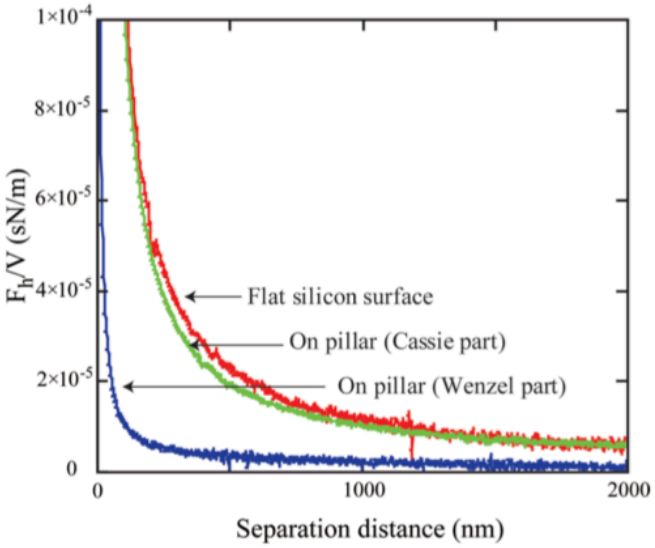

Figure 3. The measured hydrodynamic drag force F_h divided by belocity as a function of separation distance for the different surfaces (Reprinted from Maali et al., 2012)

There are many different kinds of erosion models that are used for different purposes. It is always easier to measure the velocity of the flow; however, the velocity measurement is limited to the mean-depth velocity of the flow. Indeed, the velocity profile reaches a value of zero at the interface between the water and the soil. A better model definition of erosion is the relationship between the erosion rate and the shear stress at the soil-water interface (Briaud et al., 2017).

Previous erosion models in the literature do not incorporate both shear stress and normal stress effects in one single erosion model. Shafii et al. (2016) presented a comprehensive erosion model by incorporating the effects of turbulence-driven fluctuations in normal and shear stresses acting on a particle (Eq. 1):

$$\frac{\dot{z}}{v} = \alpha \left(\frac{\tau - \tau_c}{\rho v^2}\right)^m + \beta \left(\frac{\Delta\tau}{\rho v^2}\right)^n + \gamma \left(\frac{\Delta\sigma}{\rho v^2}\right)^p \quad , \tag{1}$$

Where v, is the flow velocity, τ refers to the hydraulic shear stress, τ_c is the critical shear stress (the threshold shear stress associated with 0.1 mm/hr erosion rate), $\Delta\sigma$ refers to the net uplift normal stress fluctuations, and $\Delta\tau$ is the shear stress turbulent fluctuations. Any other parameter in Eq. 1 are the unit-less erosion model parameters. Determining all the parameters required in Eq. (1) is not practical at this time; therefore, a more practical erosion model is presented in this study (Eq. 2):

$$\frac{\dot{z}}{0.1} = \left(\frac{\tau}{\tau_c}\right)^{\alpha} \times \left(\frac{\sigma}{\sigma_c}\right)^{\beta} \quad , \tag{2}$$

Where, $\dot{z}$ is the erosion rate (mm/hr), τ_c (Pa) and σ_c (Pa) are the critical shear stress and critical normal stress associated with 0.1 mm/hr erosion rate, and α and β are the unit-less erosion model parameters.

Eq. 2 is expected to capture the influence of both shear and normal stresses during erosion.

2.2 Problem Summary

The measurement methods of hydrodynamic forces that are developed so far are not practical and precise enough. A new method needs to be created to measure or calculate the normal and shear stress acting on the soil particles before detachment during the erosion process. The erosion model showed in Eq. (1) is involves many different parameters difficult to determine at this time. Therefore a more practical erosion model needs to be developed, considering both shear stress and normal stress effects.

In this study, the erosion phenomenon is monitored using image analysis techniques for five gravel size particle samples and the movement of these particles is recorded in the Erosion Function Apparatus (EFA). Through derivative calculations, the velocity and the acceleration of each particle, and consequently the forces acting on each particle before detachment are obtained. The results of this analysis can show the roles that the hydrodynamic shear and normal forces play in the detachment of the gravel particle from the river bed, and help develop the new erosion model that is more practical while considering several influencing forces.

3. EXPERIMENTS

3.1 Experimental Device

The experiment device used in this study is called the Erosion Function Apparatus (EFA). The soil sample is taken in the field by pushing an ASTM standard Shelby tube with a 76.2 mm outside diameter (ASTM 1999a). A soft rock core sample can also be obtained and placed in the Shelby tube. One end of the Shelby tube full of soil or soft rock is placed through a circular opening in the bottom of a 1.22m long rectangular cross section pipe (Figure 4, Briaud et al., 2001). The water is driven through the pipe by a pump, the flow rate is measured by a flow meter with a range of 0.1 to 6 m/s. The end of the sample in the Shelby tube is held flush with the bottom of the pipe, a piston at the bottom end of the sample pushes the sample to maintain it flush with the bottom o fthe conduit. The advance of the piston is the erosion rate and the flow meter gives the velocity. The shear stress is obtained from the velocity and the surface roughness by using the Moody chart.

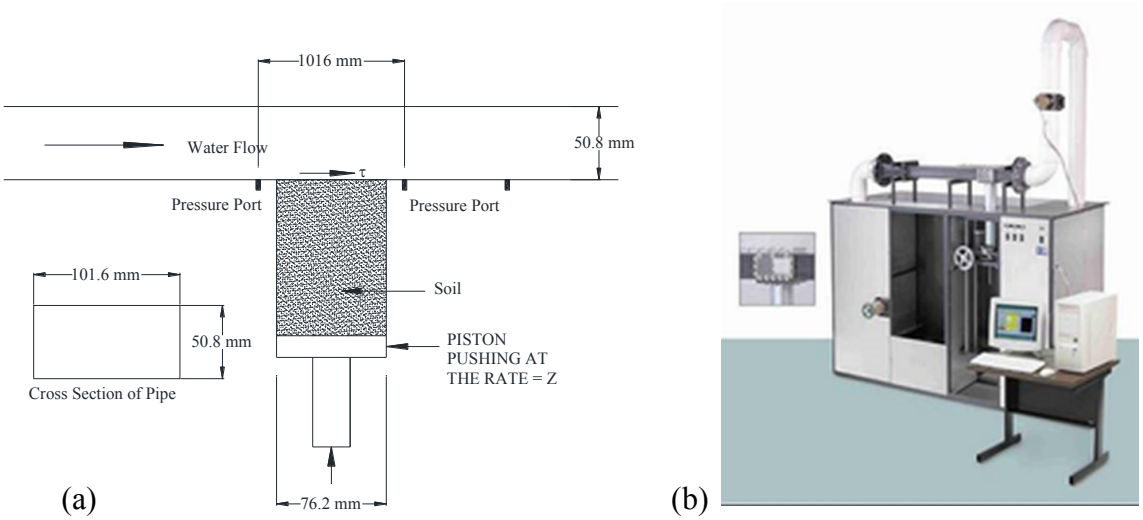

Figure 4. Erosion Function Apparatus: (a) Conceptual Diagram; (b) Photograph of Test Section (Texas A&M University)

3.2 Experimental Procedure and Measurement

The procedure for the EFA test is as follows (Briaud et al., 2001):

1) Place the sample in the Shelby tube then connect to the EFA, fill the pipe with water and wait one hour.

2) Set the velocity to 0.3 m/s.

3) Push the soil to be flush with the bottom of the flow conduit.

4) advance the piston to maintain the soil surface flush with the bottom of the conduti as erosion takes place.

5) After a 30 mm period or after 25 mm of soil sample is erode, whichever comes first, increase the velocity to 0.6 m/s.

6) Repeat step 4.

7) Repeat step 5 and 6 for velocities equal to 1 m/s, 1.5 m/s, 2 m/s, 3 m/s, 4.5 m/s, and 6 m/s.

The test result can be shown as erosion rate $\dot{z}$ versus mean-depth velocity; this curve is called the erosion function. For each flow velocity, the erosion rate $\dot{z}$ (mm/h) is obtained by dividing the length of sample eroded by the time required to do so.

In this study, five different samples were tested in the EFA. All five samples were coarse-grained samples classified as GP according to the USCS classification system. Particle size properties of each sample are shown in Table 1.

Table 1. Particle Size Properties of the Gravel Samples

Sample name	Sample symbol	USCS	D_{50}	C_c	C_u	G_s
			mm	-	-	-
Gravel 1	G1	GP	11	0.93	2.17	2.3
Gravel 2	G2	GP w/ sand	6	1.23	2.41	2.2
Teflon balls	TB	GP	5	1	1	2.16
Sand coated Teflon balls	SB	GP	5	1	1	2.16
Gravel 3	GB	GP	5	1	1	2.3

Figure 5 shows photos of the surface of all five samples in the EFA prior to testing. G1, G2, and GB are natural gravel samples, while TB and SB are artificial samples. TB is composed of uniformly distributed 5 mm diameter "Polytetrafluoroethylene (PTFE)" or Teflon spheres. The friction at the contact surface between the particles is expected to be close to zero for TB. SB is composed of uniformly distributed 5 mm sand-coated PTFE spheres. The friction at the contact surface between the particles and the water is expected to be maximum for SB compared to almost zero for TB. The three samples GB, TB, and SB have about the same mean particle size with the only difference being their specific gravity (G_s, Table 1) and friction characteristics.

The movement of the soil particles is recorded by a camera for further image analysis.

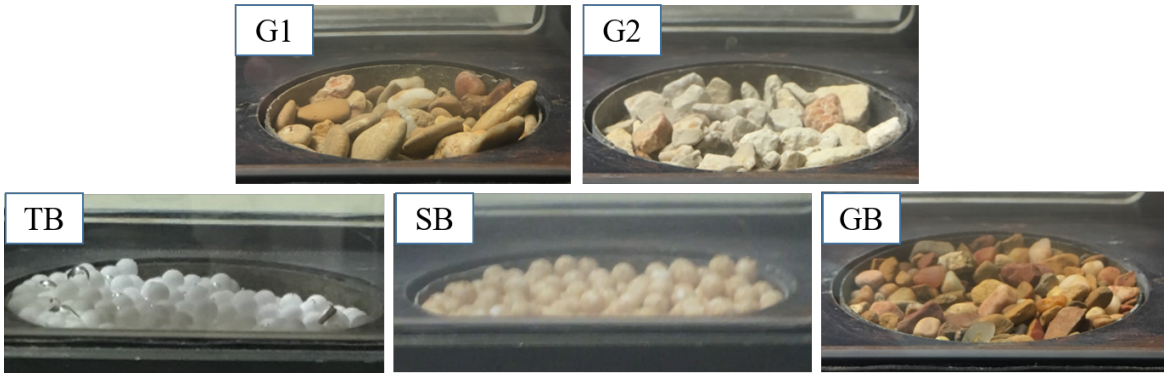

Figure 5. Photos of the Surface Samples in the Erosion Function Apparatus (EFA)

3.3 Data Collected

All five samples were tested in the Erosion Function Apparatus and the results in the format of erosion rate vs. mean-depth velocity are shown in Figure 6. GB, TB, and SB are in the high erodibility category while G1 and G2 are in the medium erodibility category when the water velocity is low. As the velocity becomes higher, finally G1 and G2 switch to the high erodibility category.

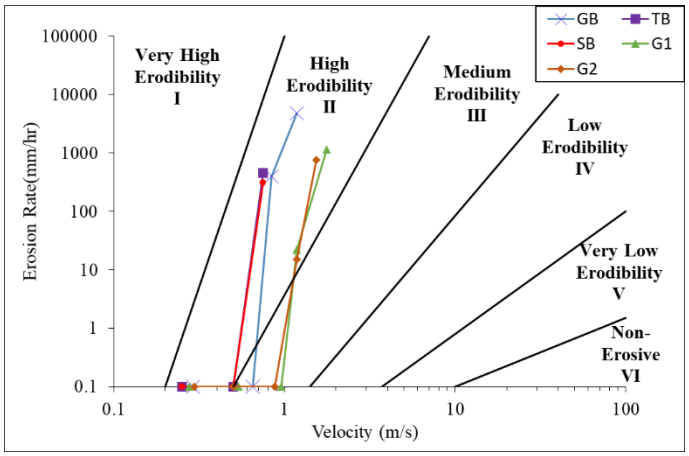

Figure 6. Erosion Function Apparatus Results (Erosion rate vs. Velocity)

Erosion Function Apparatus or EFA test results can also be presented in the format of erosion rate vs. shear stress. Shear stress in the EFA is calculated by Eq. (3):

$$\tau = \frac{1}{8} f \rho v^2 \ , \tag{3}$$

Where τ is the shears stress (Pa), v refers to the flow velocity, ρ is the density of water (1000 kg/m^3) and f is the friction factor obtained from the Moody Chart (Moody, 1944). The values of shear stress are obtained using both Eq. (3) and direct measurements through video analysis. The results are compared and the validity of Eq. (2) is studied for both cases.

Two videos of each soil sample are collected during the erosion process for further image analysis.

4. RESULTS AND ANALYSIS

4.1 Analysis Tool and Procedure

The software used for the image analysis is called Tracker. Tracker is a free video analysis and modeling tool built on the Open Source Physics (OSP) Java framework (Tracker, 2018). By importing the videos into the software, the movement of selected particles can be tracked and traced for further analysis.

To use this software, the first step is to import the video that needs to be analyzed. If it is a slow-motion video, then a time correction will be necessary for future calculations. Secondly, choose the start and ending frame in the video by dragging the little triangle under the time bar. Then use the toolbar to build a plotting scale, input the distance that is already known beforehand (76mm for the outside diameter of the tube in the EFA machine in this case), and build a 2-D reference frame in the same way. Notice that it is best to ensure that the angle of the x-axis is the same as the angle of the scale. Finally, create a new mass point and the file is ready for tracking.

Press the shift button on the computer, when the arrow of the mouse becomes an asterisk, click the point that you want to trace, then the video will move to the next frame automatically, at the same time the time and location (based on the reference frame just built) of the point will be recorded by the software in a table on the right side and also shown in a plot. The time of the start point will be recorded as 0 sec. By clicking frame by frame, the motion curve will be built and the data will be saved.

In this low budget research, the videos were taken through the EFA observation window by an iPhone using the slow-motion option that is provided by the camera system. Since the time rate will change when using the slow-motion video, the plots that are built by the software can't

be used directly. As the iPhone 7 camera can do the slow-motion video with 1080 pixels at 120 frame per second and 720 pixels at 240 frame per second, the video we used in the analysis is a 720p video, and the original video is 30 fps, so the video is actually 8 times slower than before.

The time correction is made by importing the original data into Excel, which gives us the time that needs to be corrected, as well as the distance in both x and y direction. The algorithm Tracker uses to calculate velocity and acceleration is based on the Finite Difference Method. The corrected time, velocity and acceleration in both the horizontal (x) and vertical (y) directions are generated using the following algorithm (Eqs. 4 to 6):

$$r = (x^2 + y^2)^{0.5}, \tag{4}$$

$$v_i = \frac{x_{i+1} - x_{i-1}}{2\Delta t}\ , \tag{5}$$

$$and\ \ a_i = \frac{2x_{i+2} - x_{i+1} - 2x_i - x_{i-1} + 2x_{i-2}}{7\Delta t^2}\ . \tag{6}$$

Where r refers to the resultant displacement of the particle, v_i is the velocity of the particle, and a_i is the acceleration of the particle. From the acceleration values, the drag force and the normal force on the particle were calculated by multiplying the acceleration by the mass of the particle. The shear stress and the normal stress were then obtained by dividing the force by the area. The calculations of forces and stresses are detailed in the next section.

4.2 Experimental Results

For each of the soil type, four particles were analyzed using Tracker. The particle properties that will be used in the future calculation are shown in Table 2. The diameter, volume and area of particles can be directly measured or estimated from Tracker, assuming the gravel particles are Ellipsoid or Sphere. For TB and SB particles, the volume, surface area and cross-section area can be calculated since they are spheres with a diameter of 5mm. The equations will be V=$\frac{4}{3}\pi r^3$; As=2 πr^2; Ac= πr^2. For G1, G2 and GB particles, based on the shape of the chosen particles, some of them can be estimated as spheres and use the same equations, others can be seen as ellipsoid, and the equations used will be V=$\frac{4}{3}\pi abc$; As=$2\pi(\frac{(ab)^{1.6}+(ac)^{1.6}+(bc)^{1.6}}{3})^{1/1.6}$; Ac= πab, where a is the radius on the semi-major axis of ellipsoid, c is the radius on the semi-minor axis of ellipsoid, and b is the radius on the third direction that is perpendicular to both the semi-major axis and semi-minor axis. The values of a,b, and c can be measured from Tracker by using the scaleplate in the toolbar.

Table 2. Particle Properties of the Gravel Samples

Properties		Unit Weight	Volume V	Mass M	Surface Area As	Cross-Section Area Ac
Unit		g/cm3	cm3	g	cm2	cm2
G1	1	2.65	0.685	1.815	1.9	0.9
	2		0.612	1.622	1.8	0.75
	3		0.589	1.561	1.5	0.67
	4		0.63	1.670	1.6	0.8
G2	1	2.65	0.103	0.273	0.565	0.3
	2		0.123	0.326	0.623	0.35
	3		0.115	0.305	0.6	0.33
	4		0.11	0.292	0.62	0.32
TB	1	2.2	0.065	0.143	0.39	0.195
	2		0.065	0.143	0.39	0.195
	3		0.065	0.143	0.39	0.195
	4		0.065	0.143	0.39	0.195
SB	1	2.2	0.065	0.143	0.39	0.195
	2		0.065	0.143	0.39	0.195
	3		0.065	0.143	0.39	0.195
	4		0.065	0.143	0.39	0.195
GB	1	2.65	0.065	0.172	0.39	0.195
	2		0.062	0.164	0.38	0.183
	3		0.063	0.167	0.38	0.185
	4		0.065	0.172	0.39	0.193

The drag force will be calculated by multiplying the hotizontal acceleration by the mass of the particle. The normal force will be calculated by multiplying the vertical acceleration by the mass of the particle. Then shear stress will be obtained by dividing the drag force by the surface area and the normal stress will be obtained by dividing the normal force by the cross-section area of the particles. An example of the datra reduction for one of the particles from the sample G1 is explained below.

Figure 7. Movement of Particle 1 of G1 in the Erosion Function Apparatus

One particle (Fig. 7) is selected. The trace of the particle is tracked with 30 frames per second recordings. Results of the displacement, velocity, acceleration, stress and force at incipient motion are shown in Figure 8 and 9, for horizontal and vertical directions, respectively. The dashed lines on the plots show the time associated with the detachment of the particle called the departure time.

1) Horizontal direction (x direction):

Figure 8. Horizontal displacement, velocity, acceleration, stress and force as a function of time for particle 1 of G1.

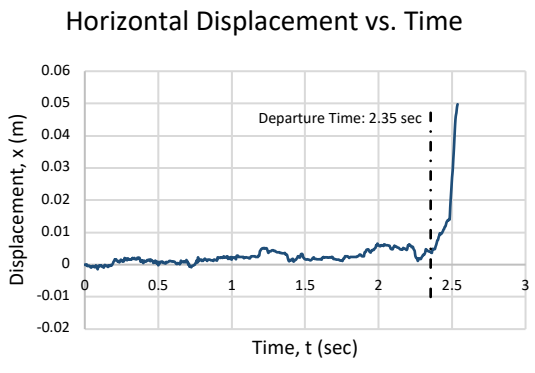

Figure 8 Continued

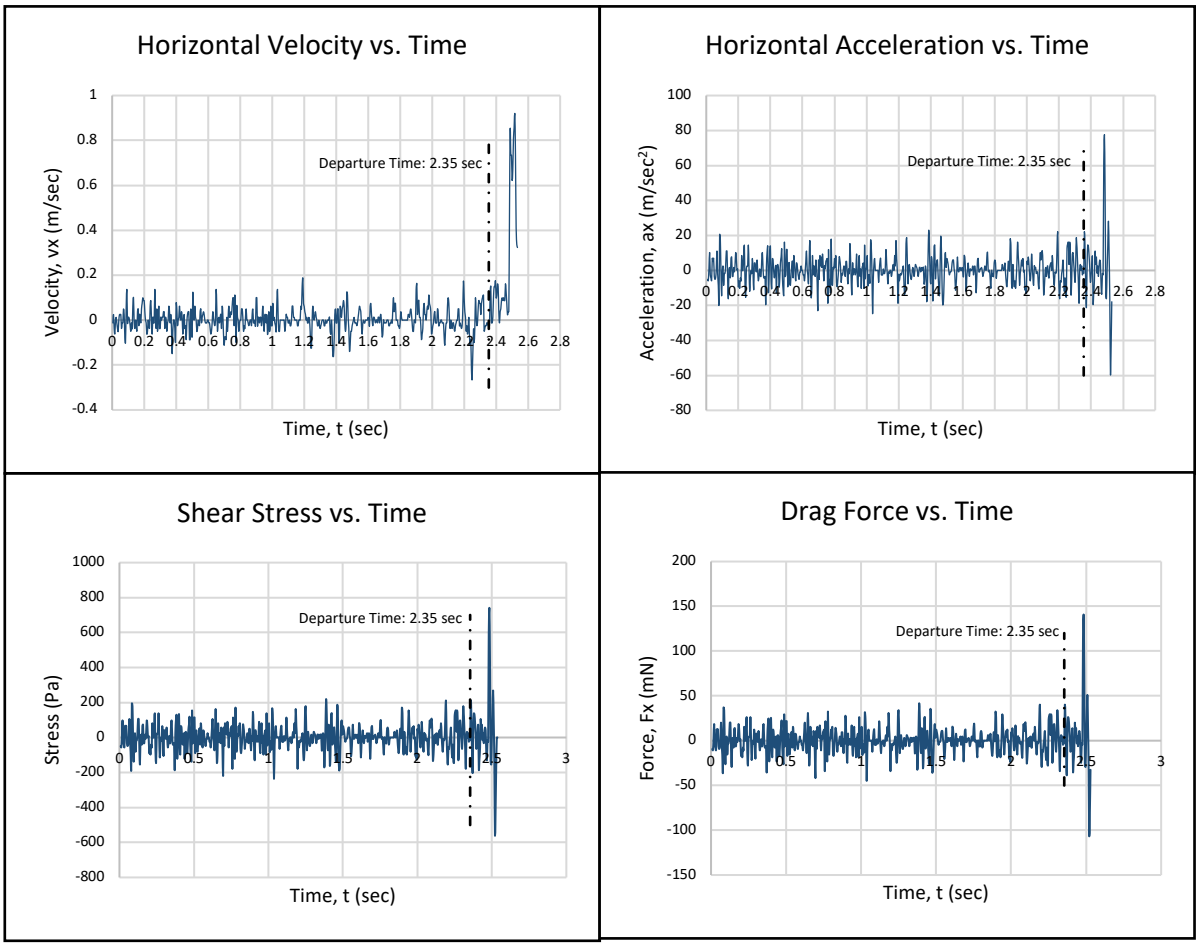

2) Vertical direction (y direction):

Figure 9. Vertical displacement, velocity, acceleration, stress and force as a function of time for particle 1 of G1.

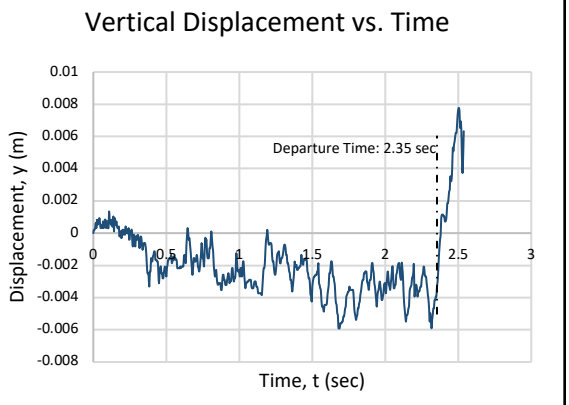

Figure 9 Continued

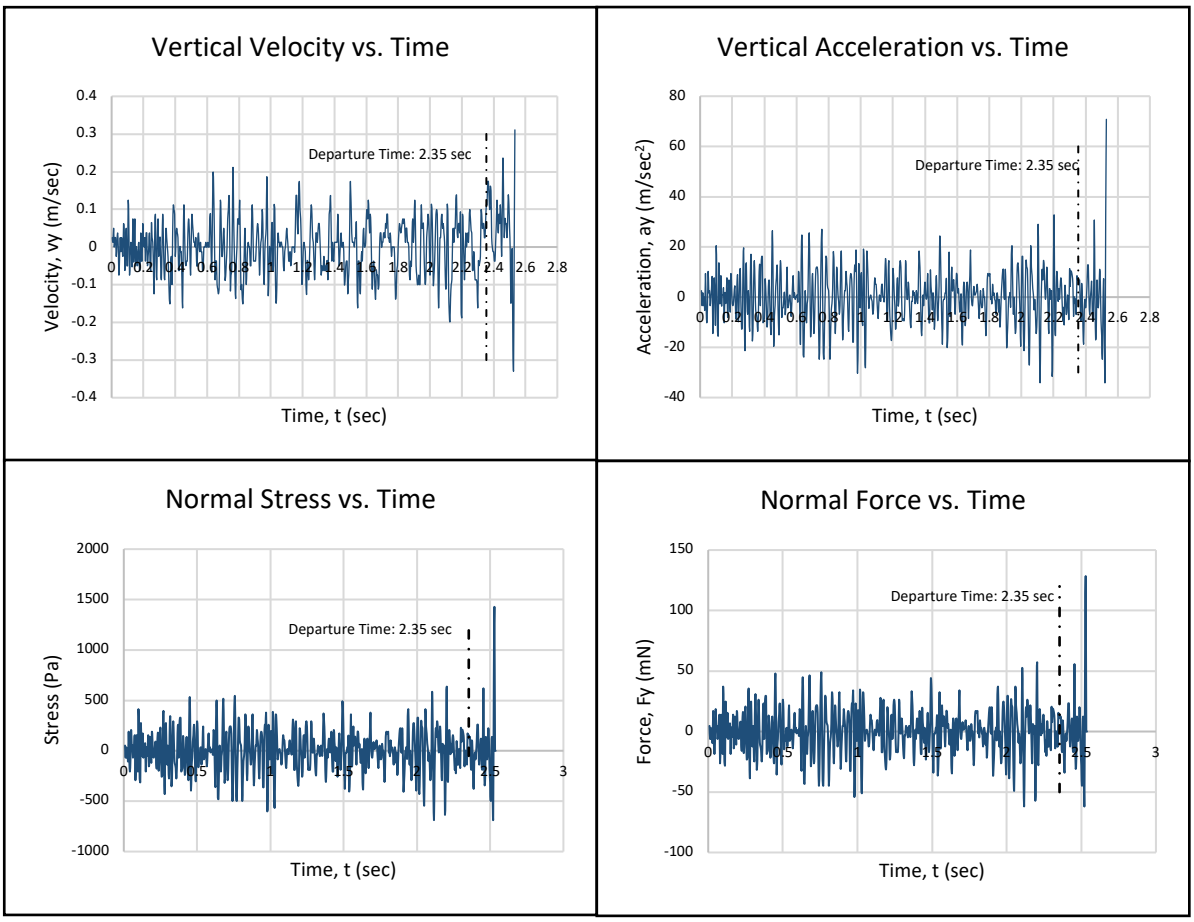

The results of other particles are shown below:

Particle 2 of G1:

Figure 10. Movement of Particle 2 of G1 in the Erosion Function Apparatus

1) Horizontal direction (x direction):

Figure 11. Horizontal displacement, velocity, acceleration, stress and force as a function of time for particle 2 of G1.

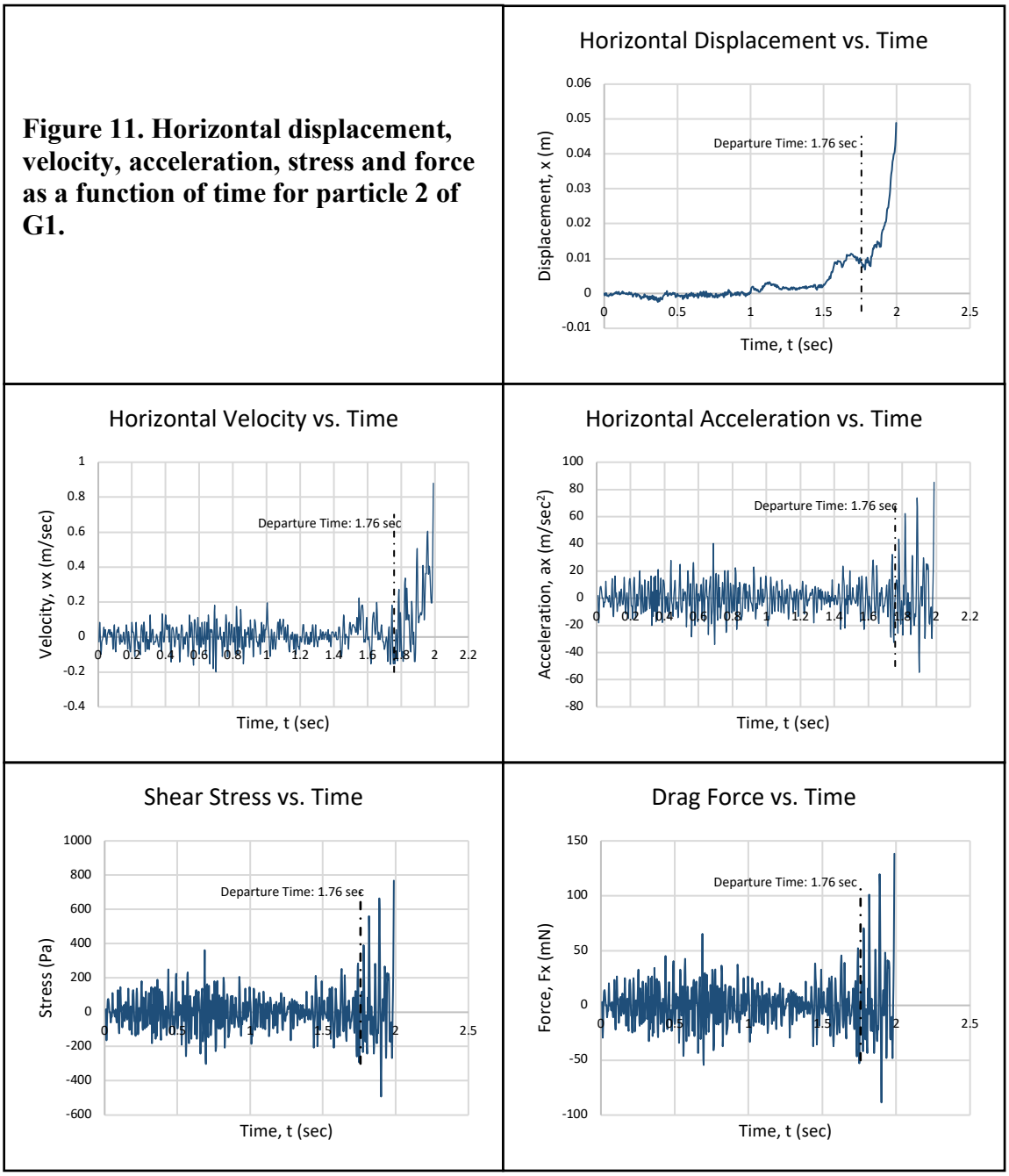

2) Vertical direction (y direction):

Figure 12. Vertical displacement, velocity, acceleration, stress and force as a function of time for particle 2 of G1.

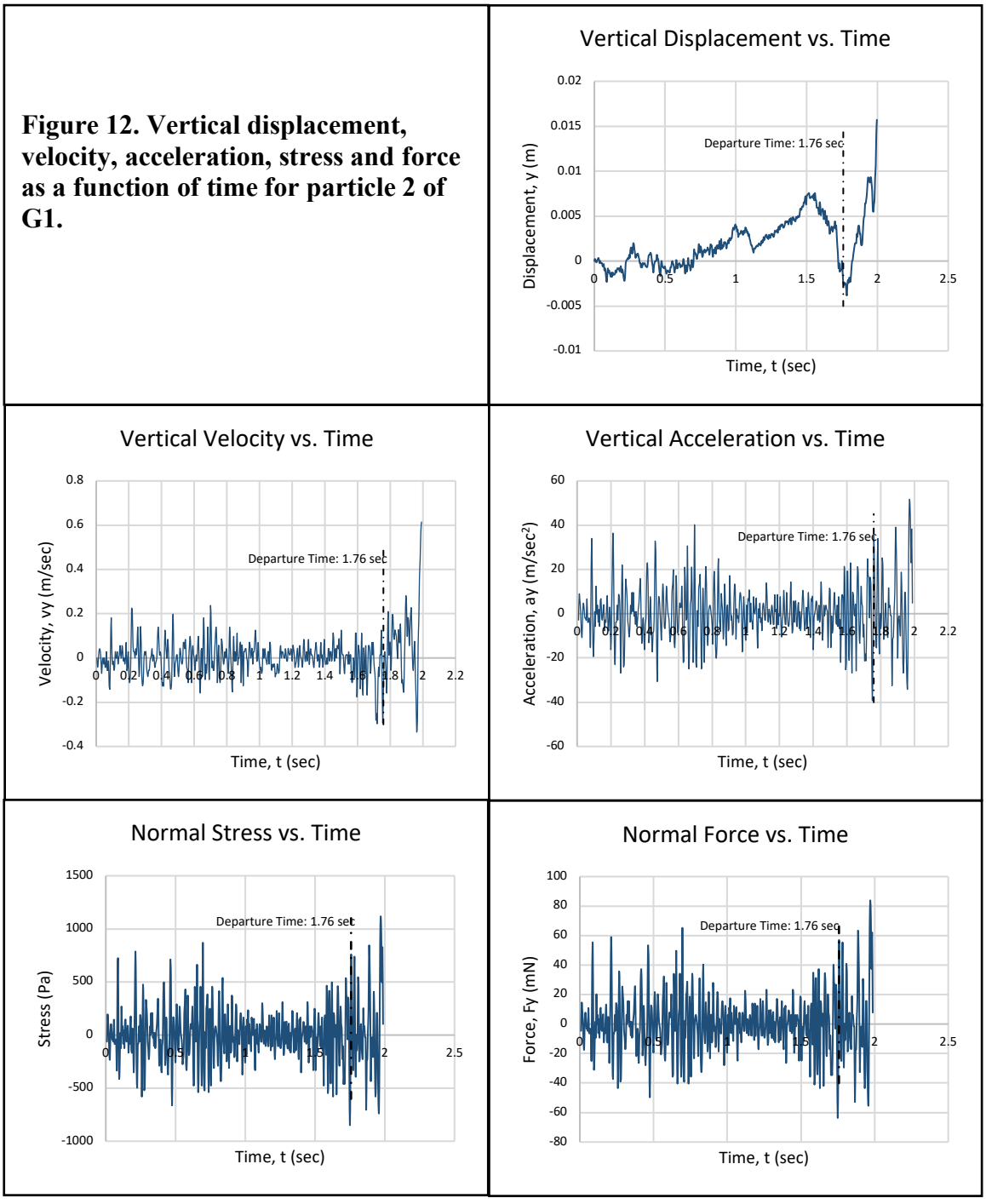

Particle 3 of G1:

Figure 13. Movement of Particle 3 of G1 in the Erosion Function Apparatus

1) Horizontal direction (x direction):

Figure 14. Horizontal displacement, velocity, acceleration, stress and force as a function of time for particle 3 of G1.

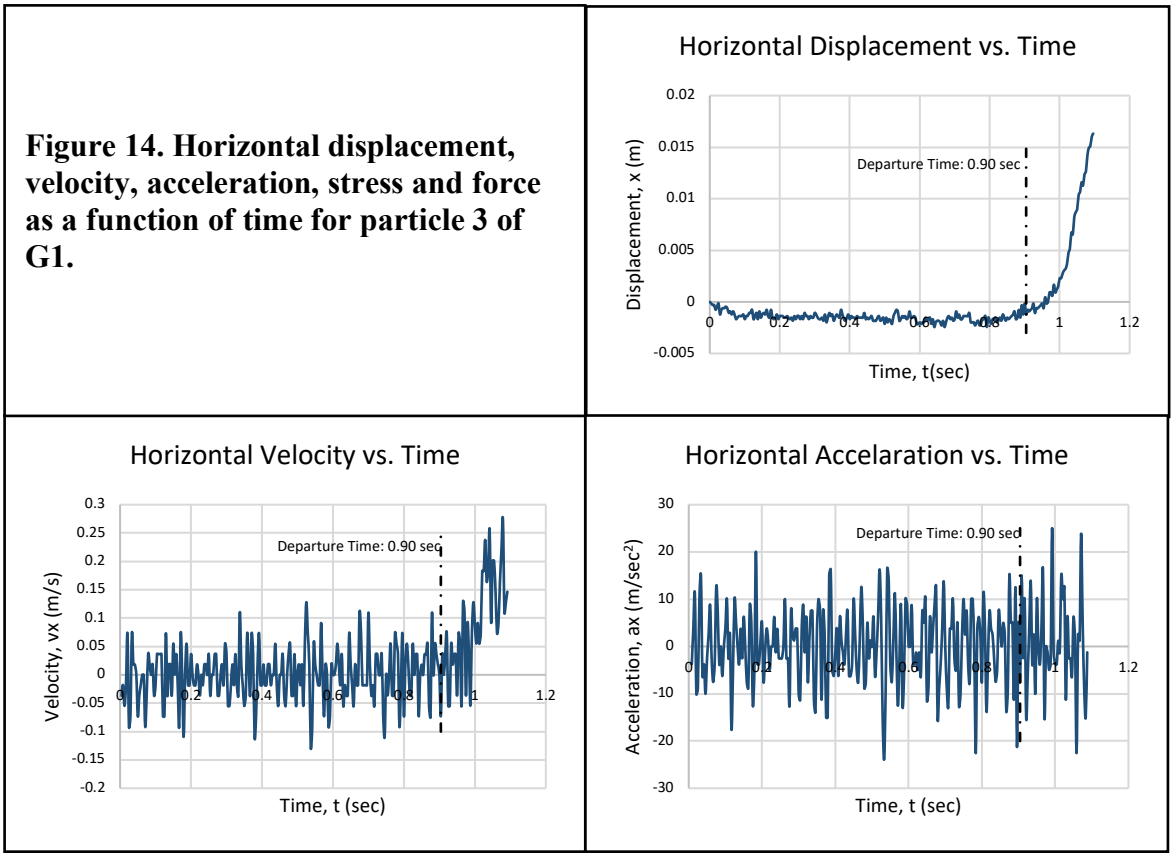

Figure 14 Continued

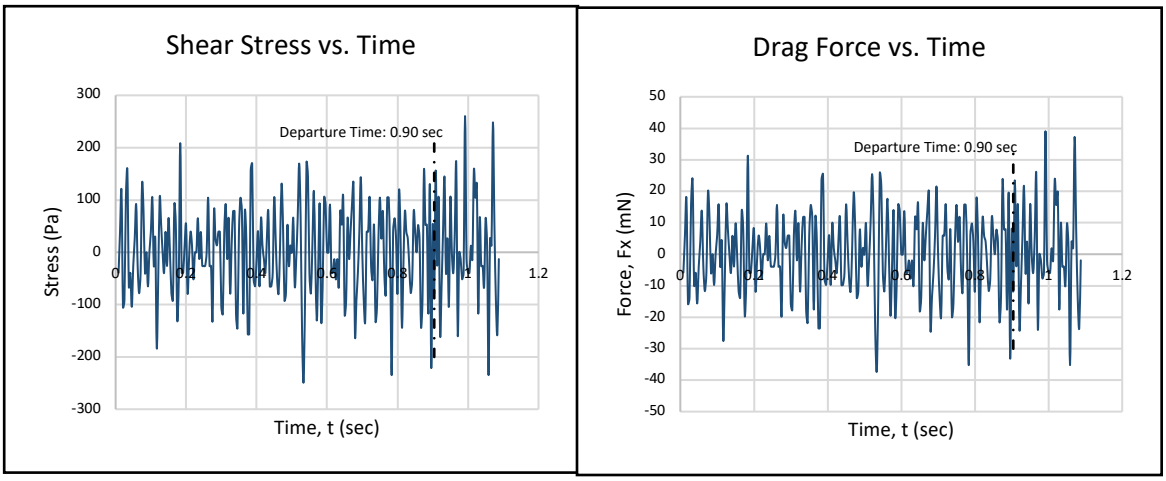

2) Vertical direction (y direction):

Figure 15. Vertical displacement, velocity, acceleration, stress and force as a function of time for particle 3 of G1.

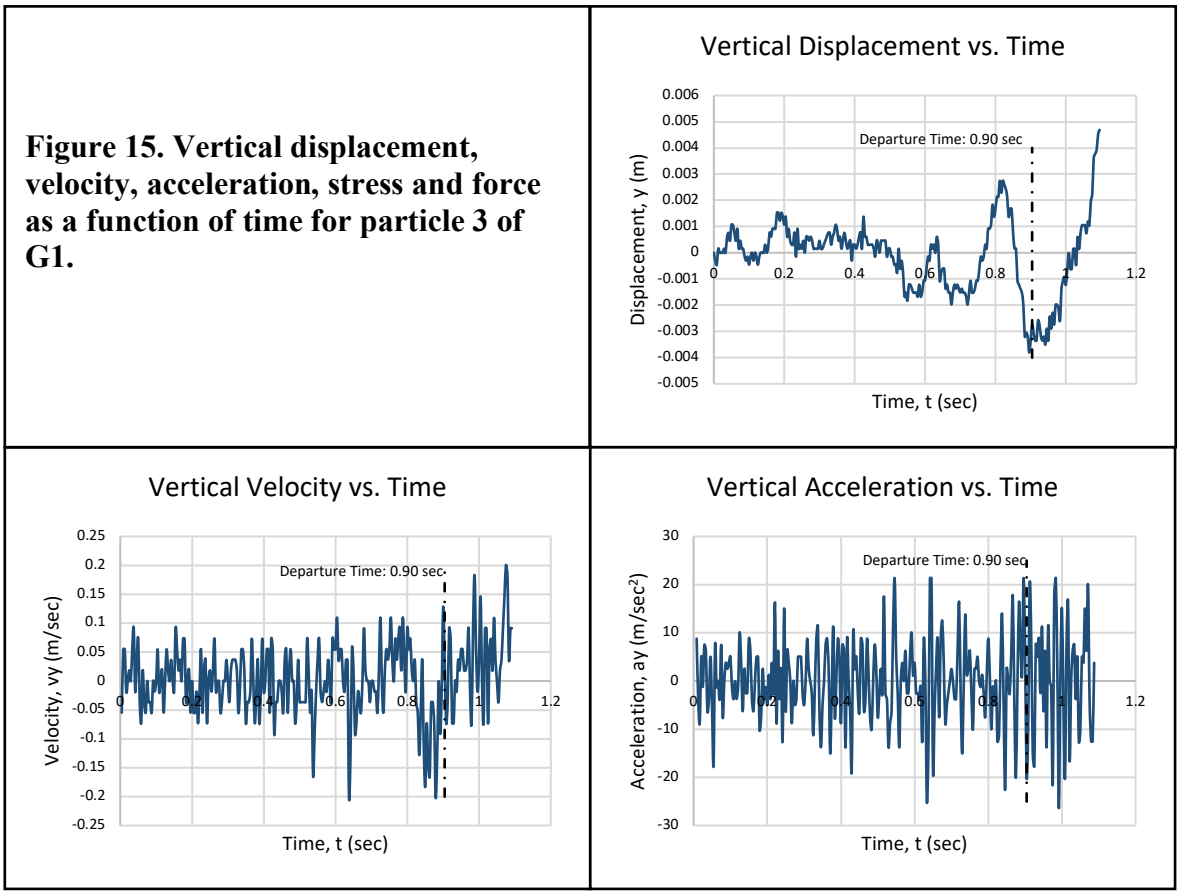

Figure 15 Continued

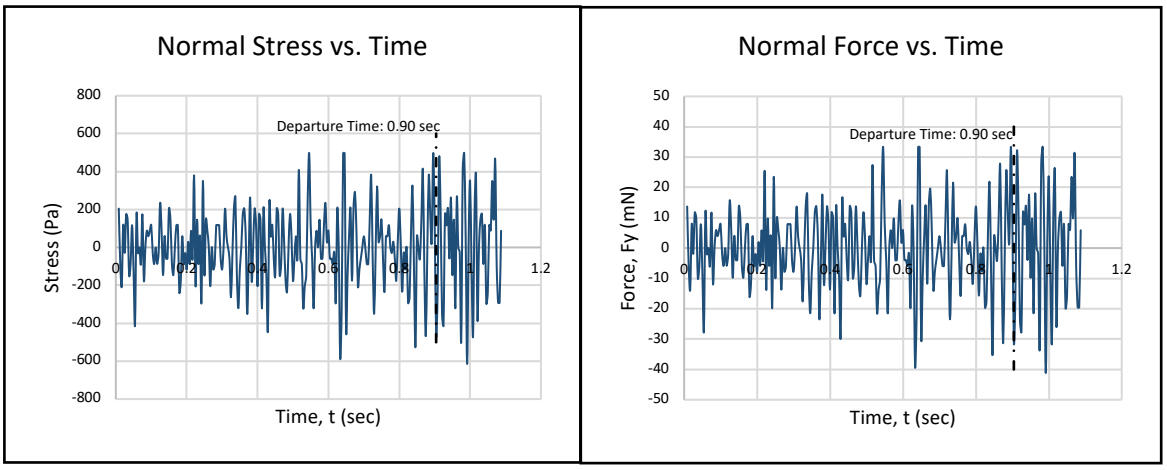

Particle 4 of G1:

Figure 16. Movement of Particle 4 of G1 in the Erosion Function Apparatus

1) Horizontal direction (x direction):

Figure 17. Horizontal displacement, velocity, acceleration, stress and force as a function of time for particle 4 of G1.

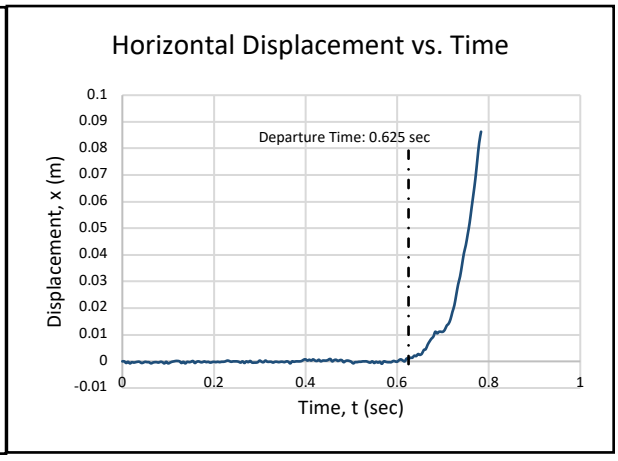

Figure 17 Continued

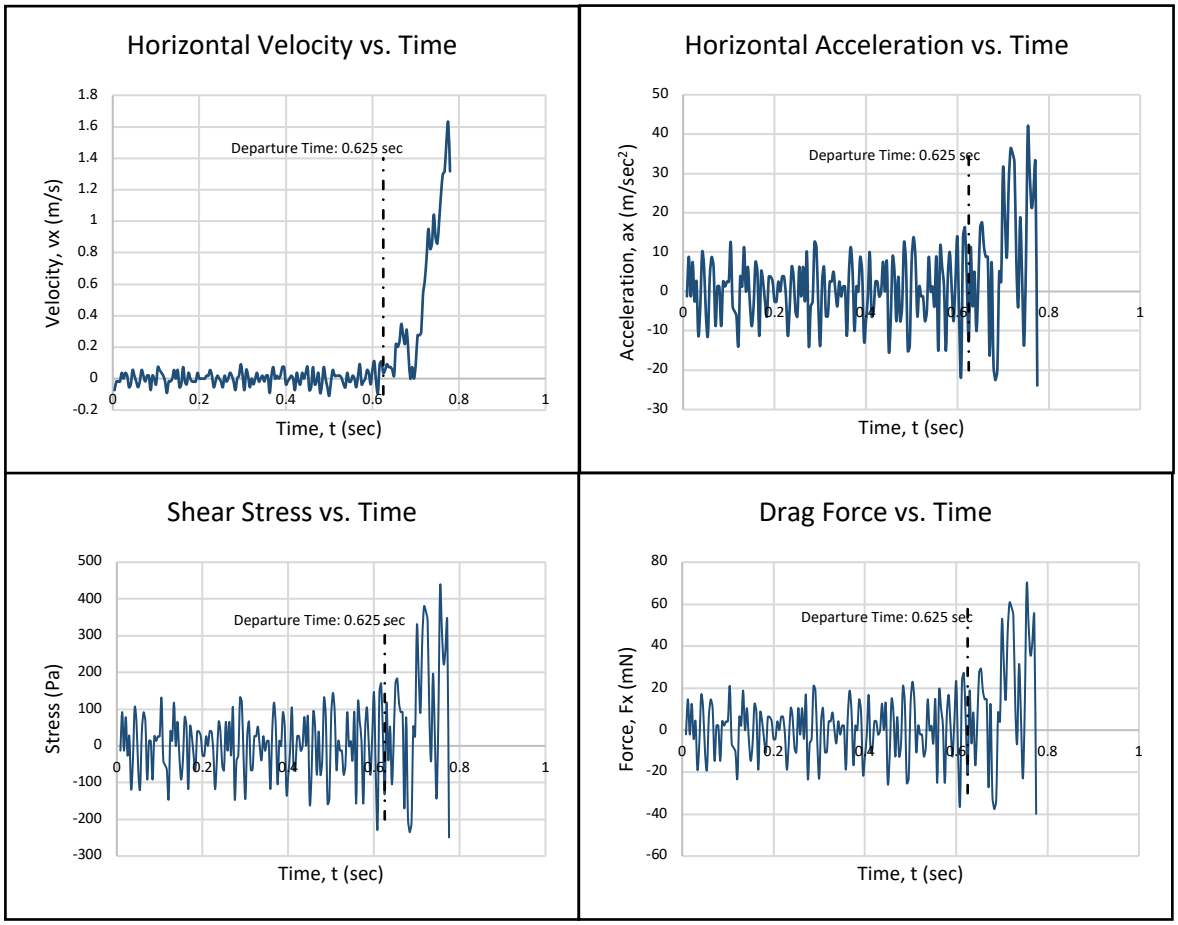

2) Vertical direction (y direction):

Figure 18. Vertical displacement, velocity, acceleration, stress and force as a function of time for particle 4 of G1.

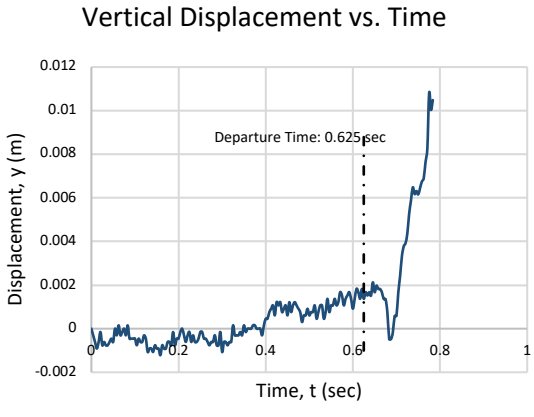

Figure 18 Continued

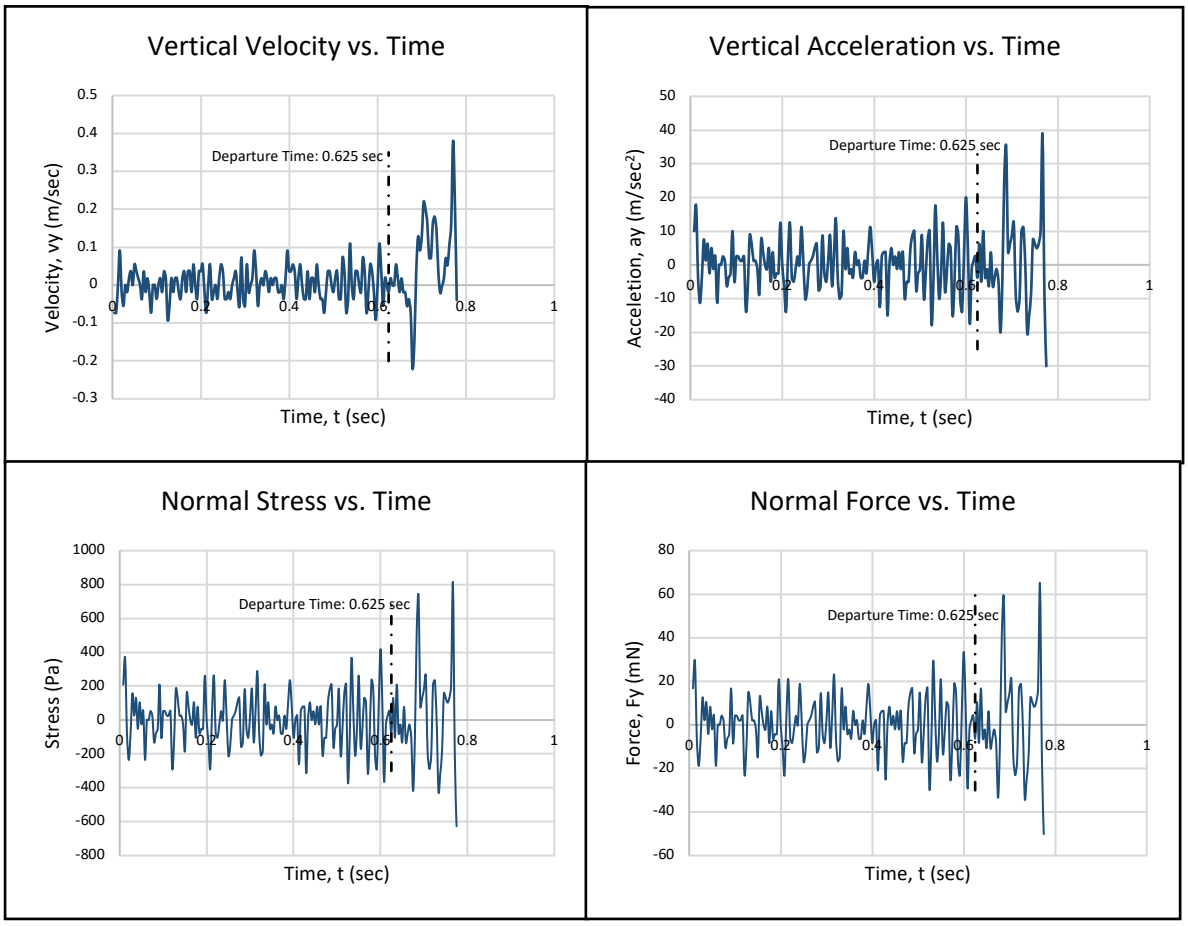

Particle 1 of G2:

Figure 19. Movement of Particle 1 of G2 in the Erosion Function Apparatus

1) Horizontal direction (x direction):

Figure 20. Horizontal displacement, velocity, acceleration, stress and force as a function of time for particle 1 of G2.

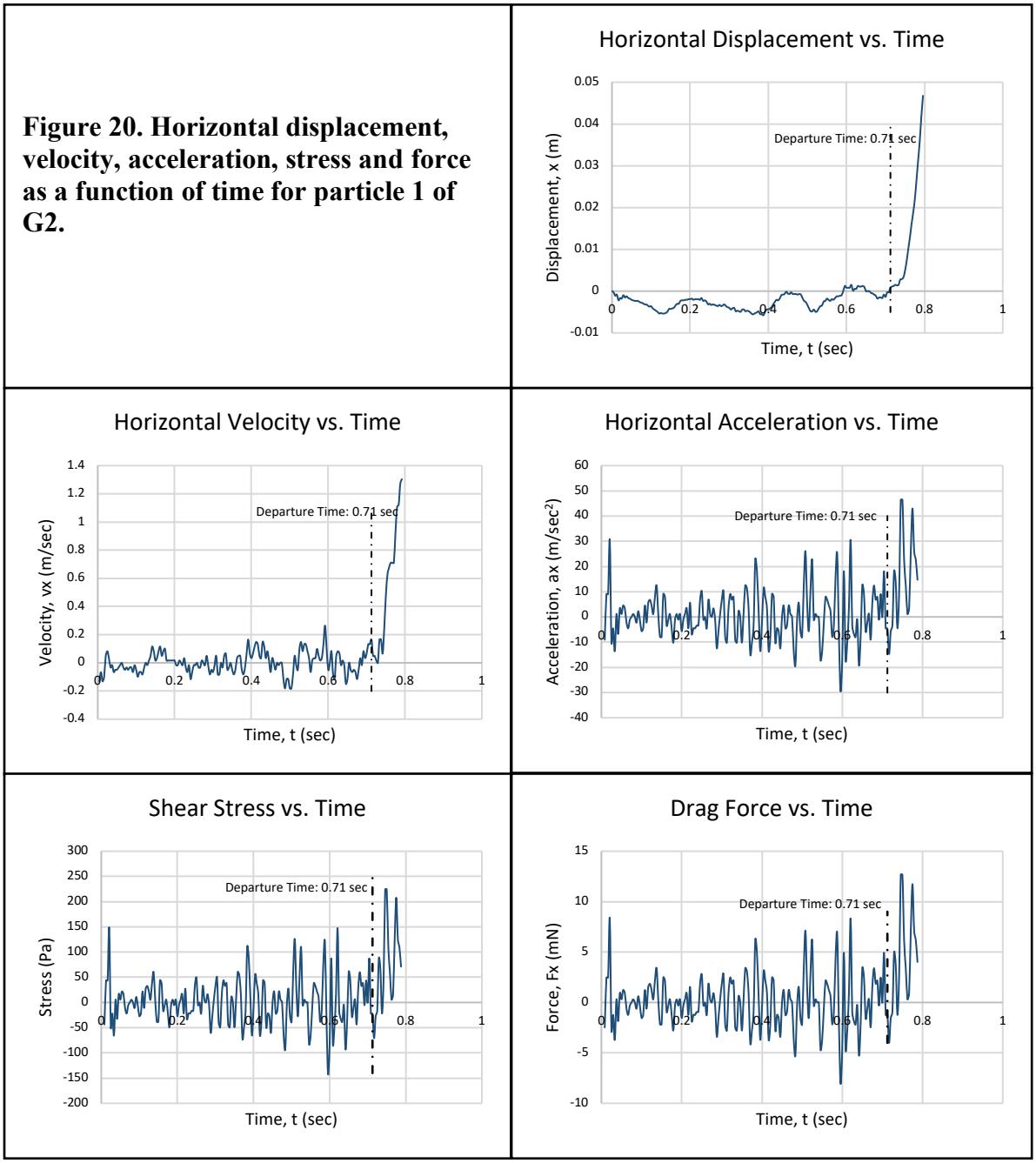

2) Vertical direction (y direction):

Figure 21. Vertical displacement, velocity, acceleration, stress and force as a function of time for particle 1 of G2.

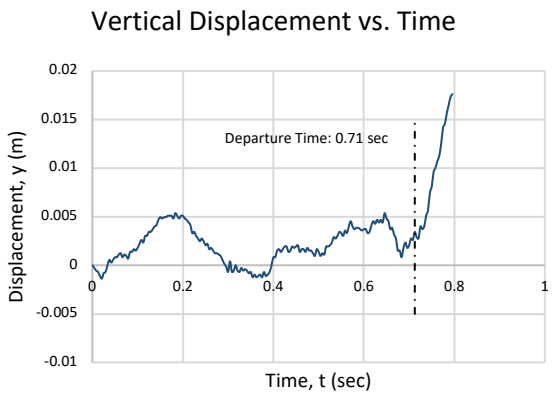

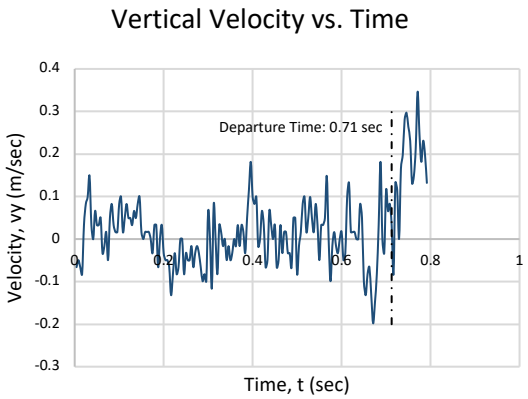

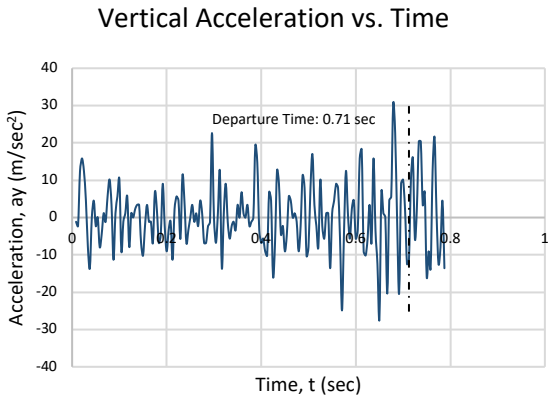

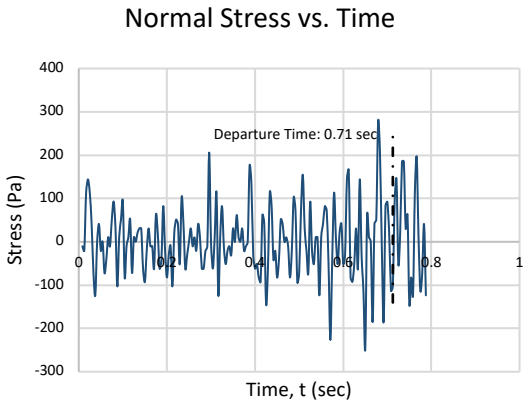

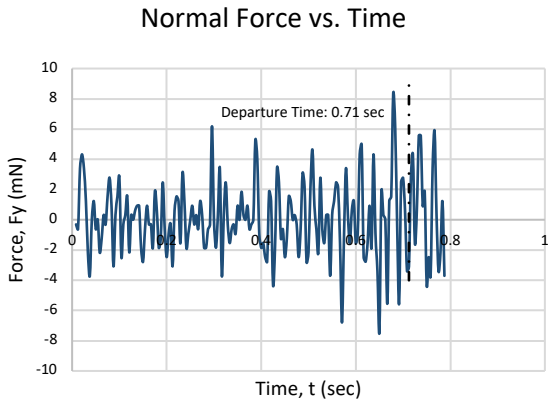

Particle 2 of G2:

Figure 22. Movement of Particle 2 of G2 in the Erosion Function Apparatus

1) Horizontal direction (x direction):

Figure 23. Horizontal displacement, velocity, acceleration, stress and force as a function of time for particle 2 of G2.

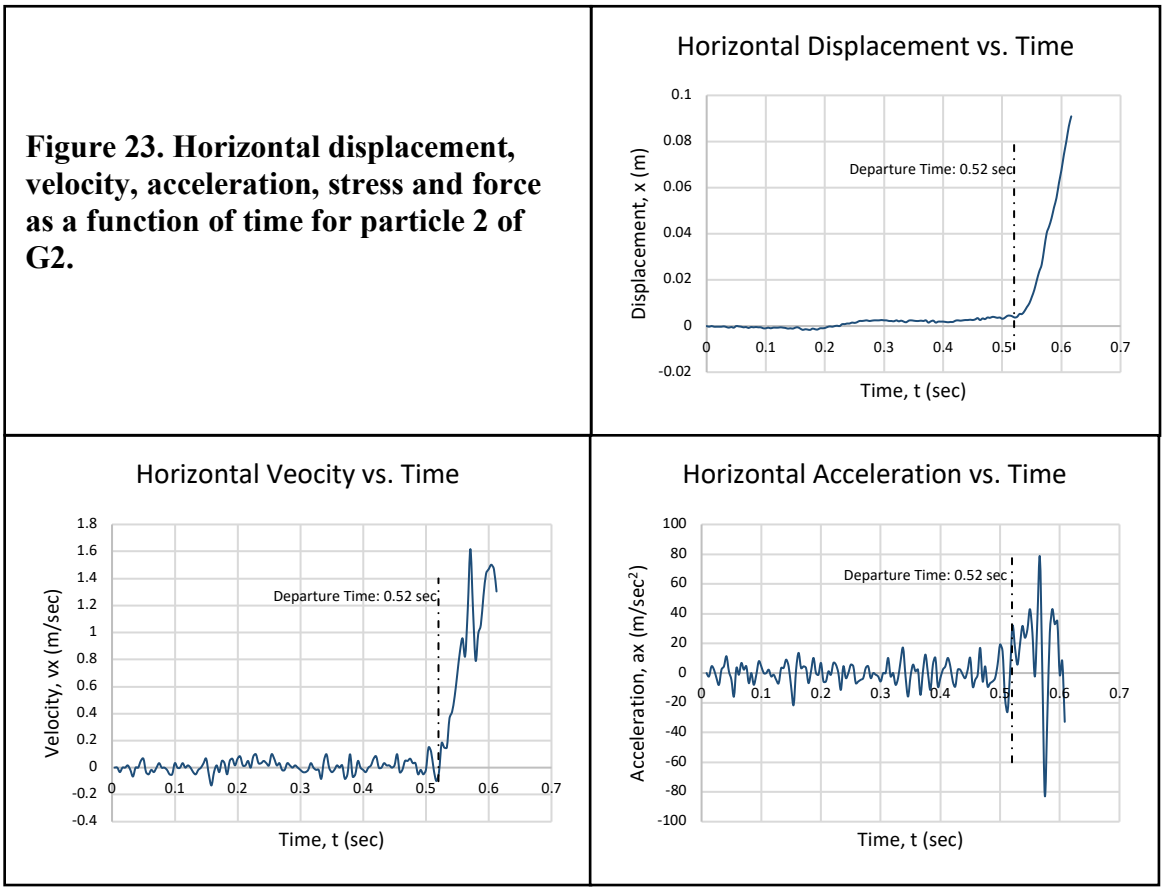

Figure 23 Continued

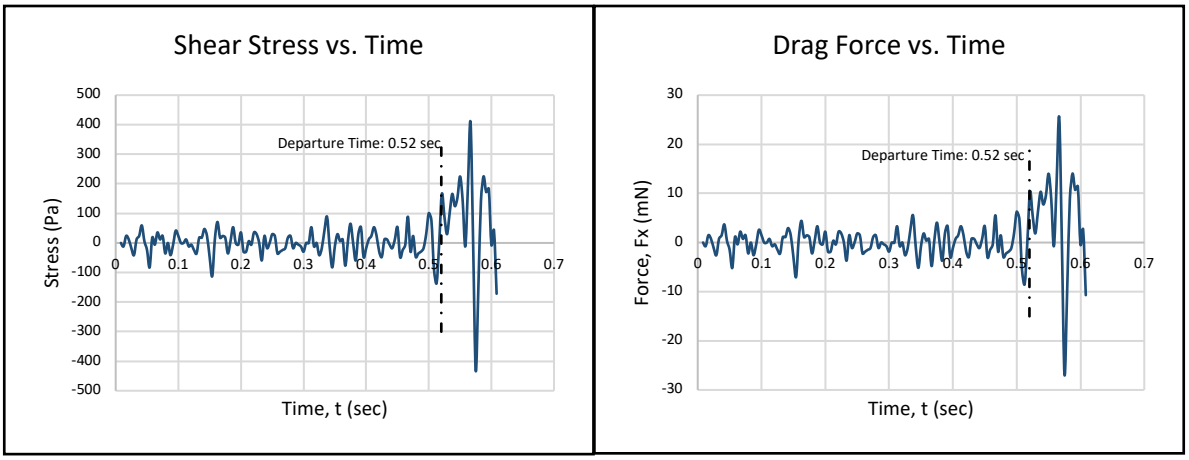

2) Vertical direction (y direction):

Figure 24. Vertical displacement, velocity, acceleration, stress and force as a function of time for particle 2 of G2.

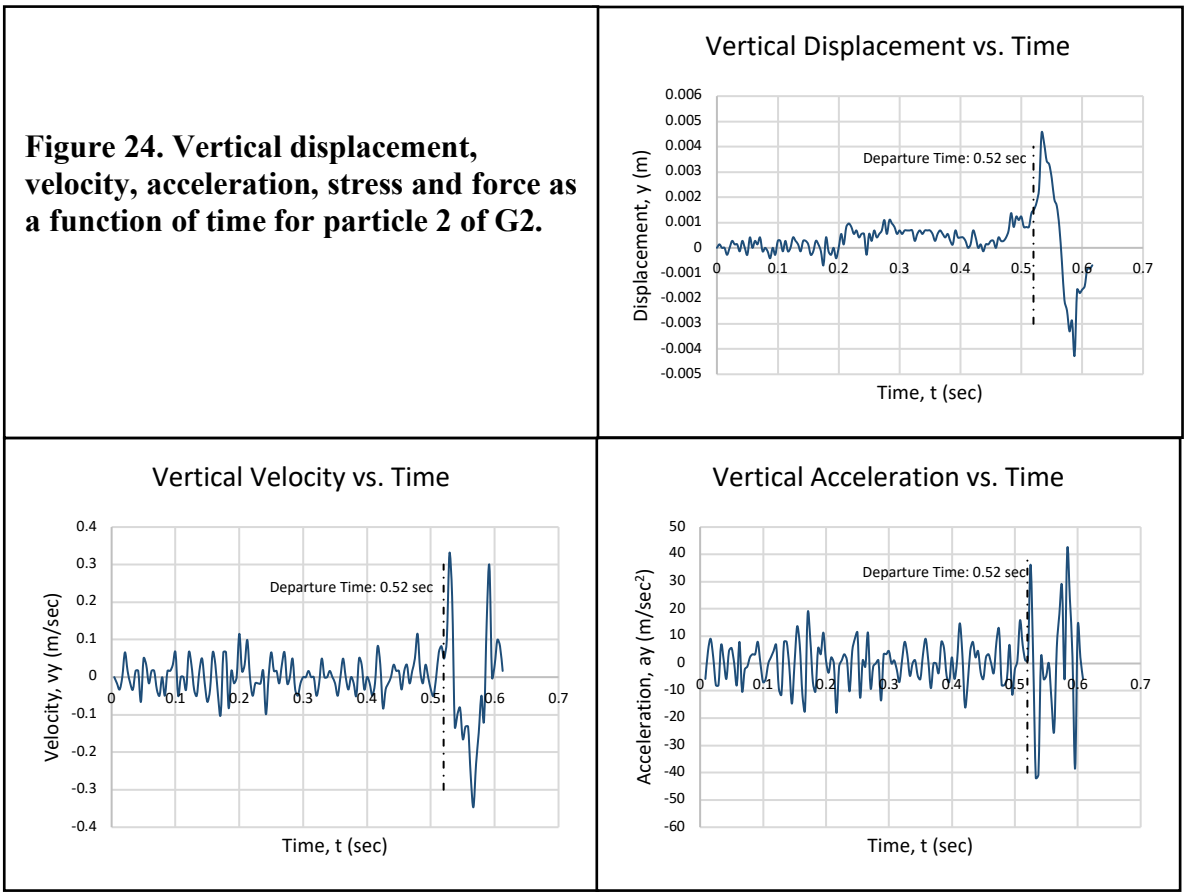

Figure 24 Continued

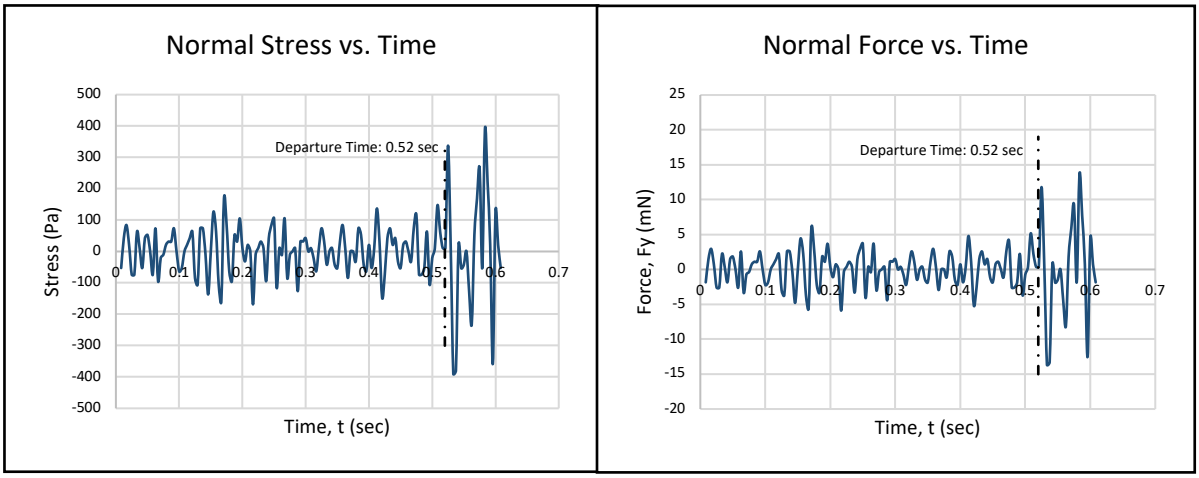

Particle 3 of G2:

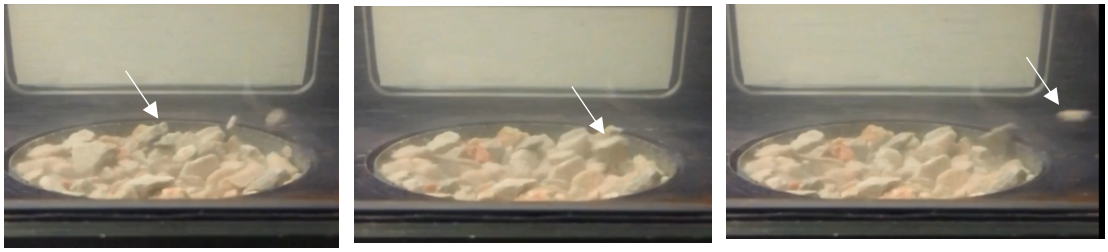

Figure 25. Movement of Particle 3 of G2 in the Erosion Function Apparatus

1) Horizontal direction (x direction):

Figure 26. Horizontal displacement, velocity, acceleration, stress and force as a function of time for particle 3 of G2.

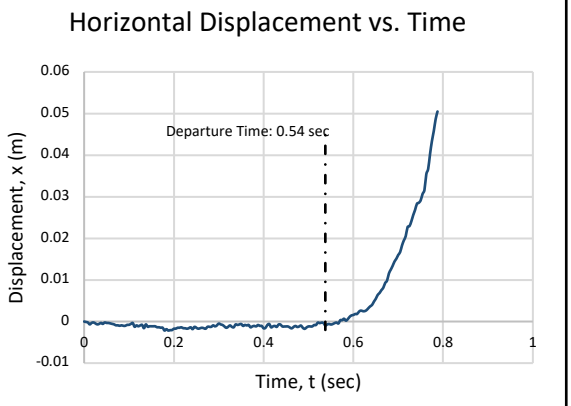

Figure 26 Continued

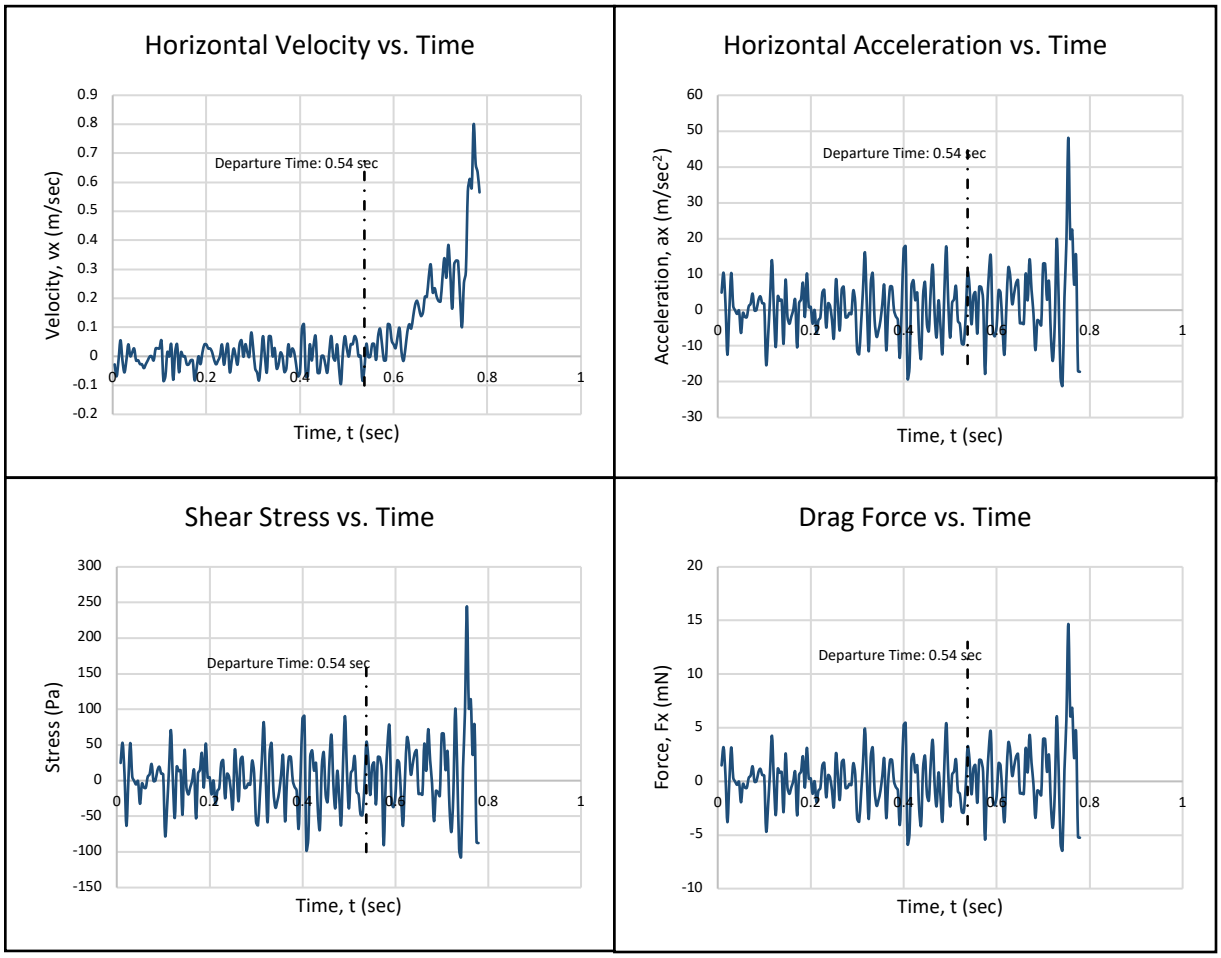

2) Vertical direction (y direction):

Figure 27. Vertical displacement, velocity, acceleration, stress and force as a function of time for particle 3 of G2.

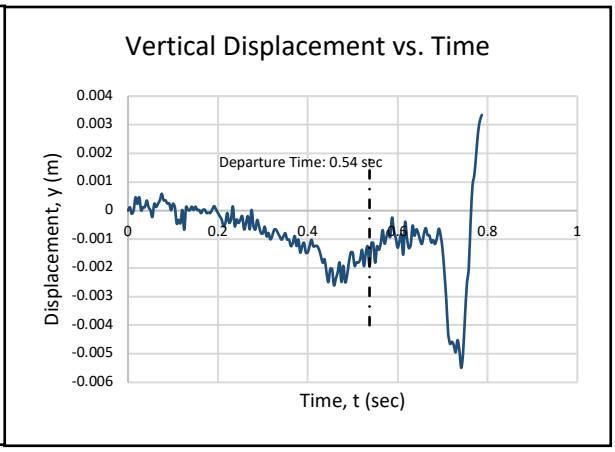

Figure 27 Continued

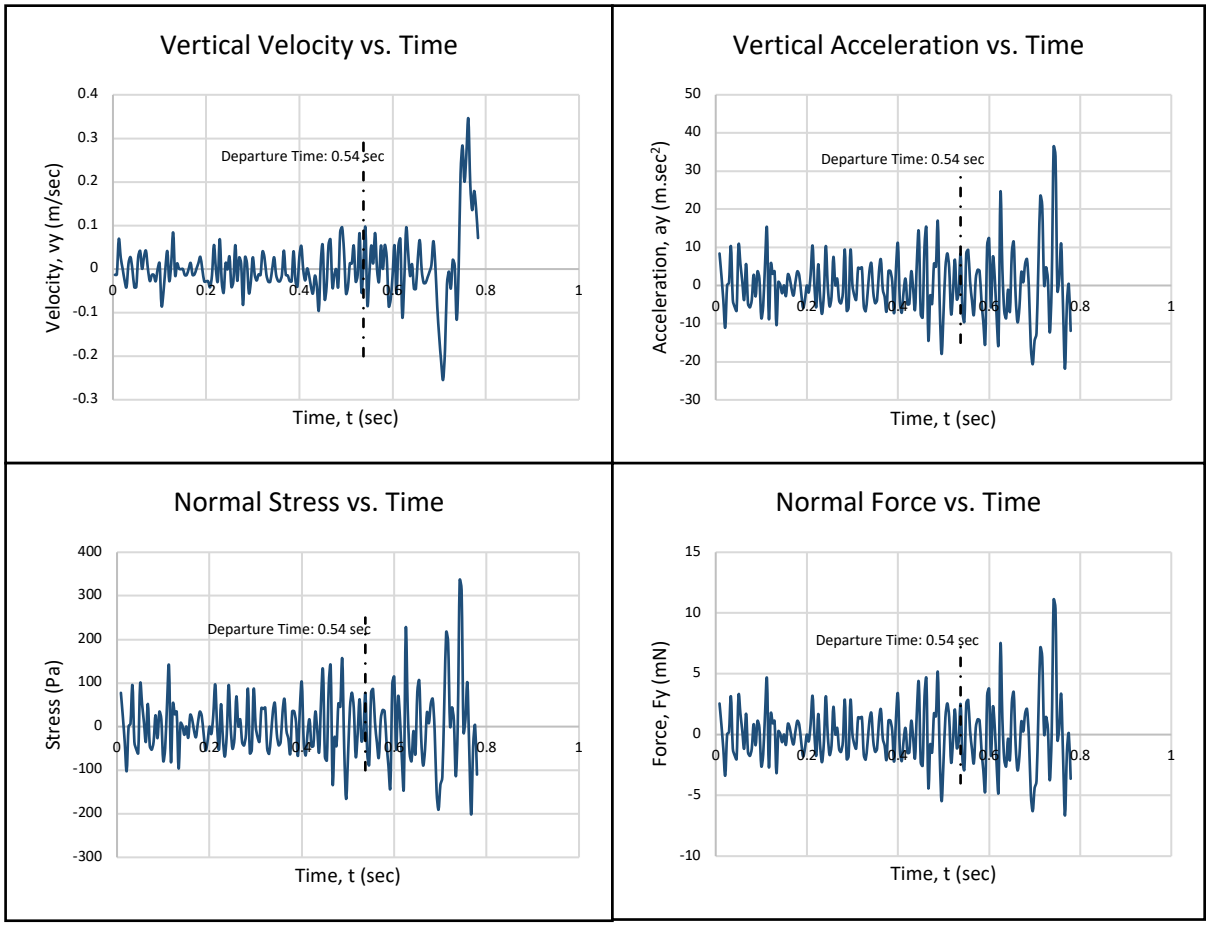

Particle 4 of G2:

Figure 28. Movement of Particle 4 of G2 in the Erosion Function Apparatus

1) Horizontal direction (x direction):

Figure 29. Horizontal displacement, velocity, acceleration, stress and force as a function of time for particle 4 of G2.

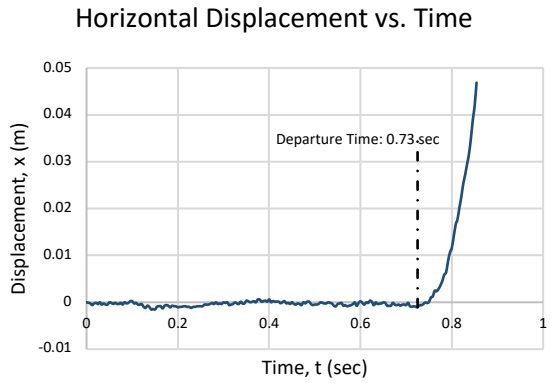

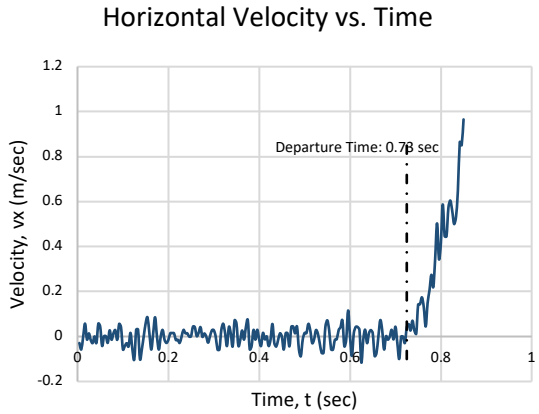

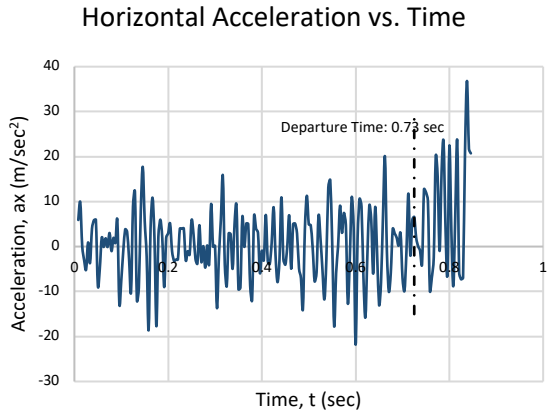

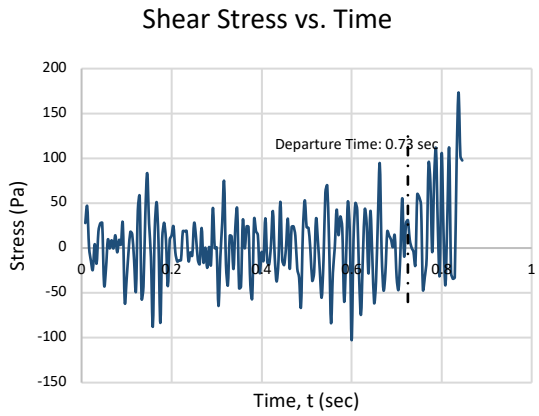

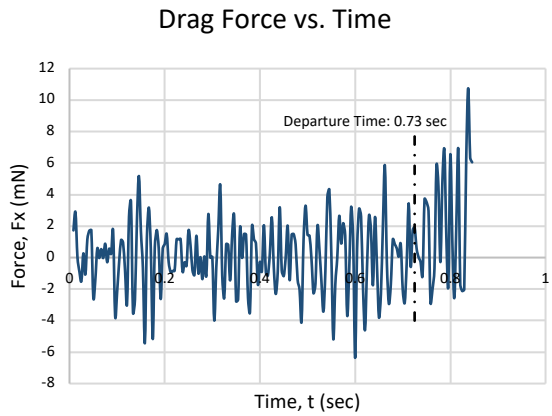

2) Vertical direction (y direction):

Figure 30. Vertical displacement, velocity, acceleration, stress and force as a function of time for particle 4 of G2.

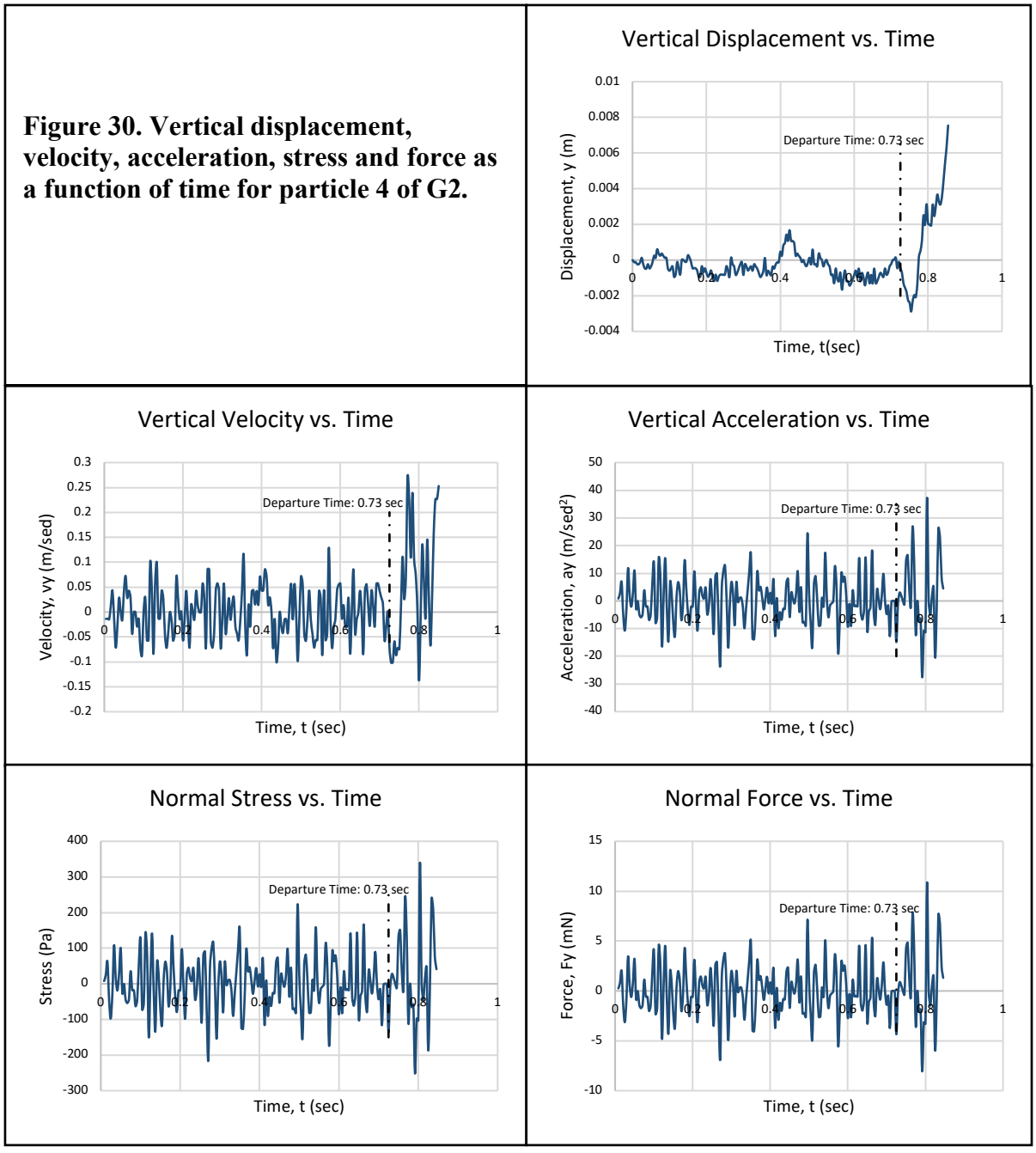

Particle 1 of TB:

Figure 31. Movement of Particle 1 of TB in the Erosion Function Apparatus

1) Horizontal direction (x direction):

Figure 32. Horizontal displacement, velocity, acceleration, stress and force as a function of time for particle 1 of TB.

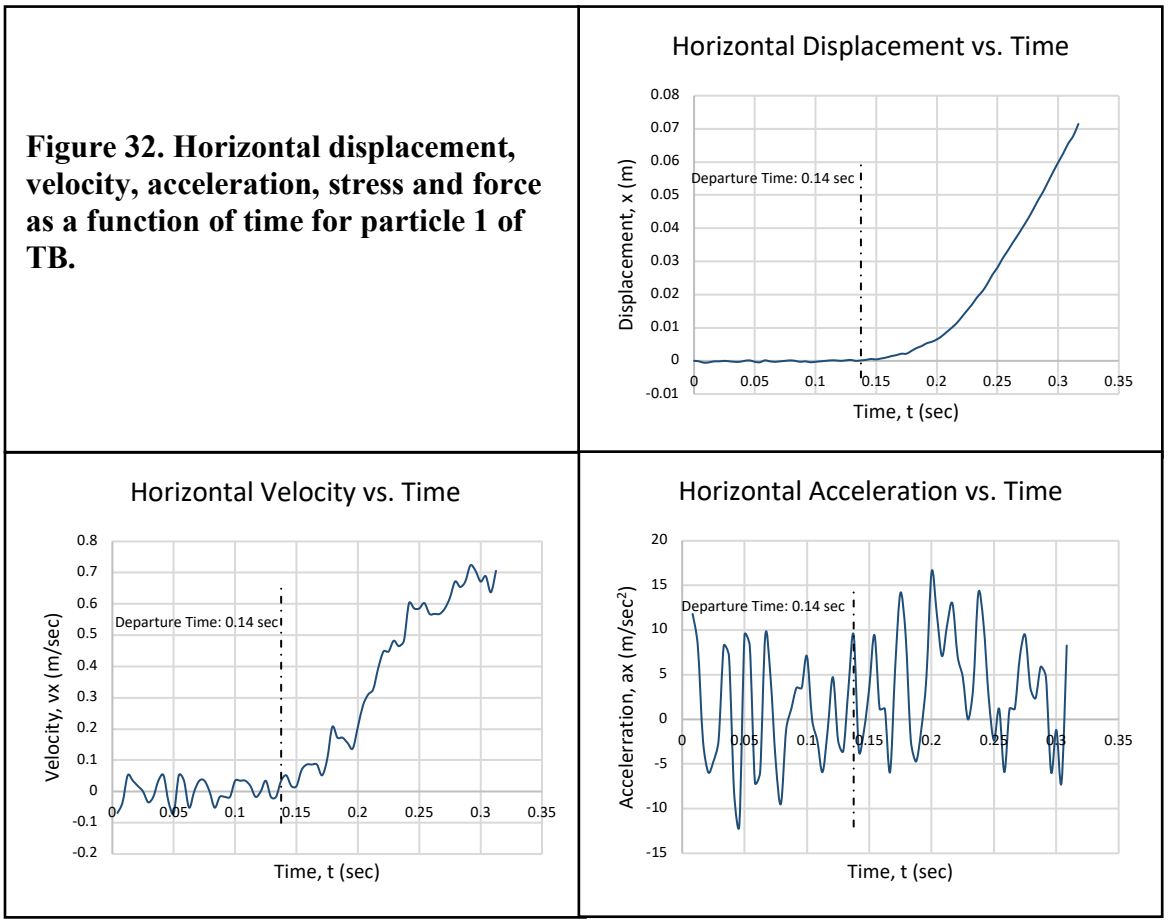

Figure 32 Continued

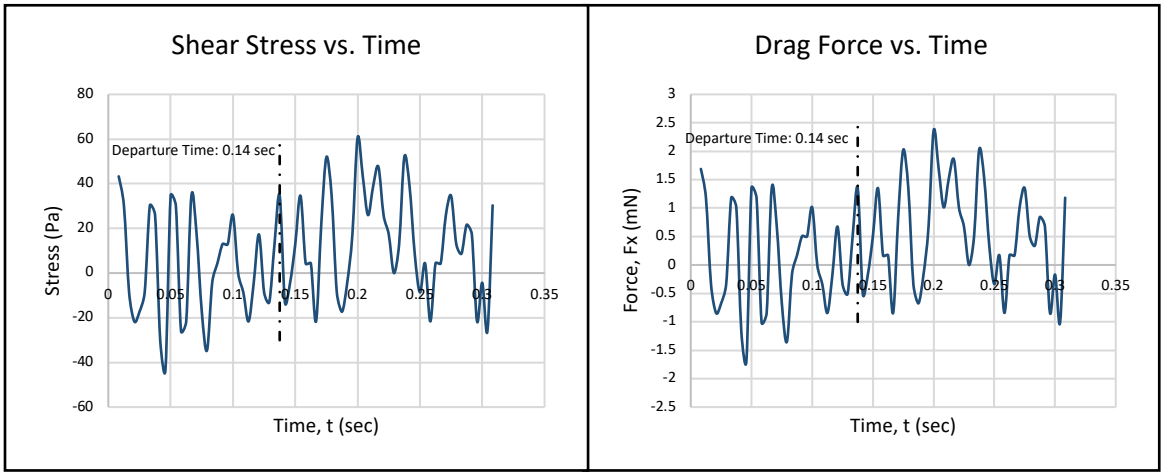

2). Vertical direction (y direction):

Figure 33. Vertical displacement, velocity, acceleration, stress and force as a function of time for particle 1 of TB.

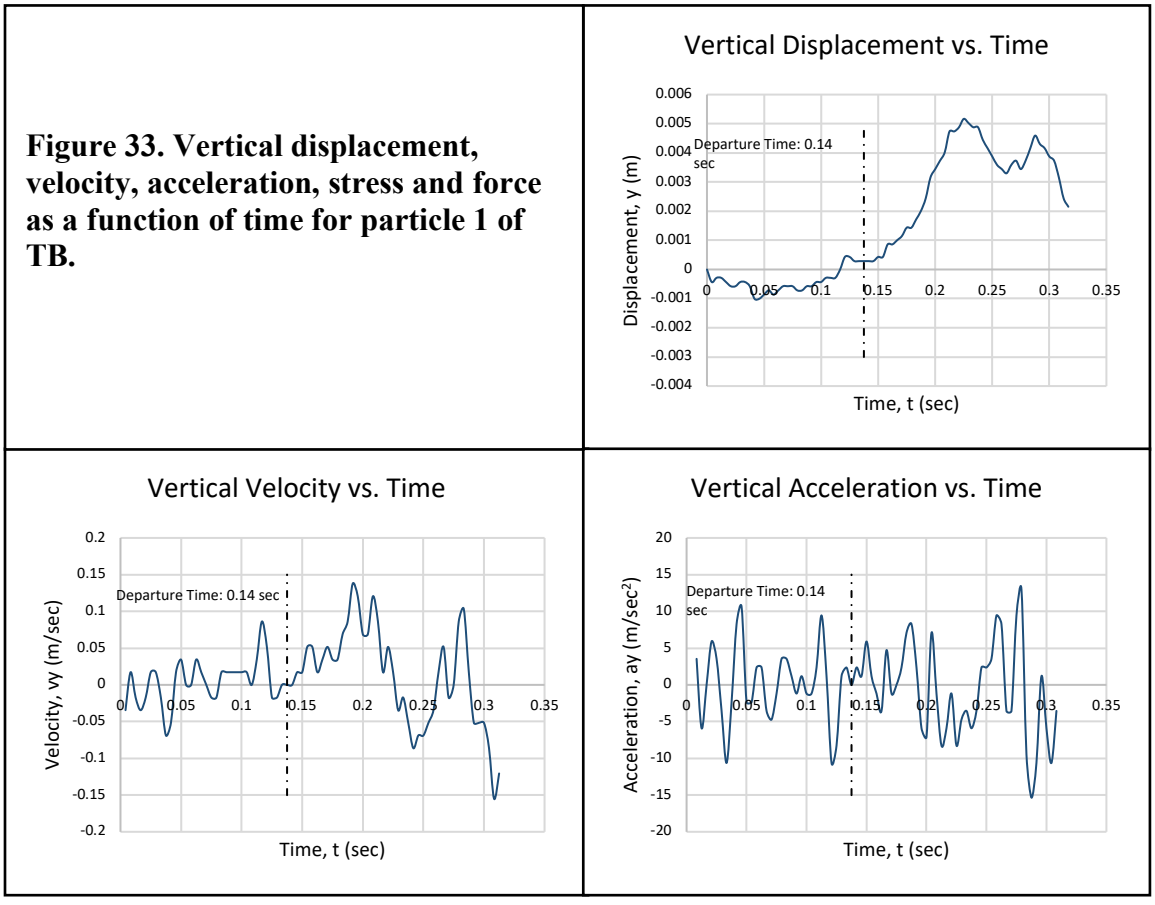

Figure 33 Continued

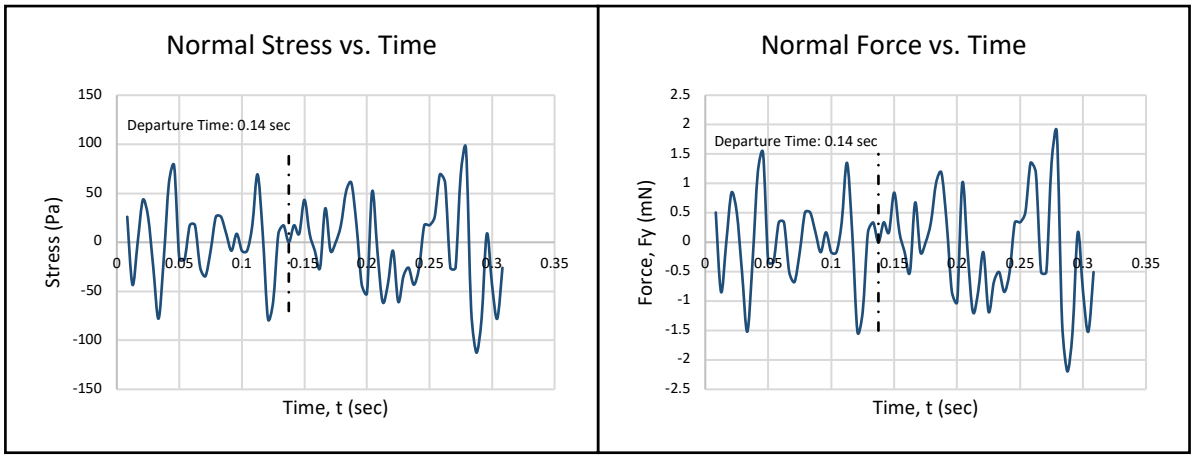

Particle 2 of TB:

Figure 34. Movement of Particle 2 of TB in the Erosion Function Apparatus

1). Horizontal direction (x direction):

Figure 35. Horizontal displacement, velocity, acceleration, stress and force as a function of time for particle 2 of TB.

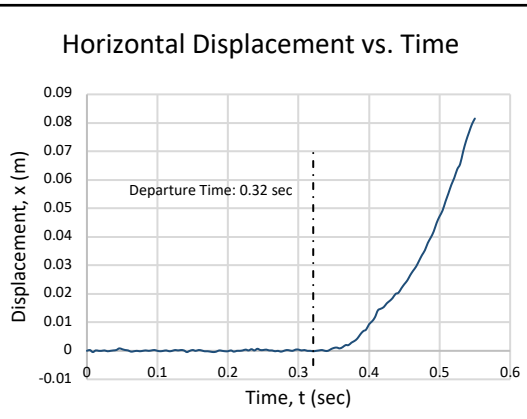

Figure 35 Continued

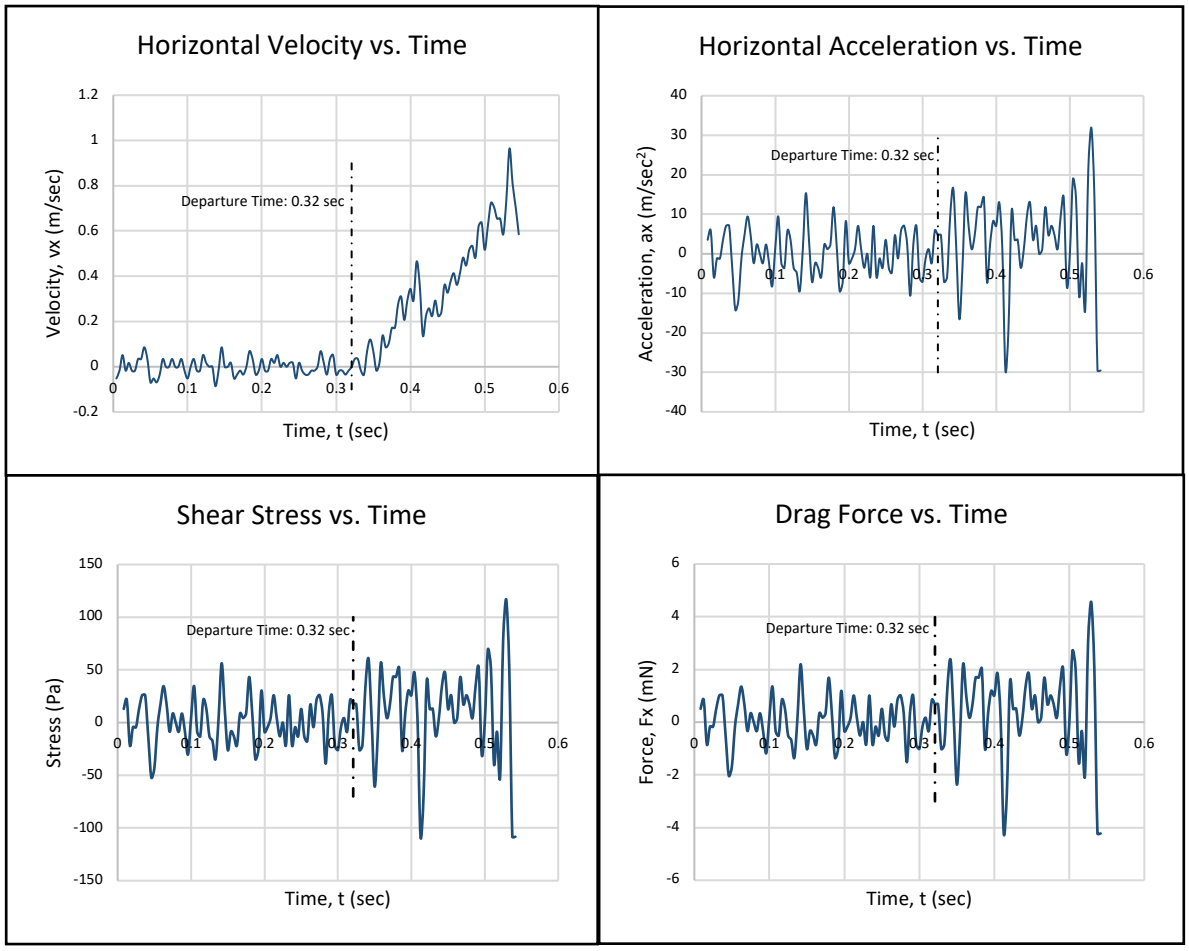

2) Vertical direction (y direction):

Figure 36. Vertical displacement, velocity, acceleration, stress and force as a function of time for particle 2 of TB.

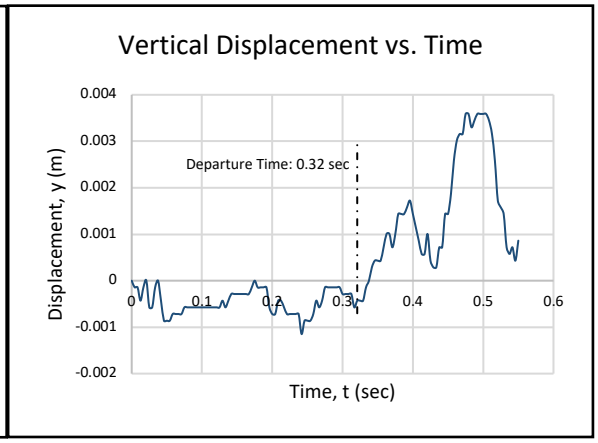

Figure 36 Continued

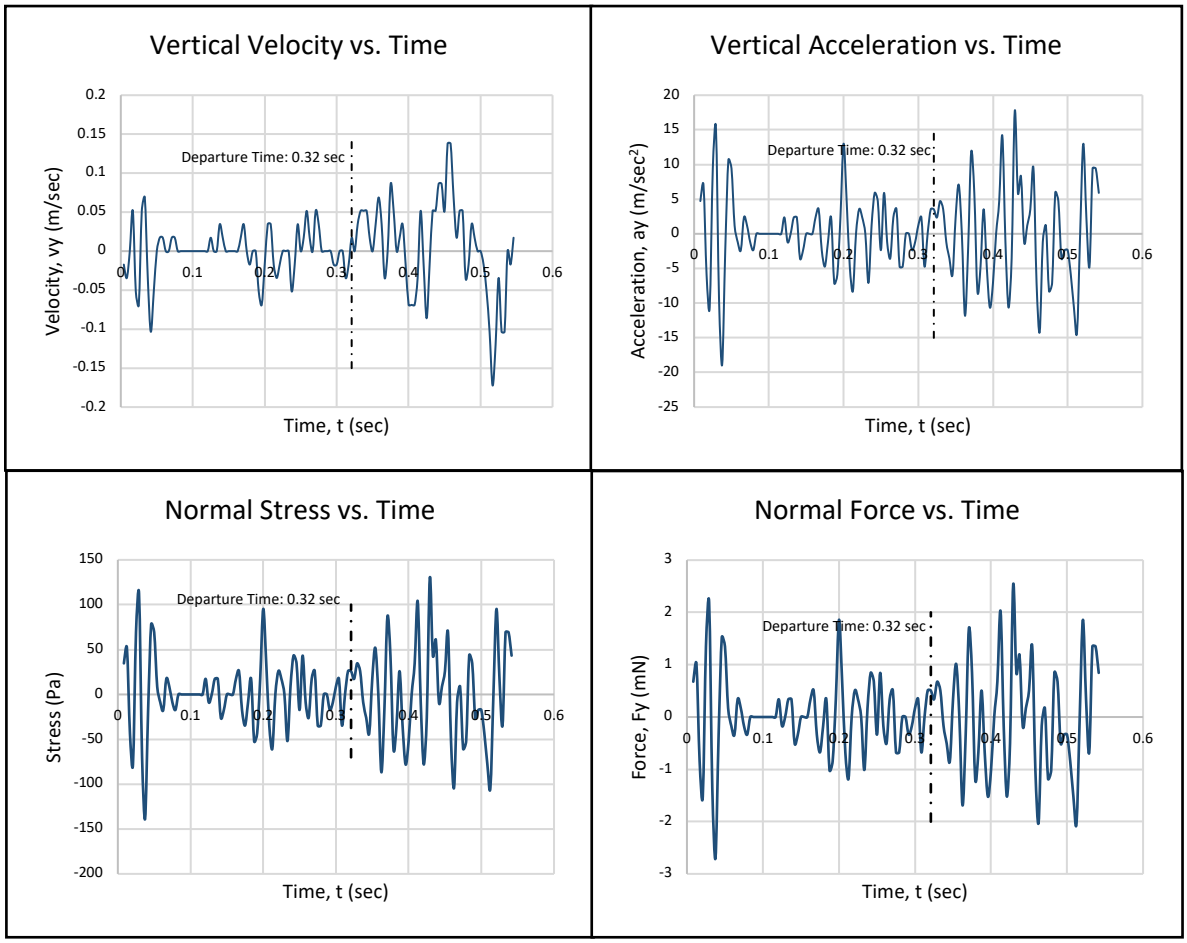

Particle 3 of TB:

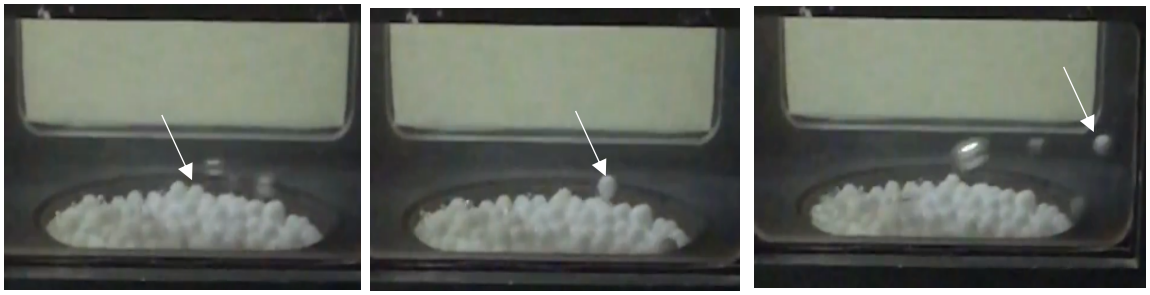

Figure 37. Movement of Particle 3 of TB in the Erosion Function Apparatus

1). Horizontal direction (x direction):

Figure 38. Horizontal displacement, velocity, acceleration, stress and force as a function of time for particle 3 of TB.

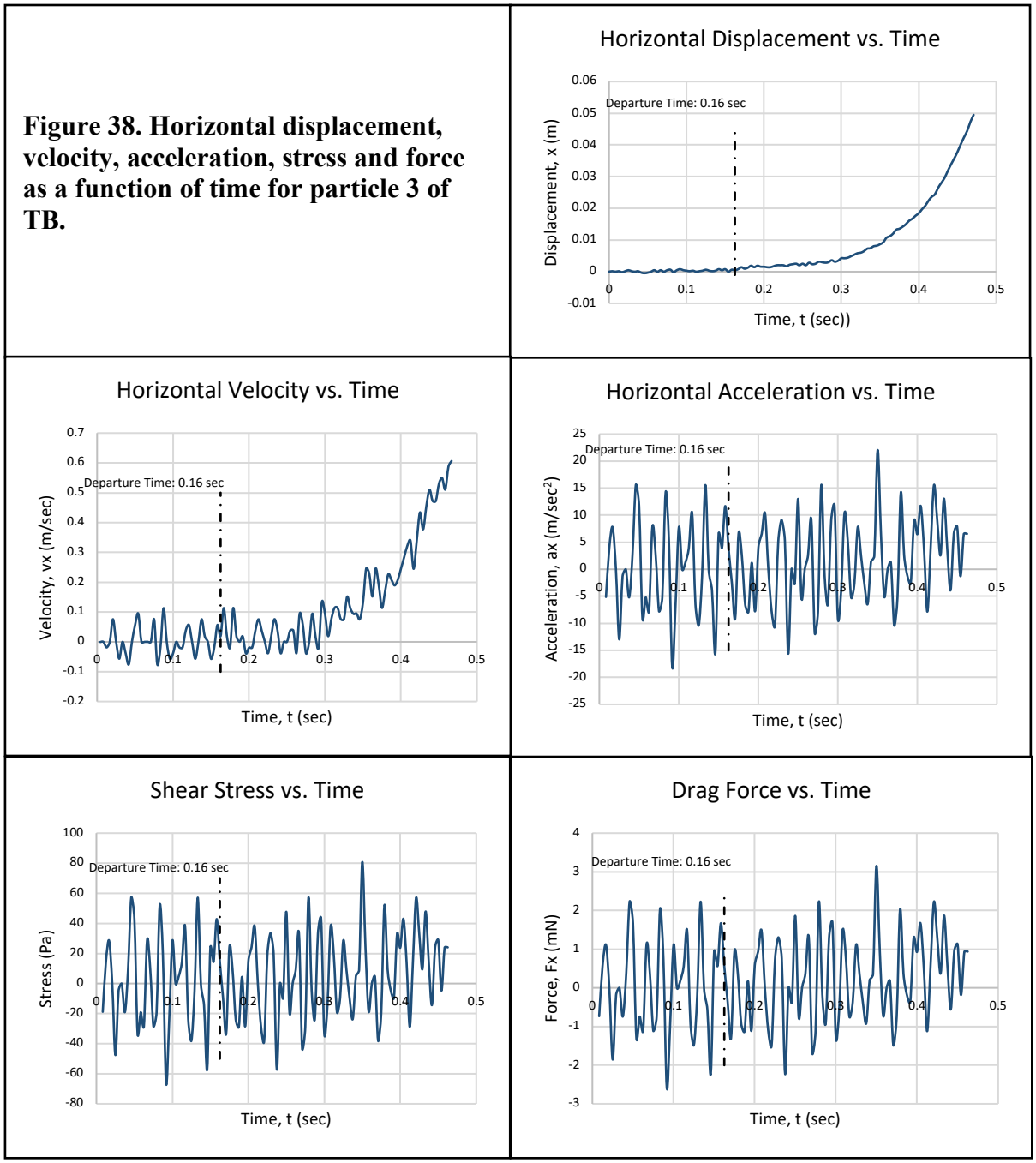

2). Vertical direction (y dire ction):

Figure 39. Vertical displacement, velocity, acceleration, stress and force as a function of time for particle 3 of TB.

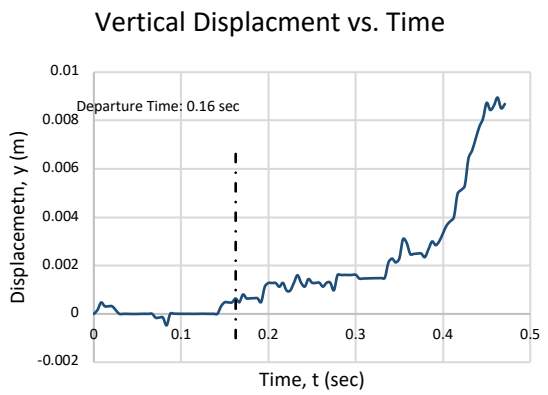

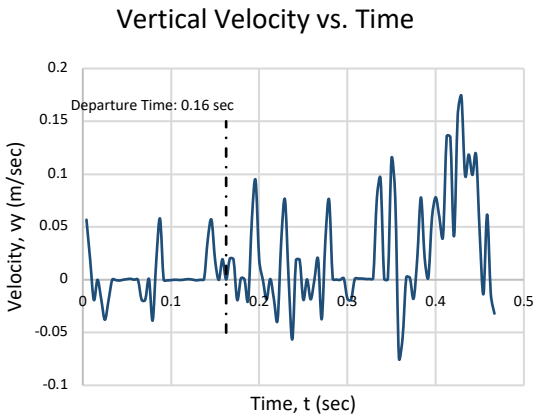

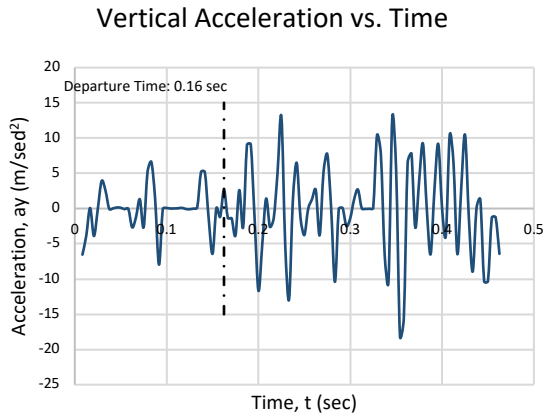

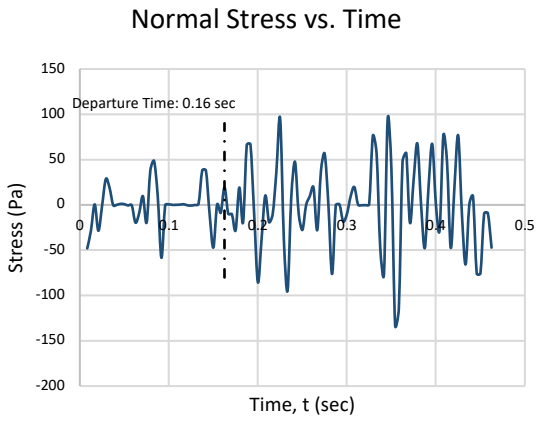

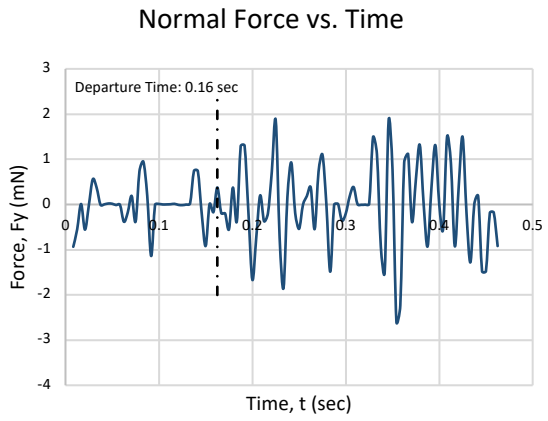

Particle 4 of TB:

Figure 40. Movement of Particle 4 of TB in the Erosion Function Apparatus

1). Horizontal direction (x direction):

Figure 41. Horizontal displacement, velocity, acceleration, stress and force as a function of time for particle 4 of TB.

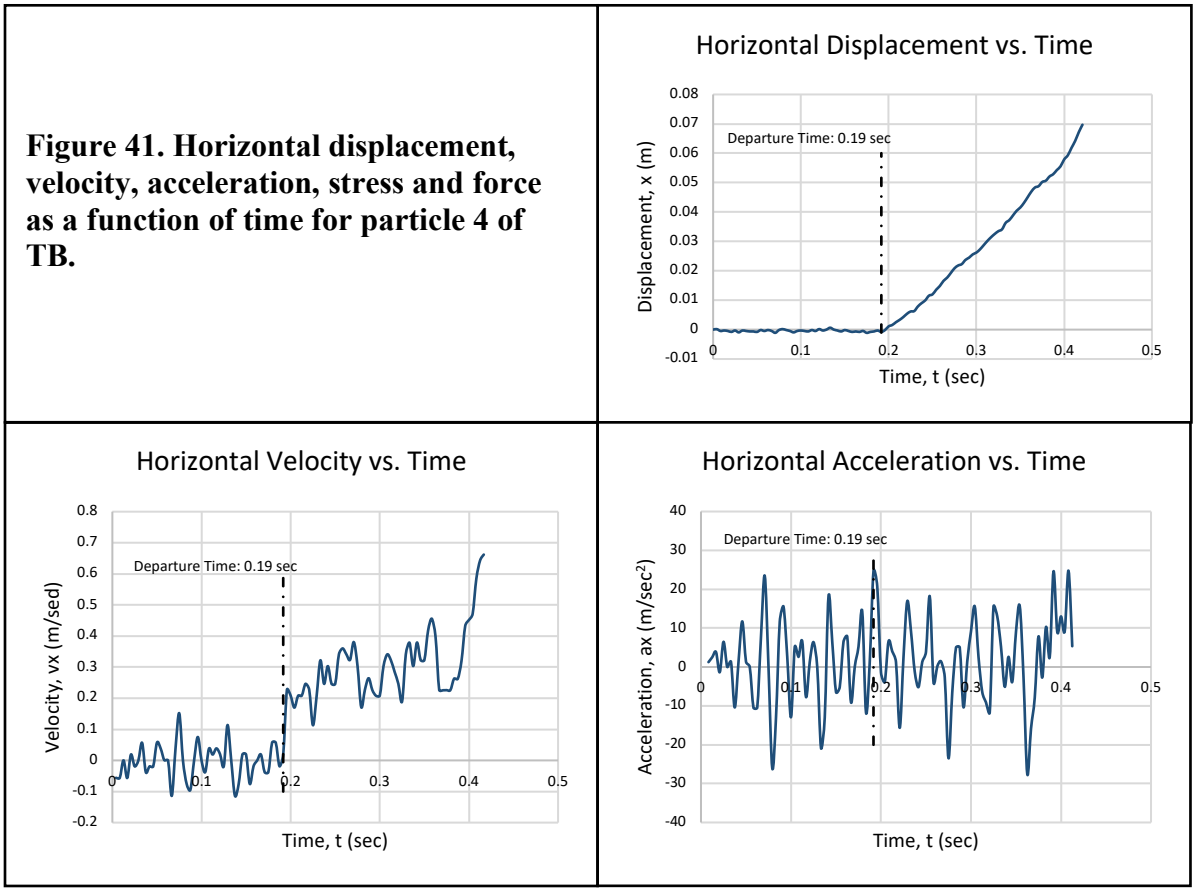

Figure 41 Continued

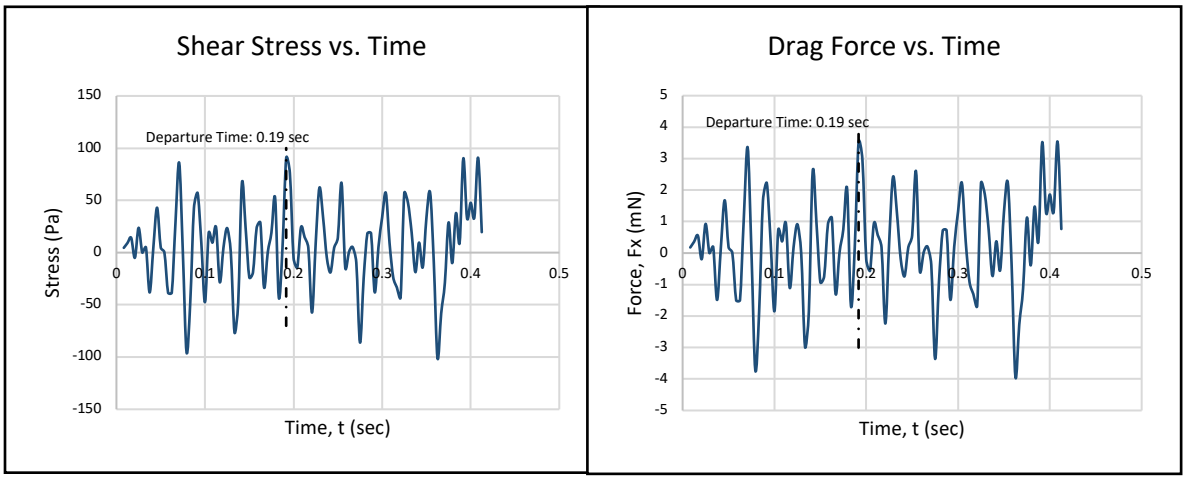

2). Vertical direction (y direction):

Figure 42. Vertical displacement, velocity, acceleration, stress and force as a function of time for particle 4 of TB.

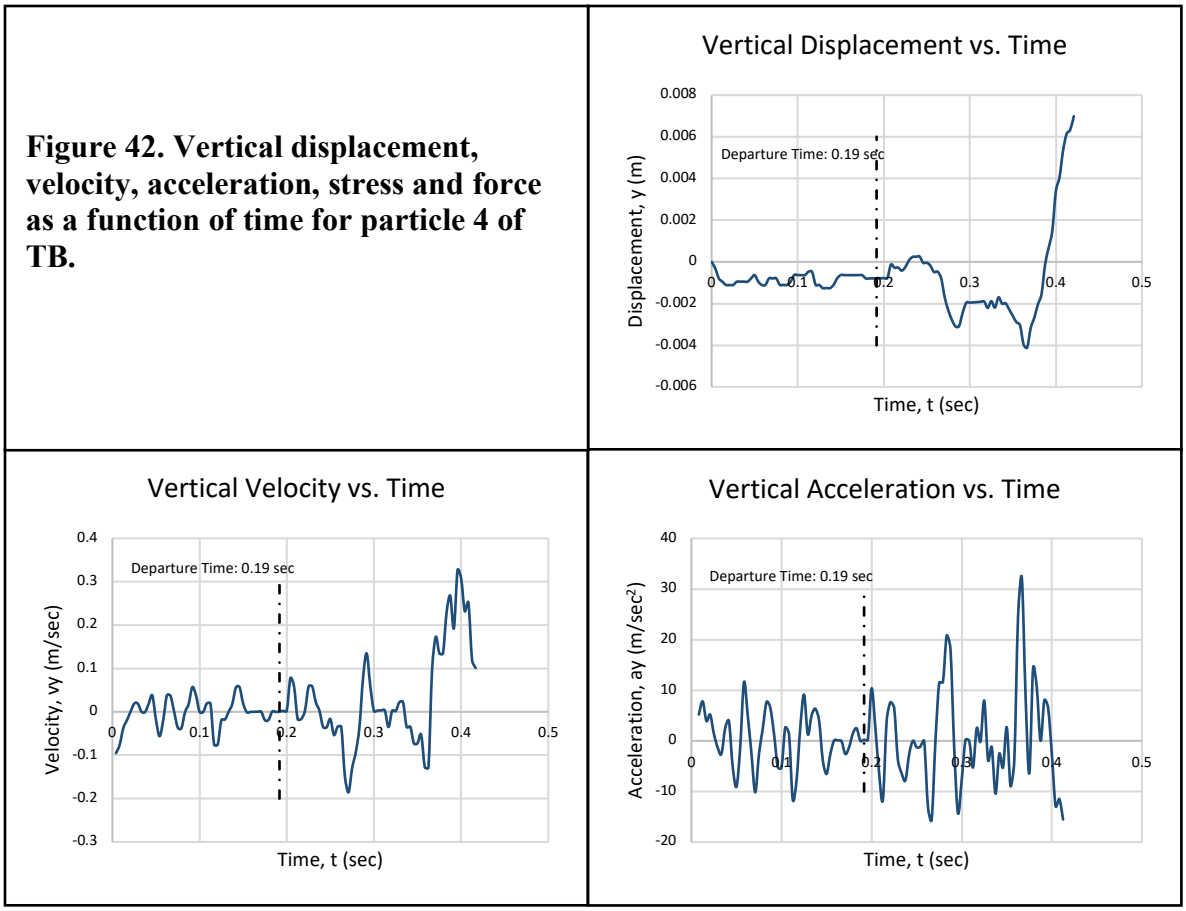

Figure 42 Continued

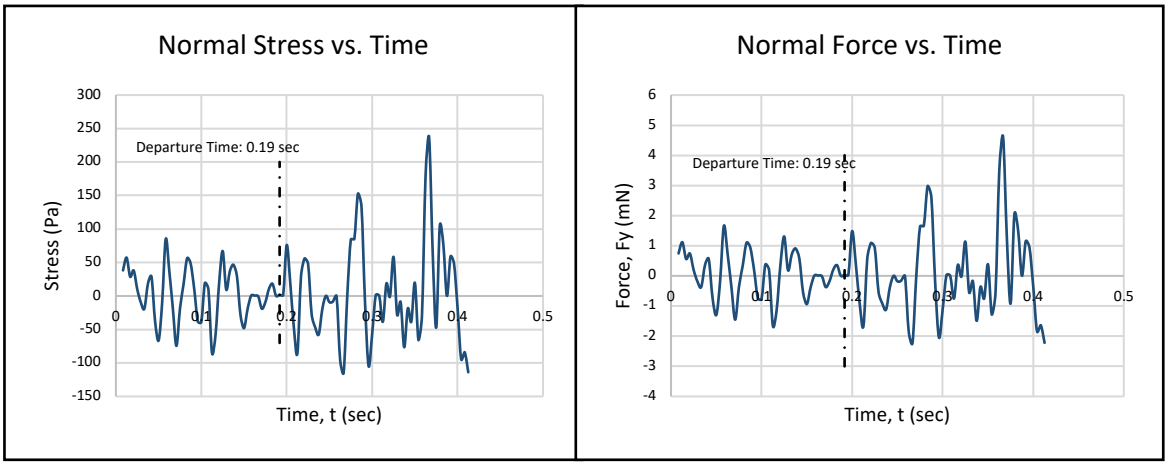

Particle 1 of SB:

Figure 43. Movement of Particle 1 of SB in the Erosion Function Apparatus

1). Horizontal direction (x direction):

Figure 44. Horizontal displacement, velocity, acceleration, stress and force as a function of time for particle 1 of SB.

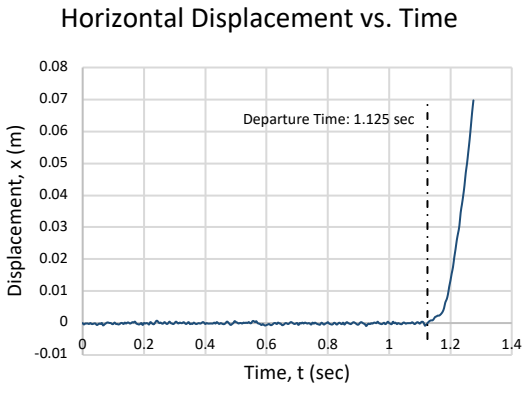

Figure 44 Continued

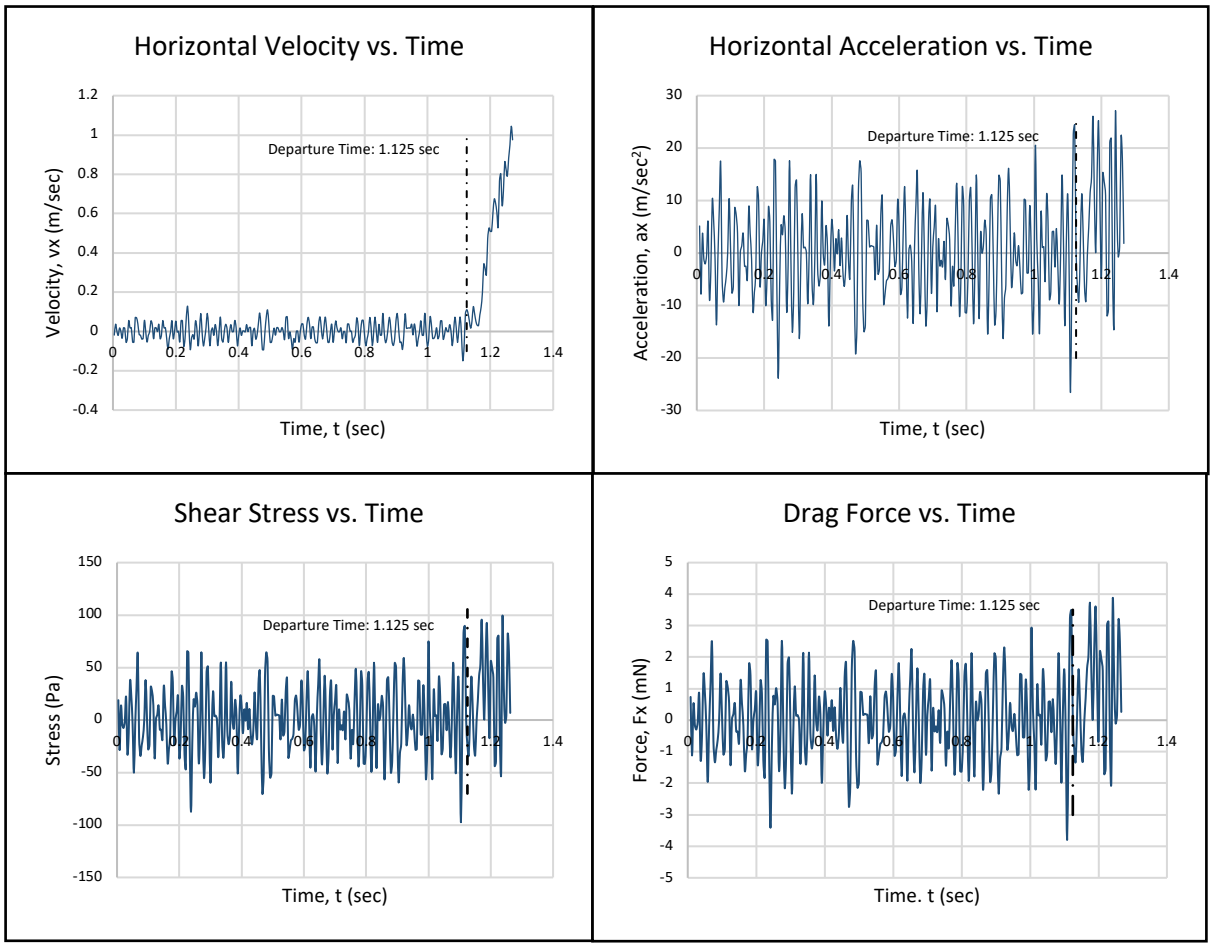

2). Vertical direction (y direction):

Figure 45. Vertical displacement, velocity, acceleration, stress and force as a function of time for particle 1 of SB.

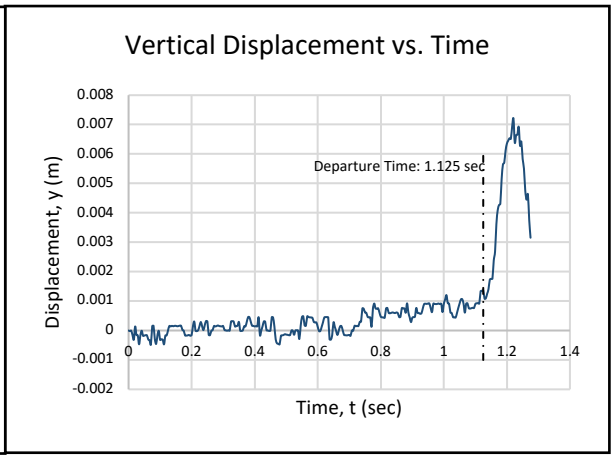

Figure 45 Continued

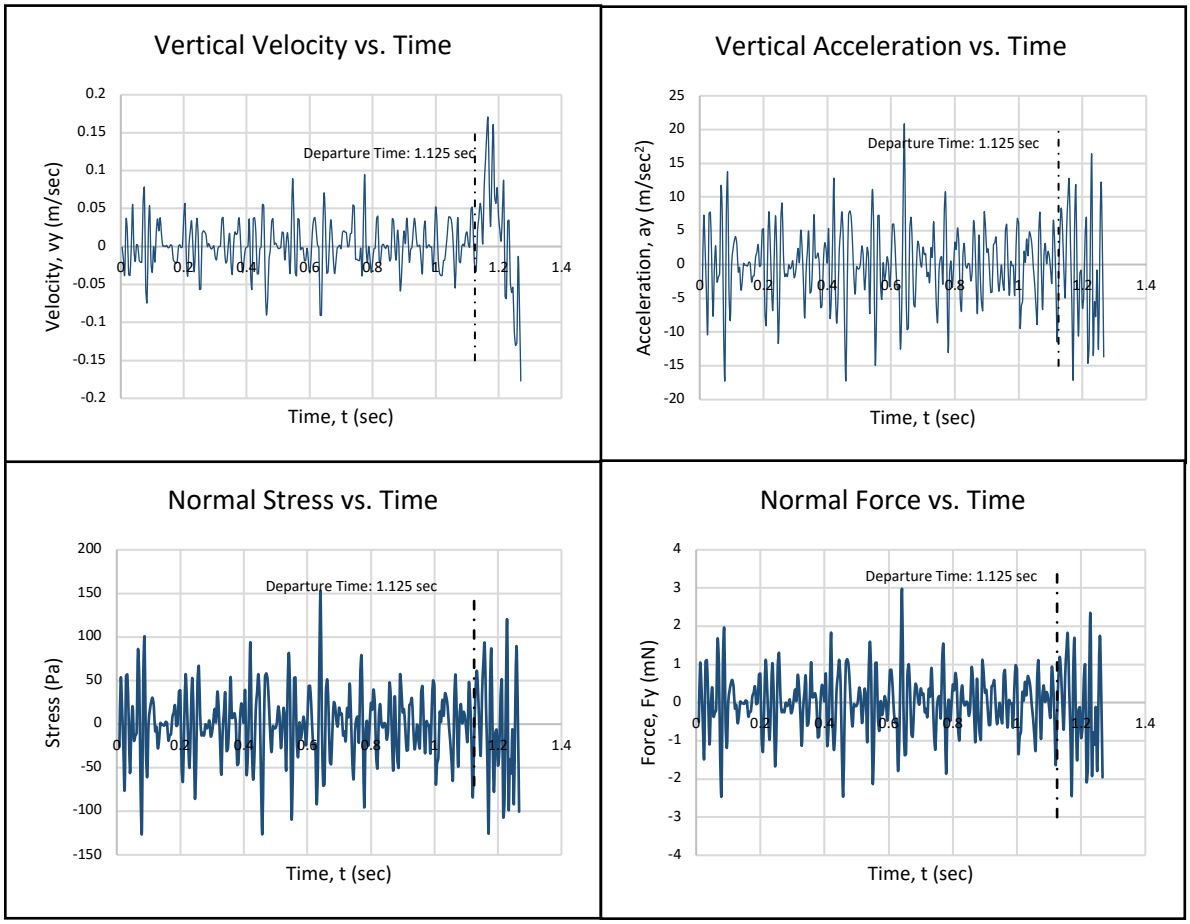

Particle 2 of SB:

Figure 46. Movement of Particle 2 of SB in the Erosion Function Apparatus

1). Horizontal direction (x direction):

Figure 47. Horizontal displacement, velocity, acceleration, stress and force as a function of time for particle 2 of SB.

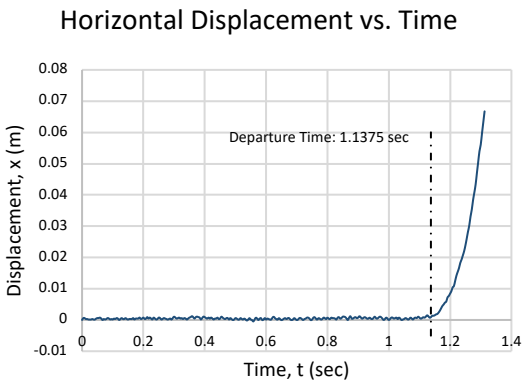

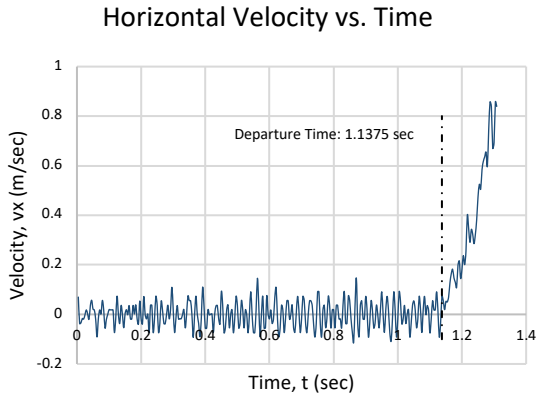

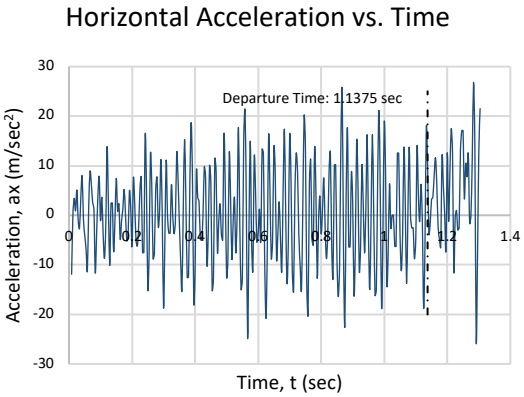

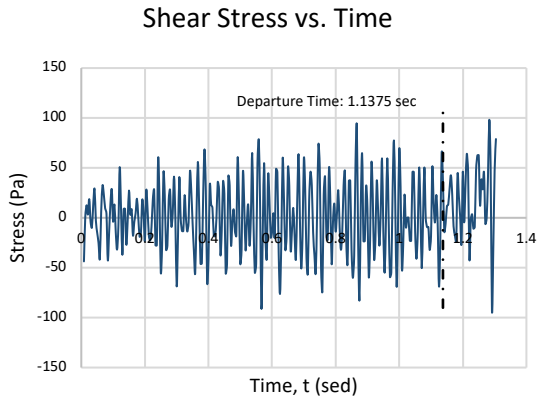

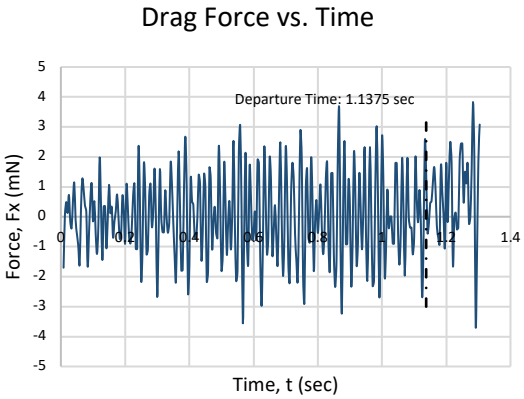

2). Vertical direction (y direction):

Figure 48. Vertical displacement, velocity, acceleration, stress and force as a function of time for particle 2 of SB.

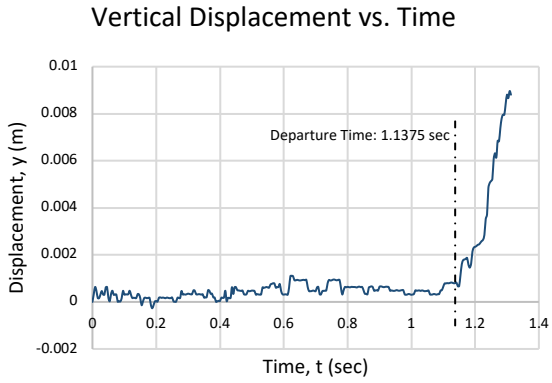

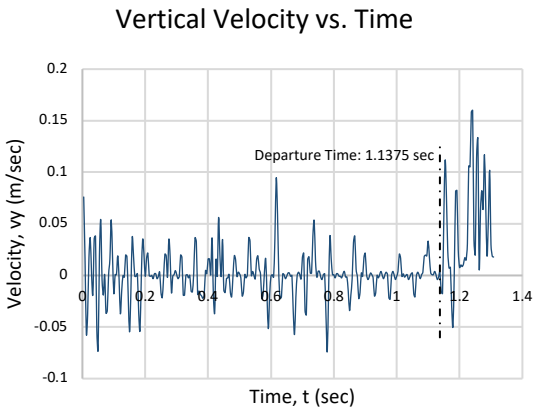

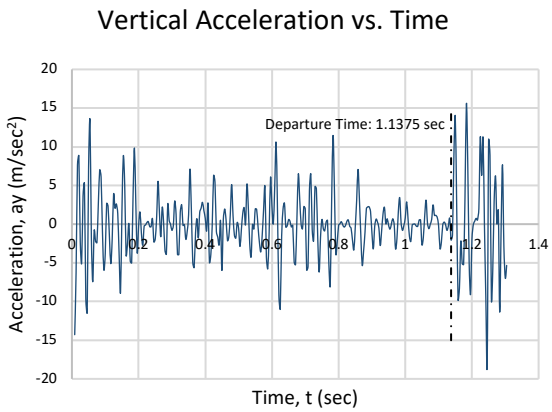

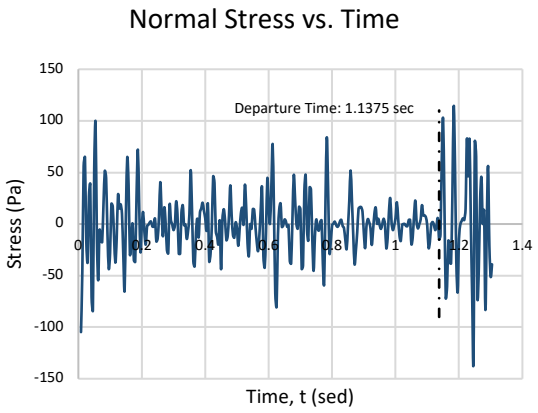

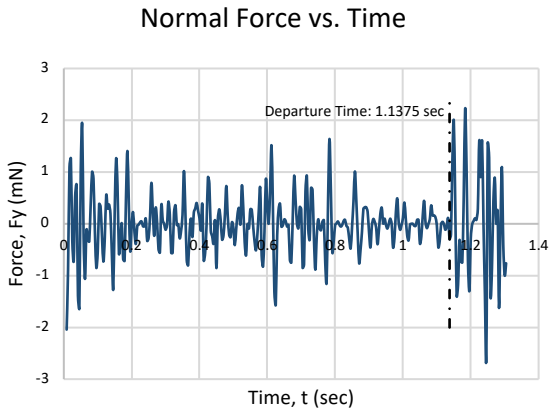

Particle 3 of SB:

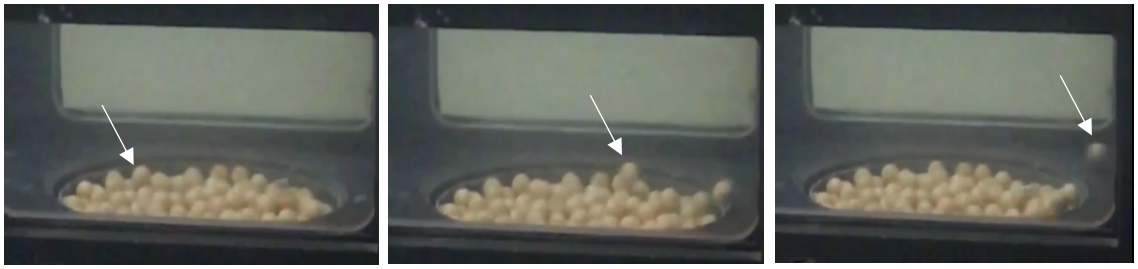

Figure 49. Movement of Particle 3 of SB in the Erosion Function Apparatus

1). Horizontal direction (x direction):

Figure 50. Horizontal displacement, velocity, acceleration, stress and force as a function of time for particle 3 of SB.

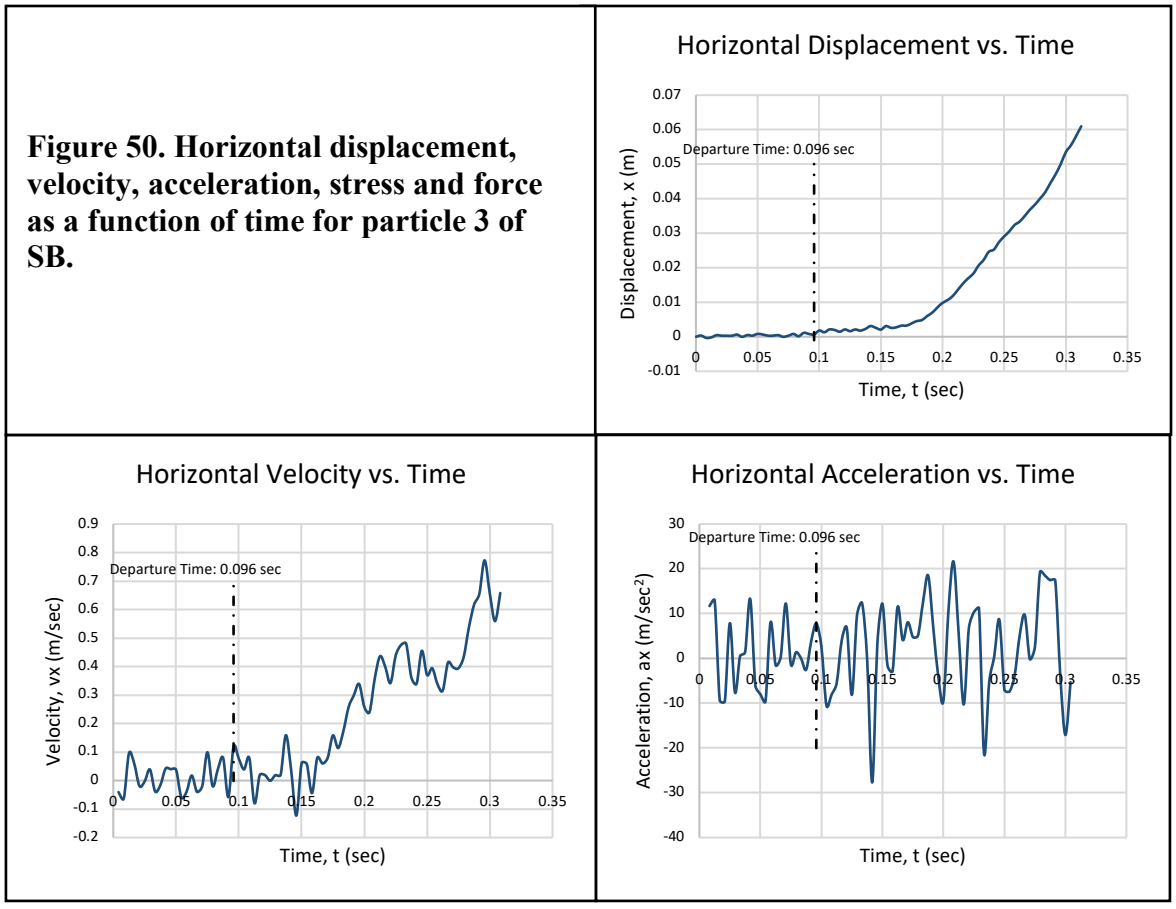

Figure 50 Continued

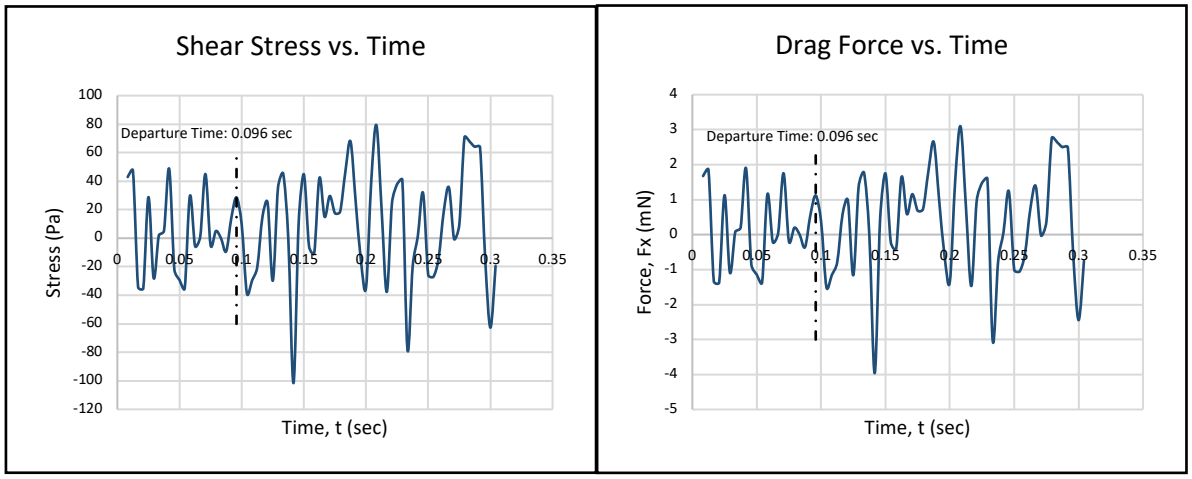

2). Vertical direction (y direction):

Figure 51. Vertical displacement, velocity, acceleration, stress and force as a function of time for particle 3 of SB.

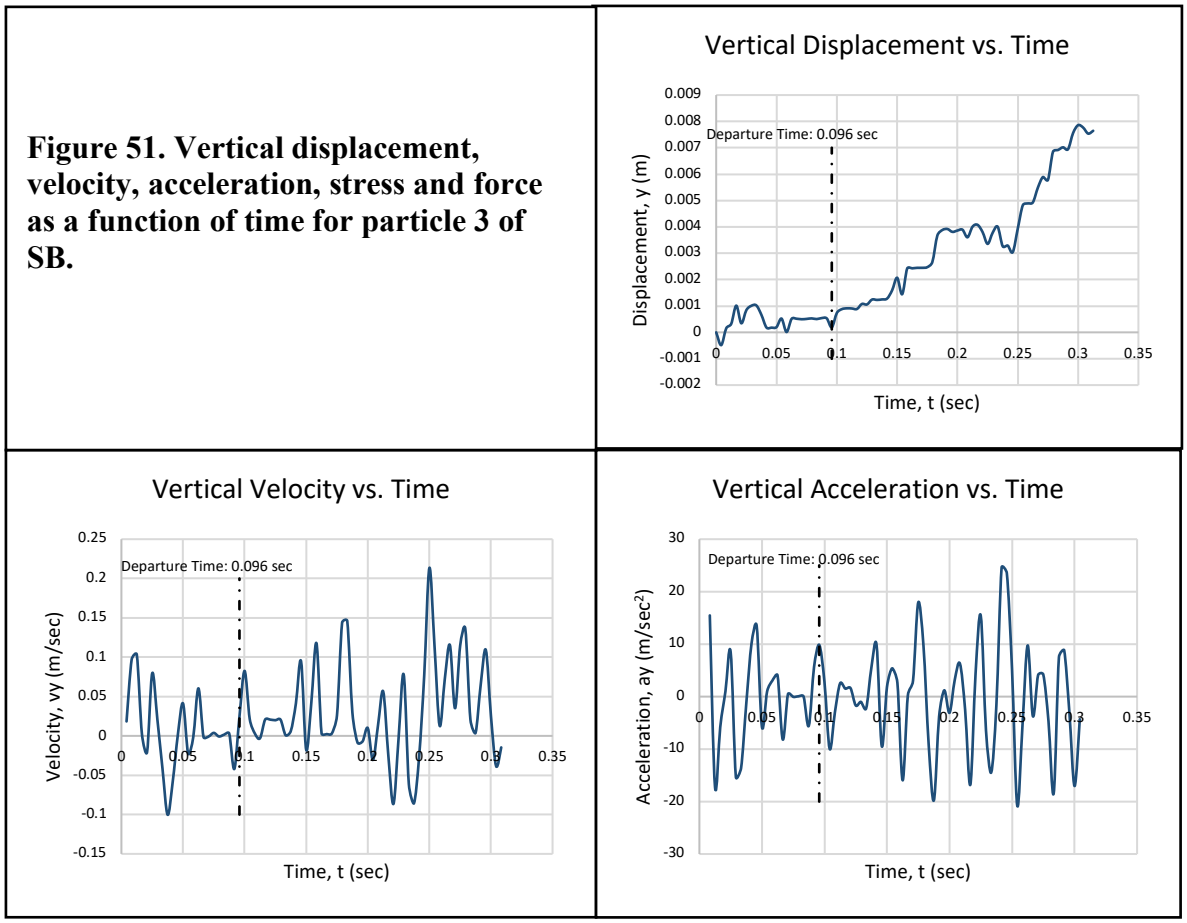

Figure 51 Continued

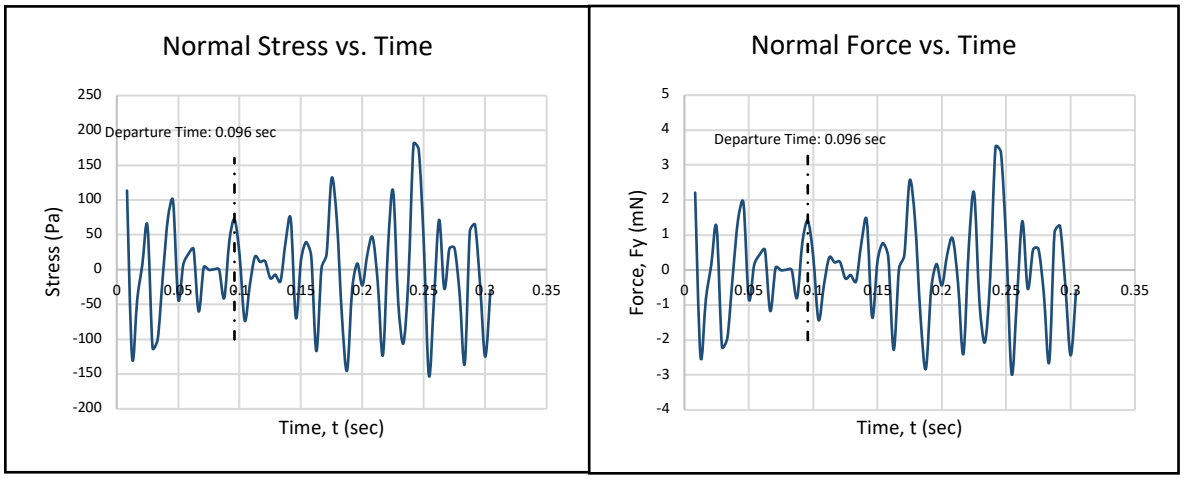

Particle 4 of SB:

Figure 52. Movement of Particle 4 of SB in the Erosion Function Apparatus

1). Horizontal direction (x direction):

Figure 53. Horizontal displacement, velocity, acceleration, stress and force as a function of time for particle 4 of SB.

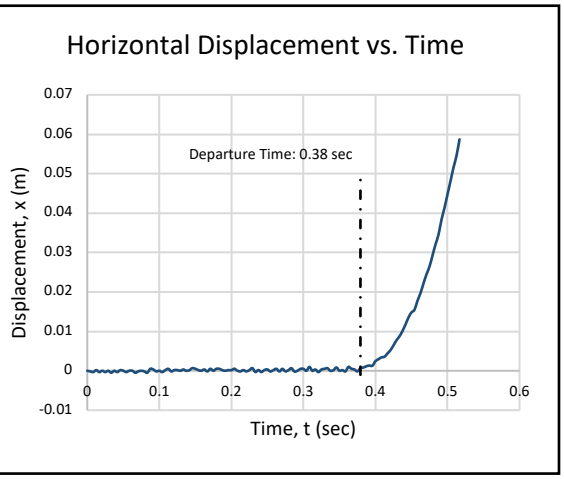

Figure 53 Continued

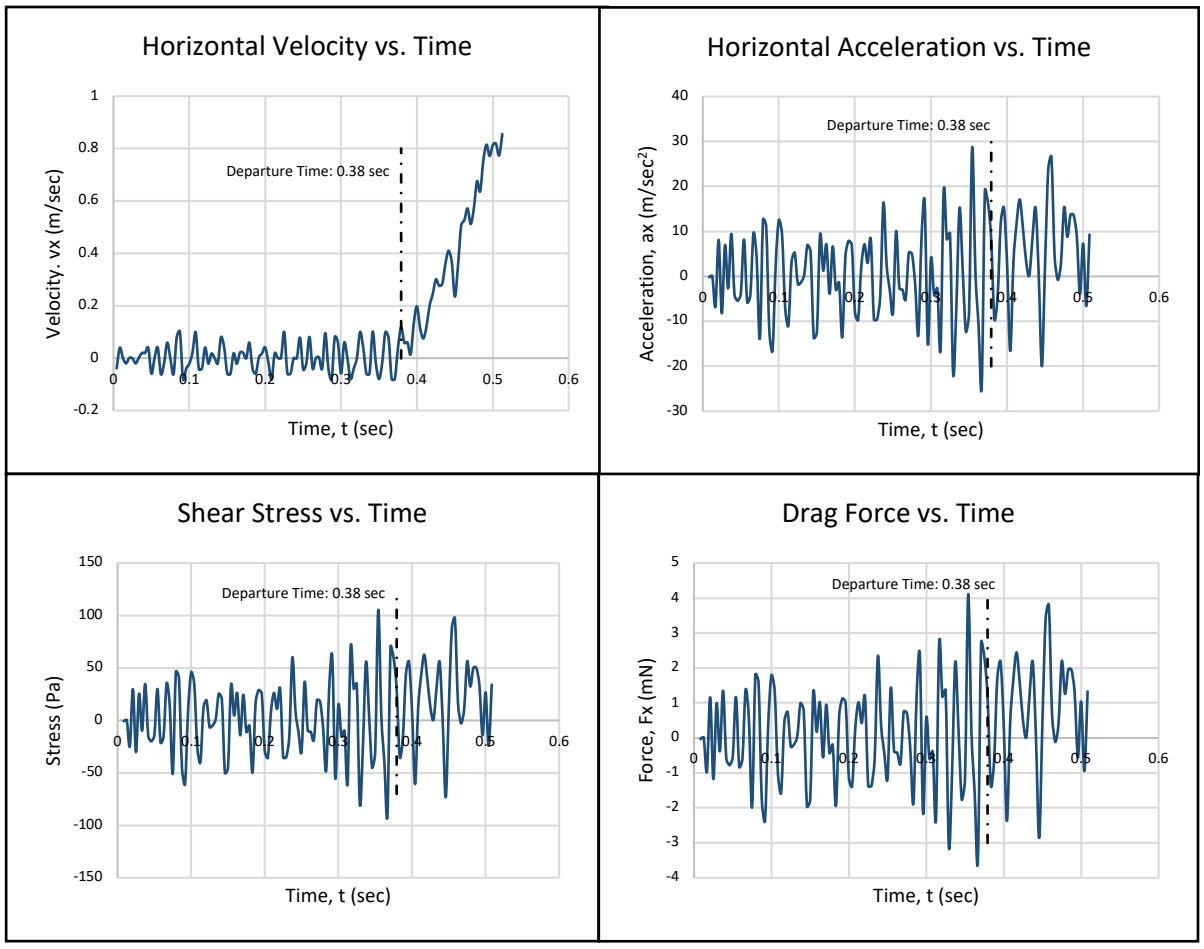

2). Vertical direction (y direction):

Figure 54. Vertical displacement, velocity, acceleration, stress and force as a function of time for particle 4 of SB.

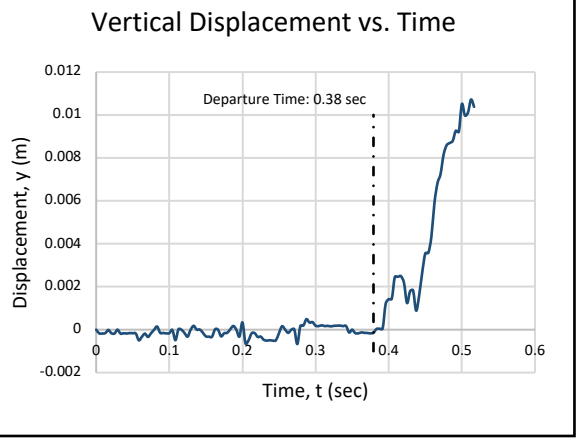

Figure 54 Continued

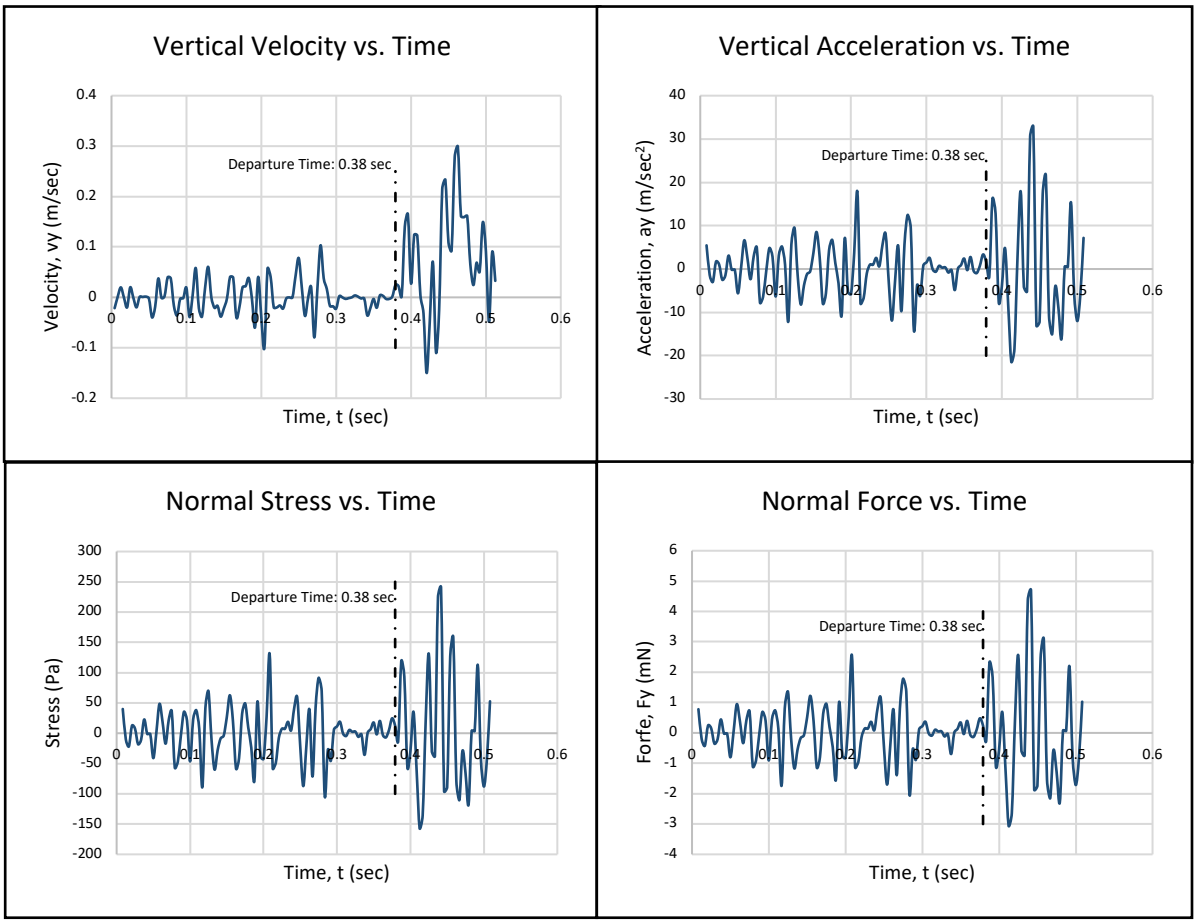

Particle 1 of GB:

Figure 55. Movement of Particle 1 of GB in the Erosion Function Apparatus

1). Horizontal direction (x direction):

Figure 56. Horizontal displacement, velocity, acceleration, stress and force as a function of time for particle 1 of GB.

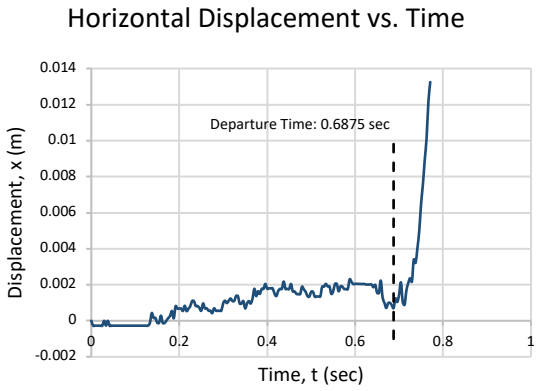

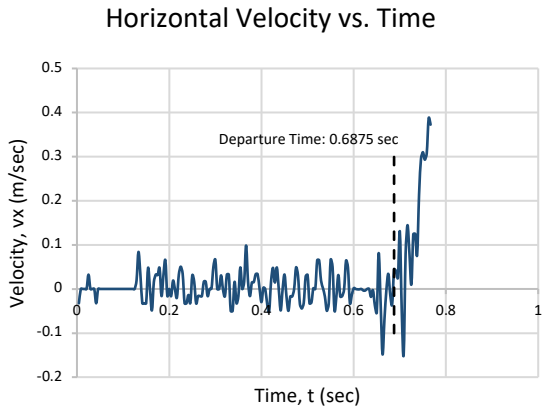

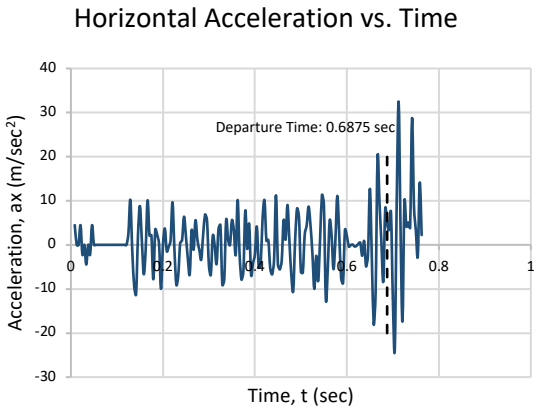

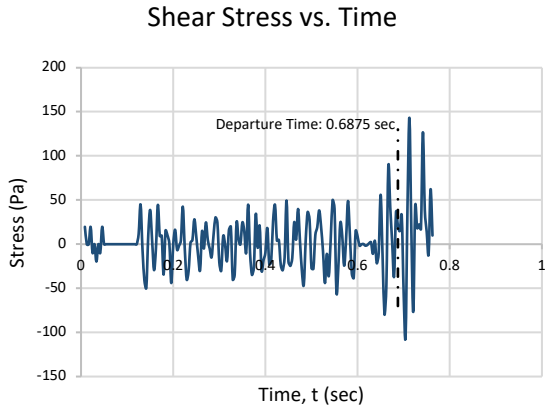

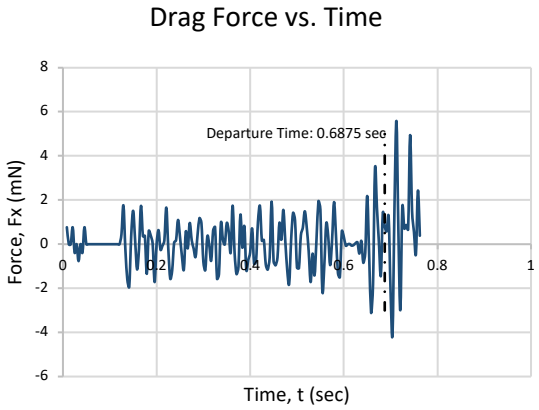

2). Vertical direction (y direction):

Figure 57. Vertical displacement, velocity, acceleration, stress and force as a function of time for particle 1 of GB.

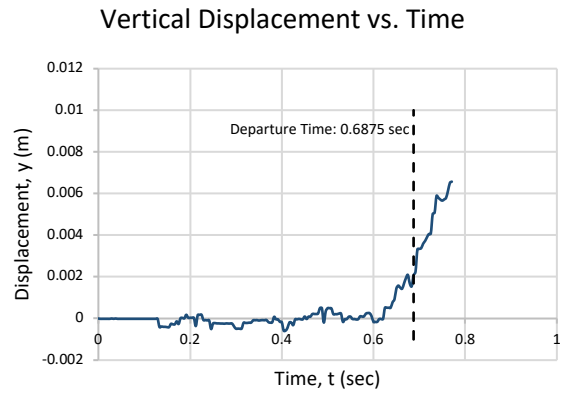

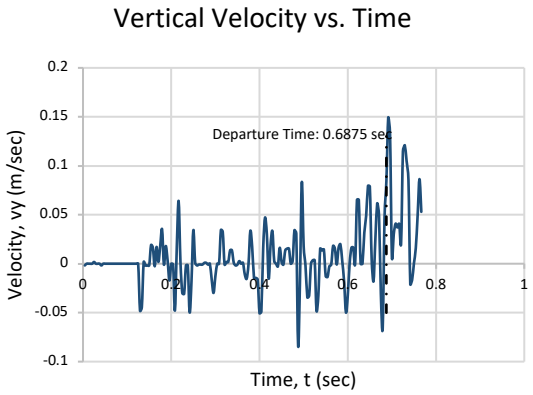

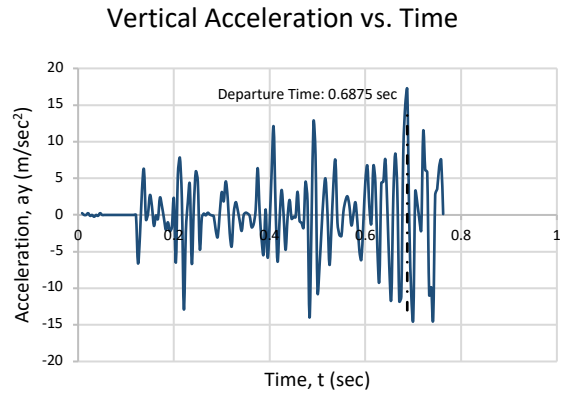

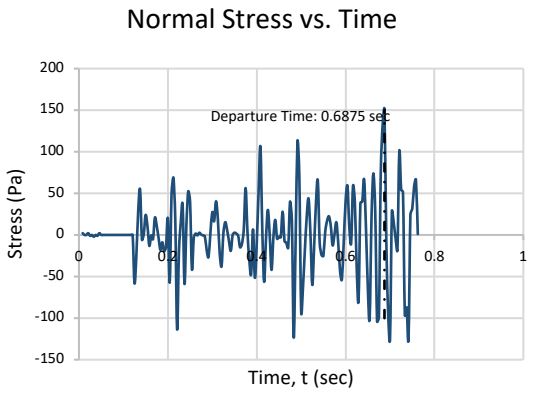

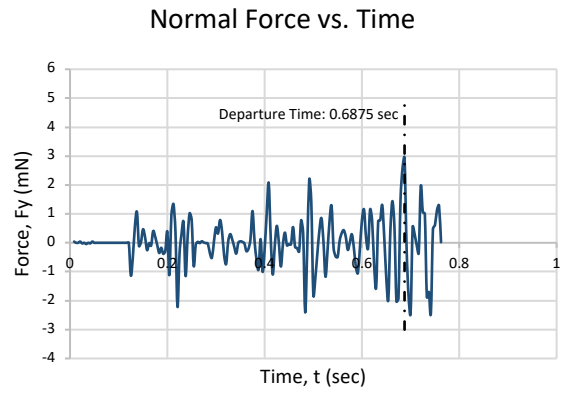

Particle 2 of GB:

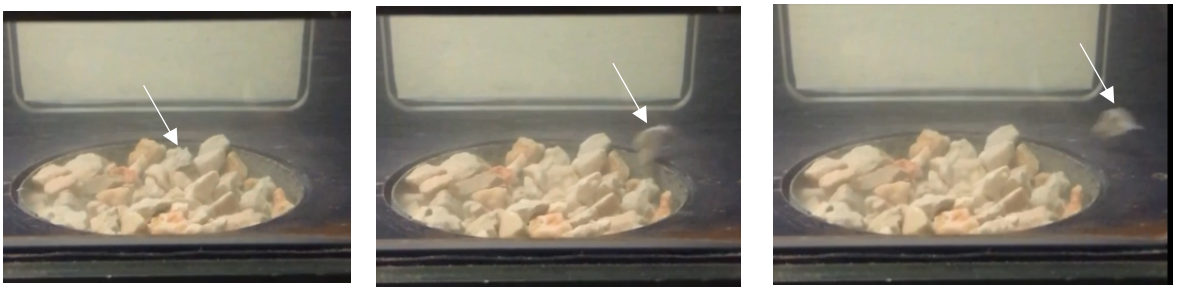

Figure 58. Movement of Particle 2 of GB in the Erosion Function Apparatus

1). Horizontal direction (x direction):

Figure 59. Horizontal displacement, velocity, acceleration, stress and force as a function of time for particle 2 of GB.

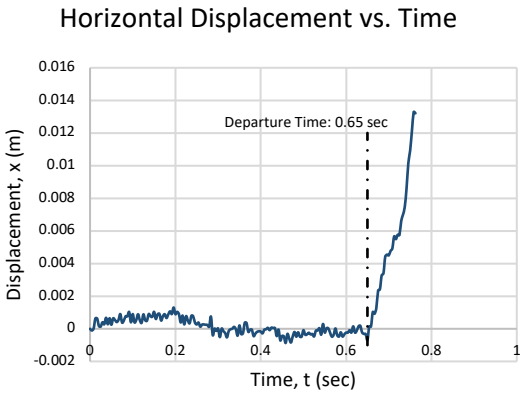

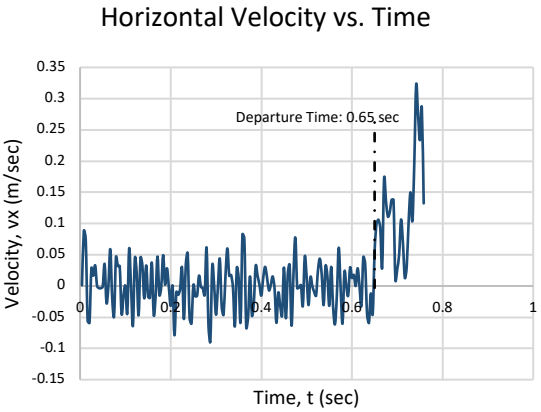

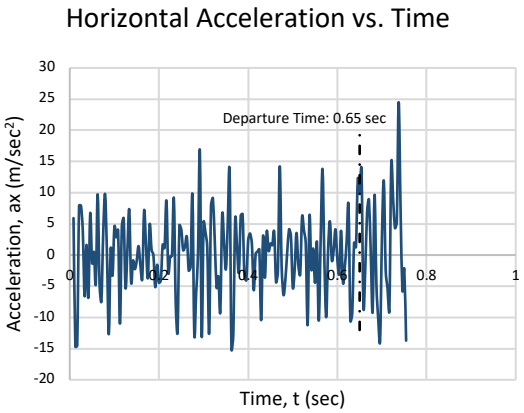

Figure 59 Continued

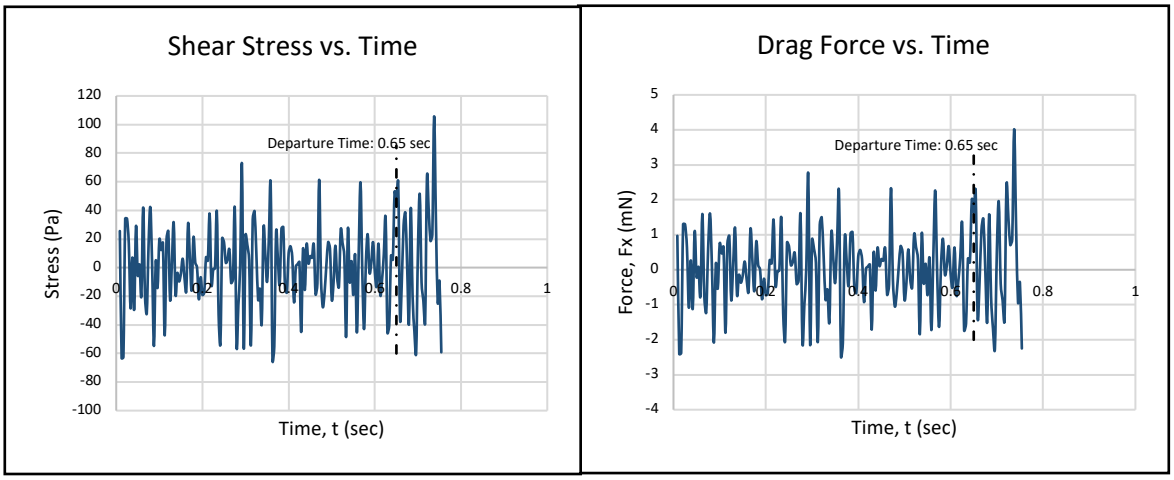

2). Vertical direction (y direction):

Figure 60. Vertical displacement, velocity, acceleration, stress and force as a function of time for particle 2 of GB.

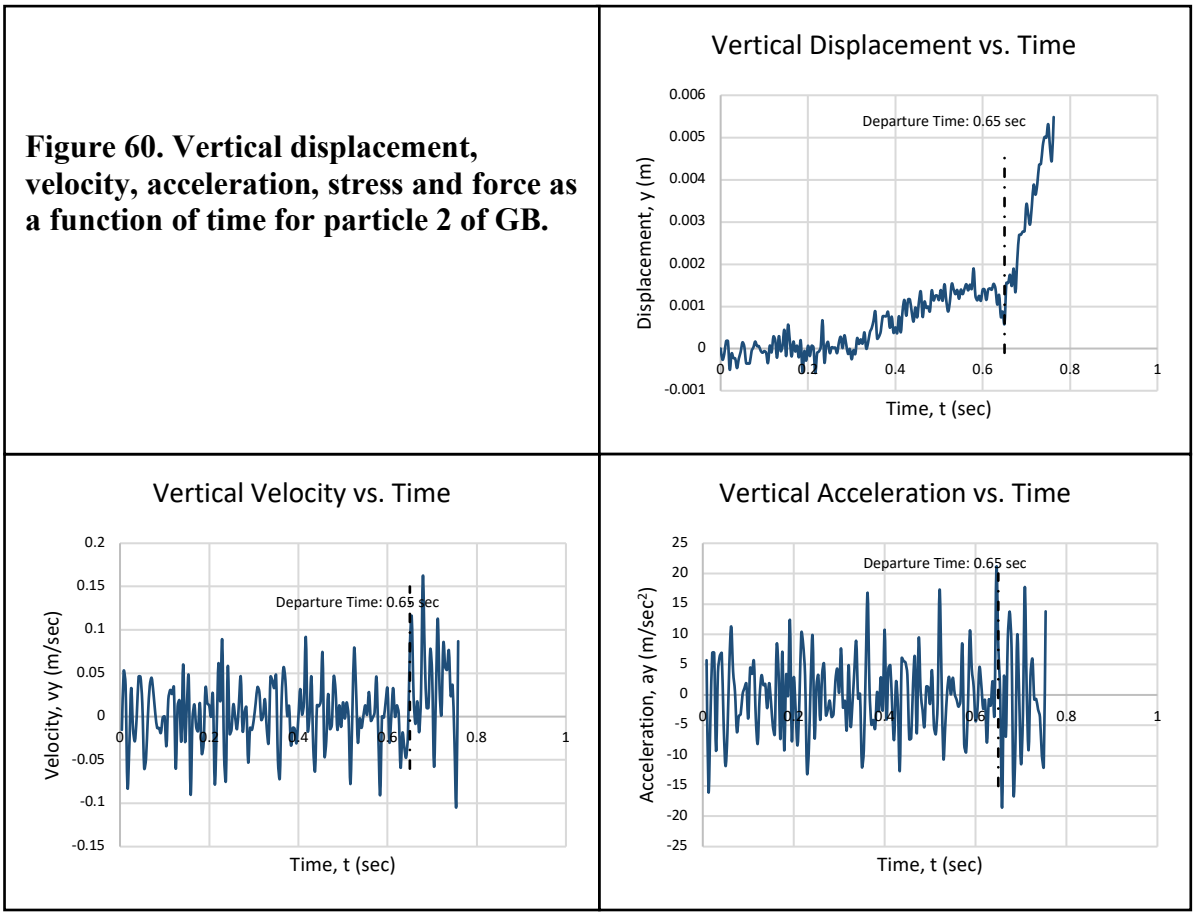

Figure 60 Continued

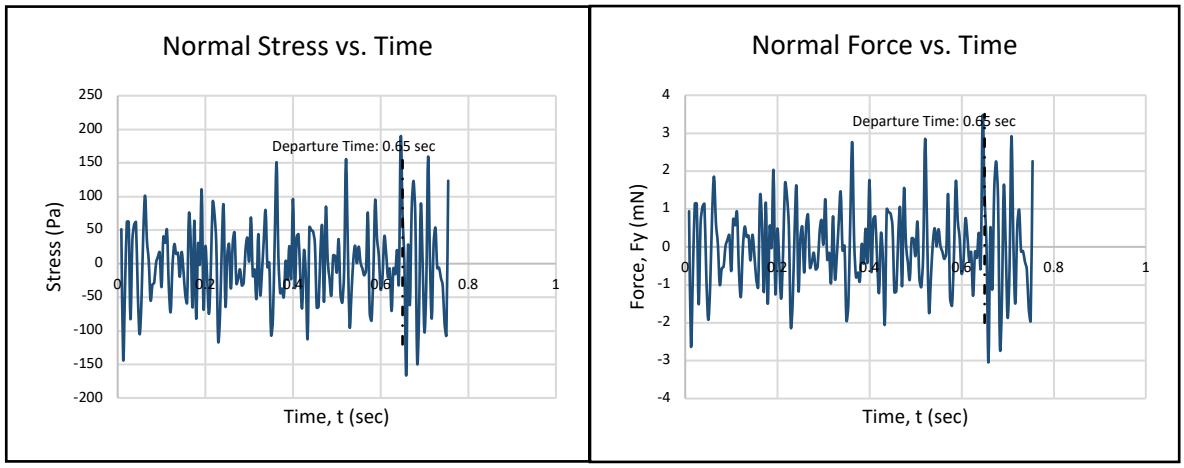

Particle 3 of GB:

Figure 61. Movement of Particle 3 of GB in the Erosion Function Apparatus

1). Horizontal direction (x direction):

Figure 62. Horizontal displacement, velocity, acceleration, stress and force as a function of time for particle 3 of GB.

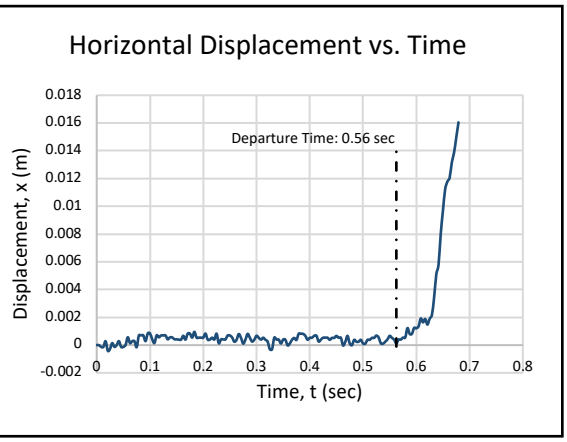

Figure 62 Continued

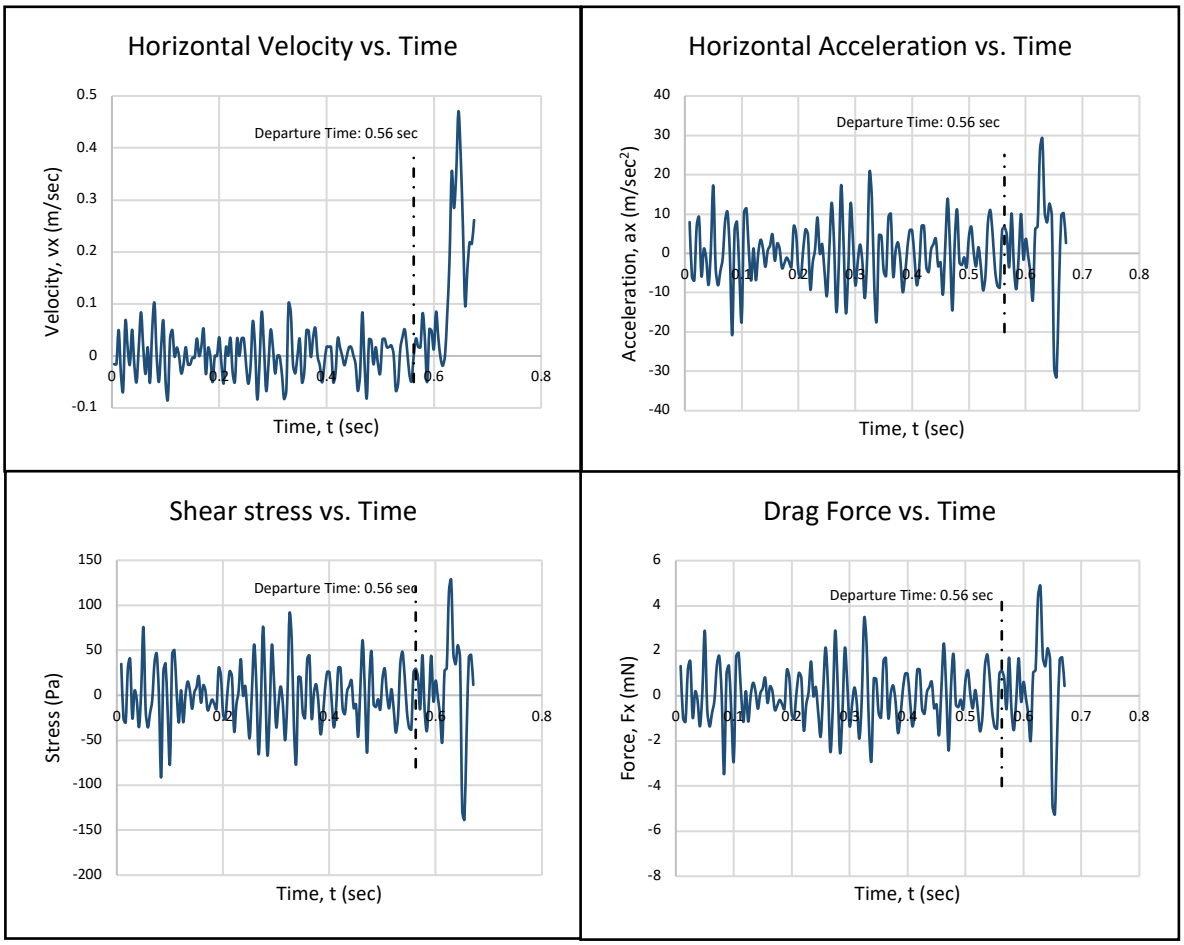

2). Vertical direction (y direction):

Figure 63. Vertical displacement, velocity, acceleration, stress and force as a function of time for particle 3 of GB.

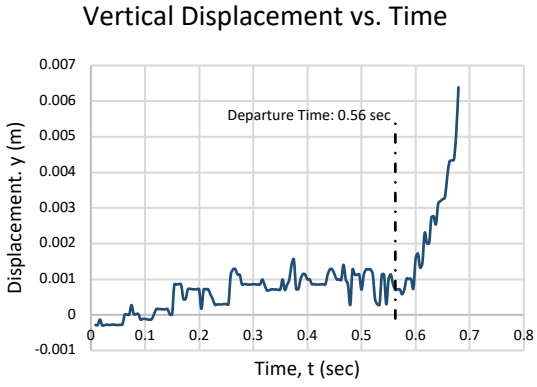

Figure 63 Continued

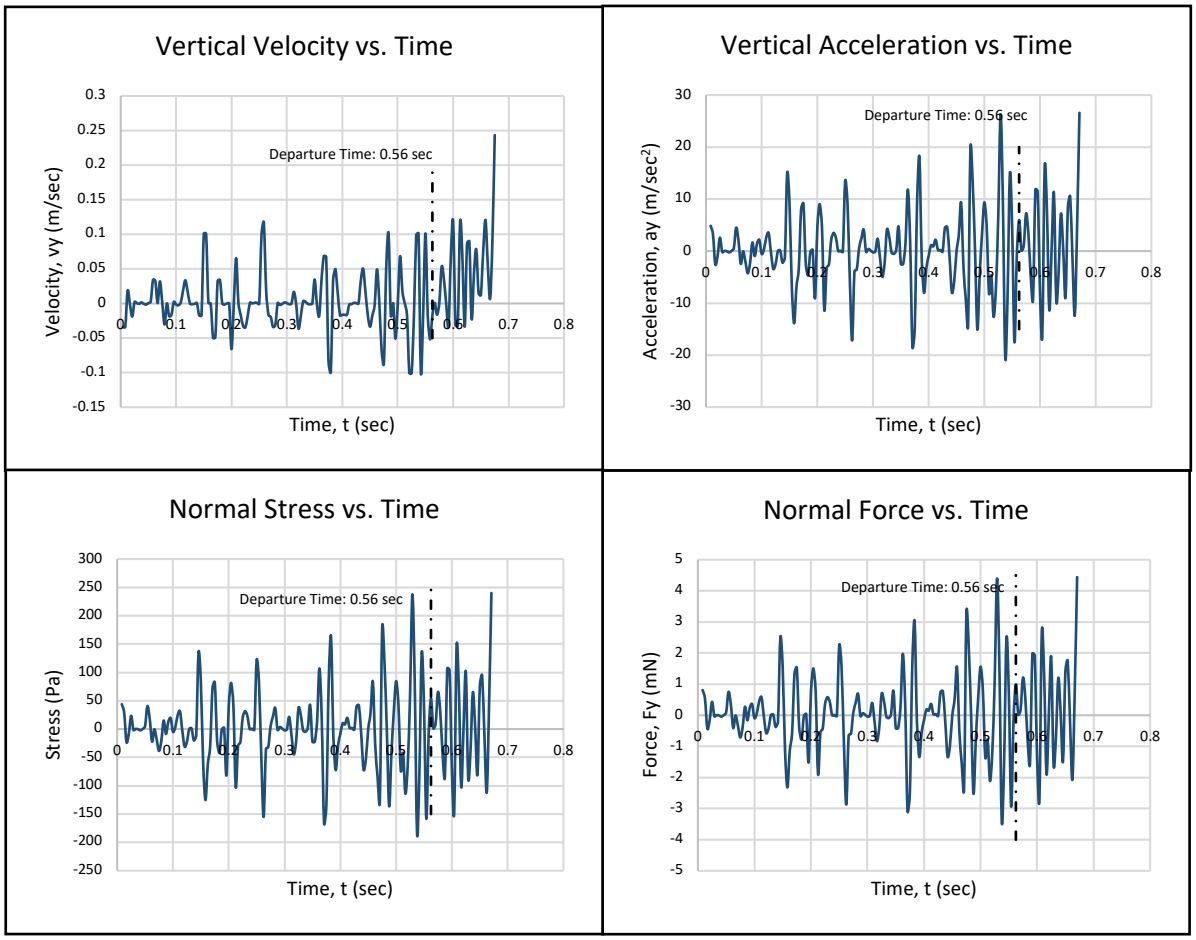

Particle 4 of GB:

Figure 64. Movement of Particle 4 of GB in the Erosion Function Apparatus

1). Horizontal direction (x direction):

Figure 65. Horizontal displacement, velocity, acceleration, stress and force as a function of time for particle 4 of GB.

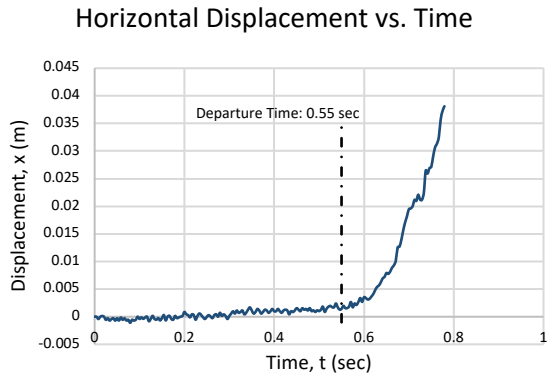

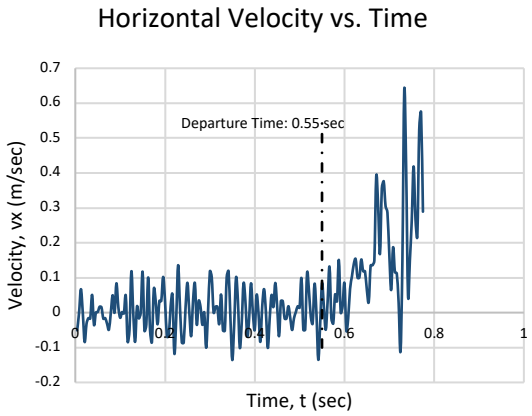

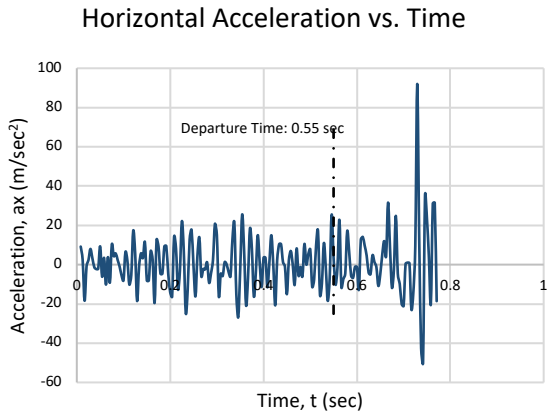

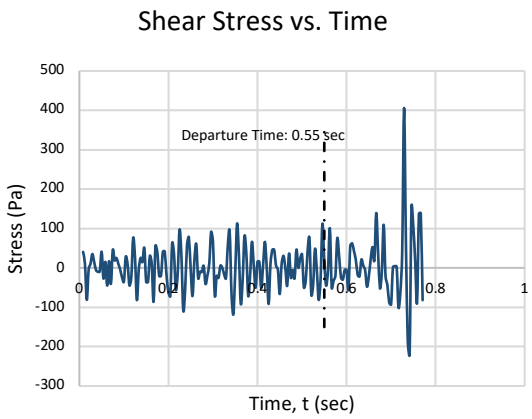

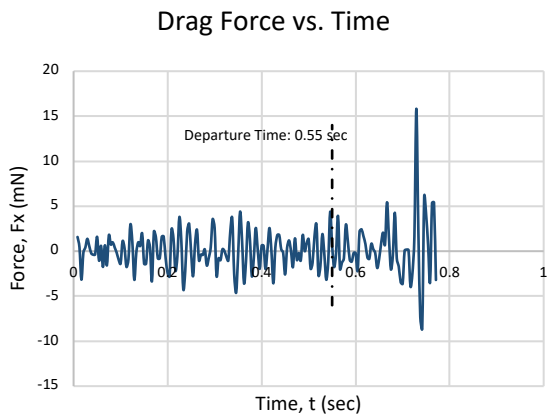

2). Vertical direction (y direction):

Figure 66. Vertical displacement, velocity, acceleration, stress and force as a function of time for particle 4 of GB.

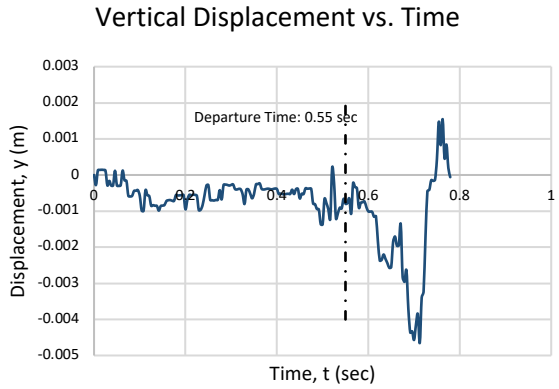

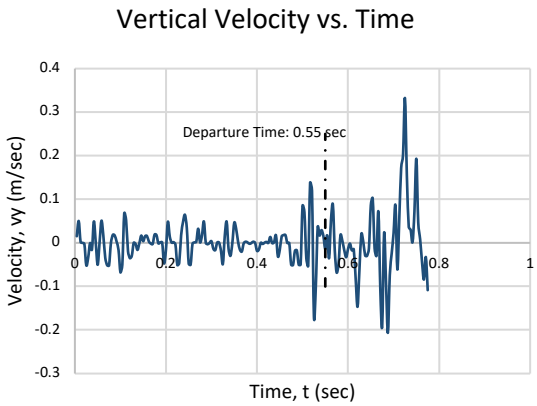

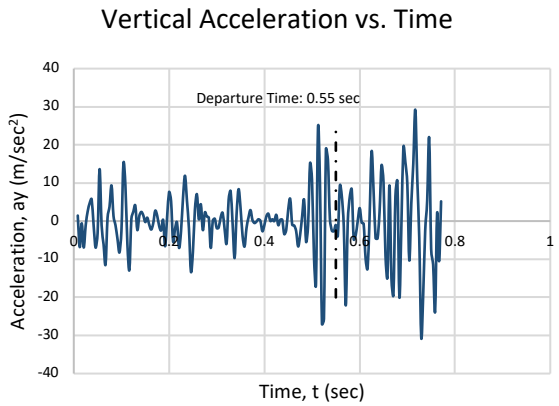

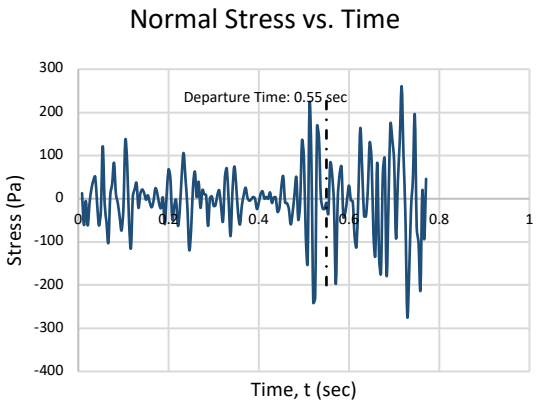

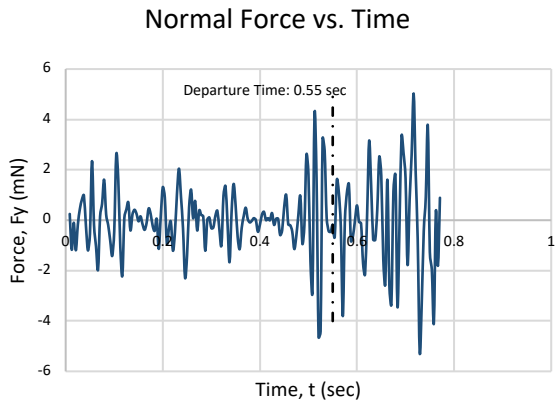

4.3 Analysis of Experimental Results

In order to calculate the average magnitude of displacement, velocity, and acceleration for a particle prior to complete detachment, the amplitude average was calculated. This was done by first determing the average of all data points. Then the amplitude of all points above the average were collected along with the amplitude of all points below the average. The average of the above amplitudes and the average of the below amplitudes were calculated. The amplitude average was then calculated as average of the above amplitudes minus average of the below amplitudes. The process for measuring the average magnitude of the horizontal velocity for particle 1 of G1 is shown in Figure 67, as an illustration. The same approach was taken to obtain the average magnitudes for the horizontal and vertical accelerations.

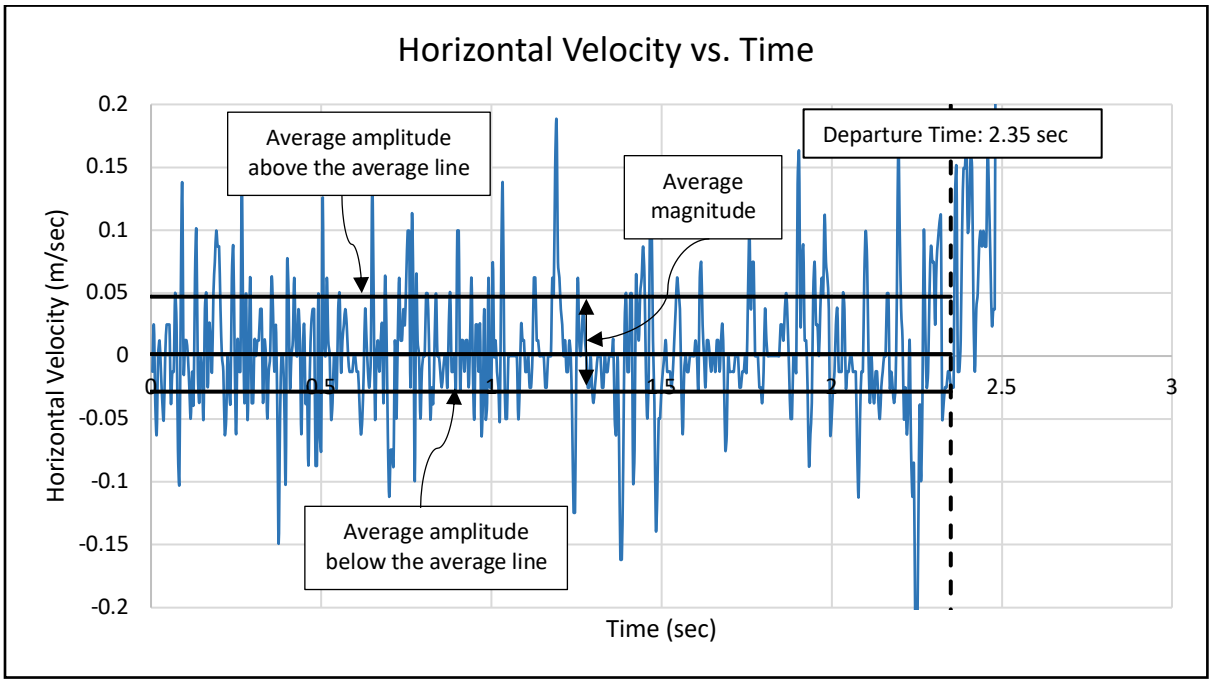

Figure 67. Example Process of Calculating the Average Magnitude of Horizontal Velocity for Particle 1 of G1

The detailed steps were as follows

1) Calculate the average horizontal velocity value by using the sum of all the values of the horizontal velocity divided the number of points used in the analysis (Figure 67).
2) Calculate the amplitude above the average value by taking the mean value of all the horizontal velocities higher than the average horizontal velocity value. This gave the average amplitude above the average line shown in Figure 67.
3) Calculate the amplitude below the average value by taking the mean value of all the horizontal velocities below the average horizontal velocity value. This gave the average amplitude below the average line shown in Figure 67.
4) Calculate the difference between the averages in step 2 and 3 above. Then use this number as the average horizontal velocity amplitude for this particle.
5) Use the same method to calculate the average horizontal velocity, average vertical velocity, average horizontal acceleration and average vertical acceleration of all the particles. The chart summarizing all the values is shown in Table 3.

Table 3. Average and Standard Deviation Values of All the Particles Tested in Erosion Function Apparatus

(Before departure)		G1					(Before departure)		G2					(Before departure)		TB				
		μ	μ+	μ-	Δu	σ			μ	μ+	μ-	Δu	σ			μ	μ+	μ-	Δu	σ
particle 1	x (m)	0.0023	0.0039	0.0011	0.0028	0.0017	particle 1	x (m)	-0.0025	-0.0010	-0.0041	0.0031	0.0018	particle 1	x (m)	-0.0001	0.0001	-0.0003	0.0003	0.0002
	y (m)	-0.0023	-0.0010	-0.0034	0.0024	0.0015		y (m)	0.0020	0.0037	0.0006	0.0031	0.0019		y (m)	-0.0004	0.0000	-0.0006	0.0007	0.0004
	r (m)	0.0035	0.0050	0.0020	0.0030	0.0018		r (m)	0.0039	0.0050	0.0027	0.0023	0.0014		r (m)	0.0006	0.0007	0.0004	0.0003	0.0002
	vx (m/s)	0.0015	0.0472	-0.0283	0.0756	0.0504		vx (m/s)	0.0015	0.0692	-0.0519	0.1211	0.0753		vx (m/s)	0.0021	0.0356	-0.0258	0.0614	0.0357
	vy (m/s)	-0.0015	0.0444	-0.0651	0.1096	0.0671		vy (m/s)	0.0046	0.0566	-0.0477	0.1042	0.0648		vy (m/s)	0.0037	0.0269	-0.0182	0.0451	0.0298
	v (m/s)	0.0021	0.0520	-0.0424	0.0945	0.0612		v (m/s)	0.0044	0.0577	-0.0502	0.1078	0.0665		v (m/s)	0.0010	0.0277	-0.0143	0.0420	0.0253
	ax (m/s2)	0.0030	5.7753	-4.9447	10.7200	7.3069		ax (m/s2)	0.2796	7.7182	-6.3828	14.1011	9.3532		ax (m/s2)	0.6643	6.6922	-4.6545	11.3467	6.5166
	ay (m/s2)	0.0456	7.7063	-7.3655	15.0718	9.9344		ay (m/s2)	0.0666	6.4652	-6.1517	12.6169	8.6219		ay (m/s2)	0.1107	3.9120	-3.6906	7.6026	5.0227
	a (m/s2)	-0.0447	6.3535	-6.6116	12.9651	8.8050		a (m/s2)	-0.1286	6.3457	-7.0059	13.3516	8.8034		a (m/s2)	-0.1101	2.7074	-3.7327	6.4400	4.2219
particle 2	x (m)	0.0015	0.0046	-0.0003	0.0049	0.0032	particle 2	x (m)	0.0011	0.0025	-0.0005	0.0030	0.0017	particle 2	x (m)	0.0001	0.0003	-0.0001	0.0004	0.0002
	y (m)	0.0017	0.0041	0.0000	0.0041	0.0024		y (m)	0.0004	0.0007	0.0000	0.0007	0.0004		y (m)	-0.0005	-0.0002	-0.0007	0.0004	0.0003
	r (m)	0.0033	0.0070	0.0015	0.0054	0.0032		r (m)	0.0018	0.0027	0.0008	0.0019	0.0011		r (m)	0.0005	0.0007	0.0003	0.0004	0.0003
	vx (m/s)	0.0051	0.0564	-0.0437	0.1001	0.0652		vx (m/s)	0.0077	0.0454	-0.0244	0.0698	0.0459		vx (m/s)	-0.0007	0.0250	-0.0318	0.0568	0.0357
	vy (m/s)	-0.0015	0.0414	-0.0616	0.1030	0.0691		vy (m/s)	0.0030	0.0411	-0.0243	0.0654	0.0416		vy (m/s)	-0.0011	0.0110	-0.0370	0.0480	0.0289
	v (m/s)	0.0050	0.0480	-0.0414	0.0894	0.0597		v (m/s)	0.0078	0.0436	-0.0227	0.0663	0.0436		v (m/s)	0.0009	0.0324	-0.0175	0.0498	0.0326
	ax (m/s2)	-0.0773	7.9890	-8.4135	16.4025	10.7548		ax (m/s2)	0.1643	6.3424	-4.5637	10.9061	7.9123		ax (m/s2)	0.0932	5.1408	-4.4514	9.5921	5.7364
	ay (m/s2)	-0.0364	7.8279	-8.3408	16.1687	11.0496		ay (m/s2)	0.1552	5.0742	-5.7413	10.8155	7.1368		ay (m/s2)	0.1243	4.6018	-2.7377	7.3395	5.1481
	a (m/s2)	-0.0523	7.9420	-8.4163	16.3583	10.5076		a (m/s2)	0.1732	6.4315	-4.7358	11.1674	7.8989		a (m/s2)	-0.1412	4.2365	-4.5920	8.8285	6.1274
particle 3	x (m)	-0.0015	-0.0011	-0.0017	0.0007	0.0004	particle 3	x (m)	-0.0011	-0.0007	-0.0014	0.0008	0.0005	particle 3	x (m)	0.0002	0.0005	0.0000	0.0005	0.0003
	y (m)	0.0000	0.0006	-0.0011	0.0018	0.0011		y (m)	-0.0007	-0.0001	-0.0015	0.0014	0.0008		y (m)	0.0001	0.0004	0.0000	0.0004	0.0002
	r (m)	0.0018	0.0023	0.0014	0.0009	0.0006		r (m)	0.0015	0.0019	0.0010	0.0010	0.0006		r (m)	0.0004	0.0006	0.0002	0.0004	0.0002
	vx (m/s)	-0.0010	0.0318	-0.0436	0.0754	0.0467		vx (m/s)	-0.0014	0.0283	-0.0407	0.0690	0.0425		vx (m/s)	0.0034	0.0619	-0.0196	0.0815	0.0457
	vy (m/s)	-0.0030	0.0363	-0.0547	0.0909	0.0575		vy (m/s)	-0.0030	0.0276	-0.0314	0.0591	0.0365		vy (m/s)	0.0029	0.0356	-0.0055	0.0411	0.0212
	v (m/s)	0.0032	0.0452	-0.0370	0.0822	0.0520		v (m/s)	0.0031	0.0369	-0.0333	0.0703	0.0419		v (m/s)	0.0046	0.0355	-0.0169	0.0524	0.0331
	ax (m/s2)	-0.0116	6.3457	-6.8726	13.2183	8.0725		ax (m/s2)	0.0826	5.6510	-5.3155	10.9665	7.0911		ax (m/s2)	0.3769	7.5761	-6.1024	13.6785	8.4684
	ay (m/s2)	-0.0174	6.2451	-6.3731	12.6181	8.1870		ay (m/s2)	0.0794	5.6128	-4.6708	10.2837	6.2076		ay (m/s2)	-0.0989	1.3218	-3.1770	4.4988	3.0892
	a (m/s2)	-0.0195	6.7510	-6.5610	13.3120	8.3902		a (m/s2)	-0.1502	5.3268	-5.6752	11.0020	7.0775		a (m/s2)	0.1833	5.0975	-5.2768	10.3743	6.4269
particle 4	x (m)	-0.0001	0.0002	-0.0003	0.0006	0.0004	particle 4	x (m)	-0.0004	-0.0001	-0.0008	0.0007	0.0004	particle 4	x (m)	-0.0004	-0.0001	-0.0007	0.0006	0.0004
	y (m)	0.0001	0.0009	-0.0005	0.0014	0.0008		y (m)	-0.0004	0.0001	-0.0008	0.0009	0.0006		y (m)	-0.0008	-0.0006	-0.0011	0.0004	0.0003
	r (m)	0.0008	0.0011	0.0004	\	0.0004		r (m)	0.0008	0.0011	0.0004	0.0007	0.0004		r (m)	0.0010	0.0012	0.0008	0.0004	0.0003
	vx (m/s)	0.0018	0.0407	-0.0296	0.0703	0.0436		vx (m/s)	-0.0011	0.0279	-0.0391	0.0670	0.0416		vx (m/s)	-0.0029	0.0316	-0.0518	0.0834	0.0542
	vy (m/s)	0.0027	0.0392	-0.0264	0.0656	0.0405		vy (m/s)	-0.0007	0.0382	-0.0416	0.0797	0.0481		vy (m/s)	-0.0033	0.0152	-0.0201	0.0353	0.0346
	v (m/s)	0.0028	0.0406	-0.0271	0.0678	0.0421		v (m/s)	0.0013	0.0403	-0.0336	0.0740	0.0461		v (m/s)	0.0041	0.0366	-0.0232	0.0598	0.0373
	ax (m/s2)	0.1096	5.6895	-6.4433	12.1328	7.4557		ax (m/s2)	0.1172	5.7724	-5.7237	11.4961	7.2935		ax (m/s2)	0.8616	7.5925	-8.3492	15.9417	10.5550
	ay (m/s2)	0.1008	5.7250	-5.3715	11.0965	7.1130		ay (m/s2)	-0.1046	6.3924	-6.1338	12.5262	8.0399		ay (m/s2)	0.4412	4.3932	-3.6904	8.0836	5.1490
	a (m/s2)	-0.1120	4.9168	-6.9828	11.8996	7.4318		a (m/s2)	-0.0317	6.4959	-6.1410	12.6369	7.9466		a (m/s2)	-0.3400	4.5674	-4.6340	9.2014	5.5547

(Before departure)		SB					(Before departure)		GB				
		μ	μ+	μ-	Δu	σ			μ	μ+	μ-	Δu	σ
particle 1	x (m)	-0.0001	0.0004	-0.0001	0.0005	0.0003	particle 1	x (m)	0.0010	0.0012	-0.0002	0.0013	0.0008
	y (m)	0.0003	0.0001	-0.0003	0.0004	0.0004		y (m)	0.0001	-0.0003	-0.0007	0.0005	0.0005
	r (m)	0.0005	0.0006	0.0002	0.0004	0.0003		r (m)	0.0012	0.0014	0.0006	0.0008	0.0007
	vx (m/s)	0.0004	0.0551	-0.0341	0.0891	0.0462		vx (m/s)	0.0016	0.0565	-0.0375	0.0940	0.0329
	vy (m/s)	0.0011	0.0262	-0.0187	0.0449	0.0288		vy (m/s)	0.0032	0.0189	-0.0321	0.0511	0.0260
	v (m/s)	0.0009	0.0344	-0.0264	0.0608	0.0272		v (m/s)	0.0033	0.0382	-0.0309	0.0691	0.0300
	ax (m/s2)	0.0891	8.3354	-7.8562	16.1917	8.5987		ax (m/s2)	0.0717	8.6364	-8.5717	17.2081	5.6945
	ay (m/s2)	-0.0148	3.9713	-4.1627	8.1341	5.1990		ay (m/s2)	0.1882	4.3928	-4.6824	9.0751	4.5556
	a (m/s2)	-0.0185	6.0577	-4.8347	10.8924	4.7222		a (m/s2)	0.1629	6.3242	-6.7533	13.0775	5.5095
particle 2	x (m)	0.0005	0.0007	0.0002	0.0005	0.0003	particle 2	x (m)	0.0001	0.0006	0.0002	0.0004	0.0005
	y (m)	0.0004	0.0007	0.0001	0.0005	0.0003		y (m)	0.0005	0.0010	0.0001	0.0009	0.0006
	r (m)	0.0007	0.0010	0.0005	0.0005	0.0003		r (m)	0.0008	0.0011	0.0005	0.0006	0.0004
	vx (m/s)	0.0007	0.0609	-0.0347	0.0956	0.0507		vx (m/s)	-0.0003	0.0345	-0.0293	0.0638	0.0372
	vy (m/s)	0.0006	0.0557	-0.0185	0.0742	0.0214		vy (m/s)	0.0019	0.0416	-0.0176	0.0592	0.0356
	v (m/s)	0.0009	0.0543	-0.0371	0.0914	0.0388		v (m/s)	0.0017	0.0337	-0.0238	0.0575	0.0344
	ax (m/s2)	0.0341	8.0639	-4.5559	12.6198	9.5605		ax (m/s2)	0.0200	5.7088	-5.7968	11.5056	6.2621
	ay (m/s2)	-0.0446	5.5805	-8.1021	13.6826	3.6140		ay (m/s2)	0.0970	5.1404	-4.6314	9.7718	6.1259
	a (m/s2)	-0.0016	8.1143	-5.4328	13.5471	7.1349		a (m/s2)	0.0402	5.0783	-5.0599	10.1381	5.9196
particle 3	x (m)	0.0004	0.0007	0.0003	0.0005	0.0003	particle 3	x (m)	0.0004	0.0006	-0.0002	0.0008	0.0003
	y (m)	0.0004	0.0006	0.0002	0.0004	0.0004		y (m)	0.0006	0.0011	0.0000	0.0011	0.0005
	r (m)	0.0007	0.0010	0.0005	0.0005	0.0003		r (m)	0.0008	0.0012	0.0005	0.0007	0.0004
	vx (m/s)	0.0110	0.0430	-0.0389	0.0819	0.0552		vx (m/s)	0.0005	0.0286	-0.0308	0.0594	0.0401
	vy (m/s)	0.0073	0.0143	-0.0132	0.0275	0.0476		vy (m/s)	0.0013	0.0307	-0.0242	0.0549	0.0402
	v (m/s)	0.0106	0.0324	-0.0290	0.0614	0.0532		v (m/s)	0.0014	0.0304	-0.0236	0.0539	0.0377
	ax (m/s2)	1.1804	8.2317	-7.3609	15.5926	7.7090		ax (m/s2)	0.0419	4.4113	-5.4531	9.8645	7.3436
	ay (m/s2)	-0.0169	2.5306	-2.5086	5.0392	8.8248		ay (m/s2)	0.0357	4.8919	-4.7602	9.6521	7.2204
	a (m/s2)	0.7250	5.8183	-5.6529	11.4712	8.1386		a (m/s2)	-0.0665	4.8093	-4.4309	9.2403	6.8079
particle 4	x (m)	0.0001	0.0003	-0.0002	0.0005	0.0003	particle 4	x (m)	0.0004	0.0016	0.0002	0.0014	0.0008
	y (m)	-0.0001	0.0006	0.0000	0.0007	0.0002		y (m)	-0.0005	0.0006	-0.0001	0.0007	0.0003
	r (m)	0.0004	0.0008	0.0003	0.0005	0.0002		r (m)	0.0010	0.0018	0.0005	0.0013	0.0005
	vx (m/s)	0.0022	0.0387	-0.0342	0.0728	0.0534		vx (m/s)	0.0031	0.0358	-0.0164	0.0522	0.0588
	vy (m/s)	0.0001	0.0263	-0.0170	0.0433	0.0312		vy (m/s)	-0.0012	0.0298	-0.0091	0.0390	0.0373
	v (m/s)	0.0017	0.0254	-0.0178	0.0432	0.0375		v (m/s)	0.0032	0.0339	-0.0138	0.0476	0.0457
	ax (m/s2)	0.2396	7.0933	-6.5598	13.6531	9.9149		ax (m/s2)	0.0981	4.7741	-3.7006	8.4748	10.7802
	ay (m/s2)	0.0851	3.7073	-4.0543	7.7616	5.4718		ay (m/s2)	-0.0409	3.7969	-2.3044	6.1013	6.8974
	a (m/s2)	0.1274	3.7225	-3.6773	7.3999	6.8233		a (m/s2)	0.0350	4.6995	-3.3874	8.0869	8.6311

G1: gravel particle 1
G2: gravel particle 2
TB: Teflon ball
SB: sand-coated Teflon ball
GB: gravel particle 3

x: horizontal displacement
y: vertical displacement
r: total displacement

vx: horizontal velocity
vy: vertical velocity
v: total velocity

ax: horizontal acceleration
ay: vertical acceleration
a: total acceleration

μ: average magnitude
μ+: average amplitude above the average
μ-: average amplitude below the average
$\Delta\mu$: average magnitude
σ: standard deviation

One major interest was to monitor the general differences between the values of horizontal/vertical acceleration, velocity, and displacement in the five samples tested. Four particles on each sample were analyzed. The plots of distance, velocity and acceleration as well as the average numbers shown in Table 3 and summarized in Figures 68 and 69 indicate that:

1) The amplitude of vibrations in the horizontal acceleration is larger in Sand Coated Teflon Balls SB than in Uncoated Teflon Balls TB. This implies that when the surface is rougher, the shear stress tends to be larger.
2) The amplitude of vibrations in the vertical acceleration is larger in Gravel 1 G1 and Gravel 2 G2 compared to other samples. This shows that when D_{50} increases, the normal stress tends to be larger.
3) The total displacement for Gravel 1 G1, Gravel 2 G2 is larger than the total displacement of the uncoated Teflon Balls TB and Sand Coated Teflon Balls SB. In other words, the displacement vs. time curve for TB and SB is smoother than the same curve for other samples. This implies that when the particles are more uniform in size, the displacement of the particles prior to detachment tends to be smaller.
4) The vertical acceleration prior to departure time for TB, SB, and GB tends to be smaller than the vertical acceleration for G1 and G2. This is most likely because the D_{50} is smaller for TB, SB, and GB compared to G1 and G2. The vibration frequency of the particle movement seems to be smaller when the soil is composed of smaller particles.

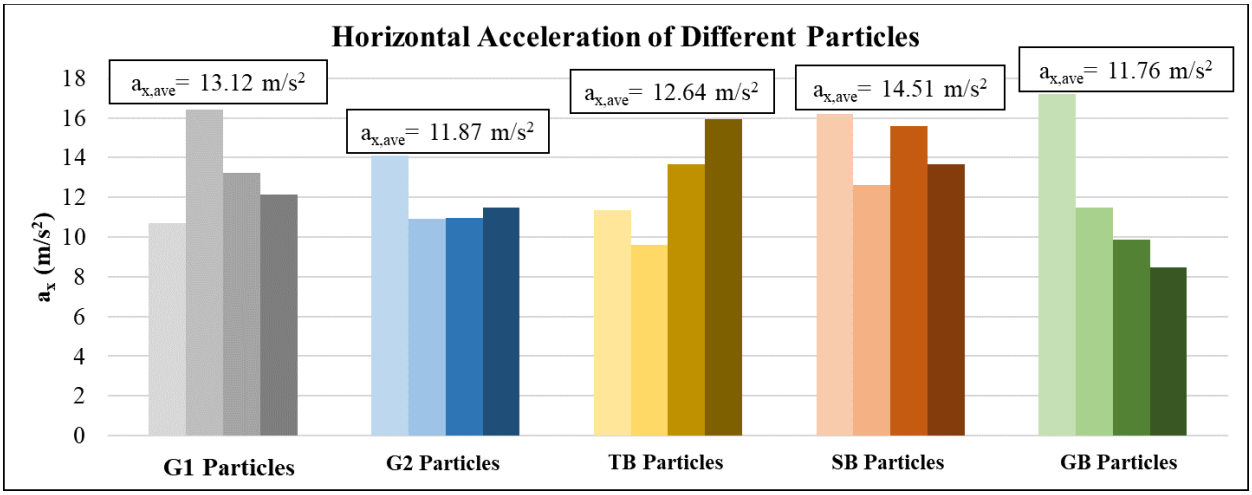

Figure 68. Horizontal Acceleration for Different Particles

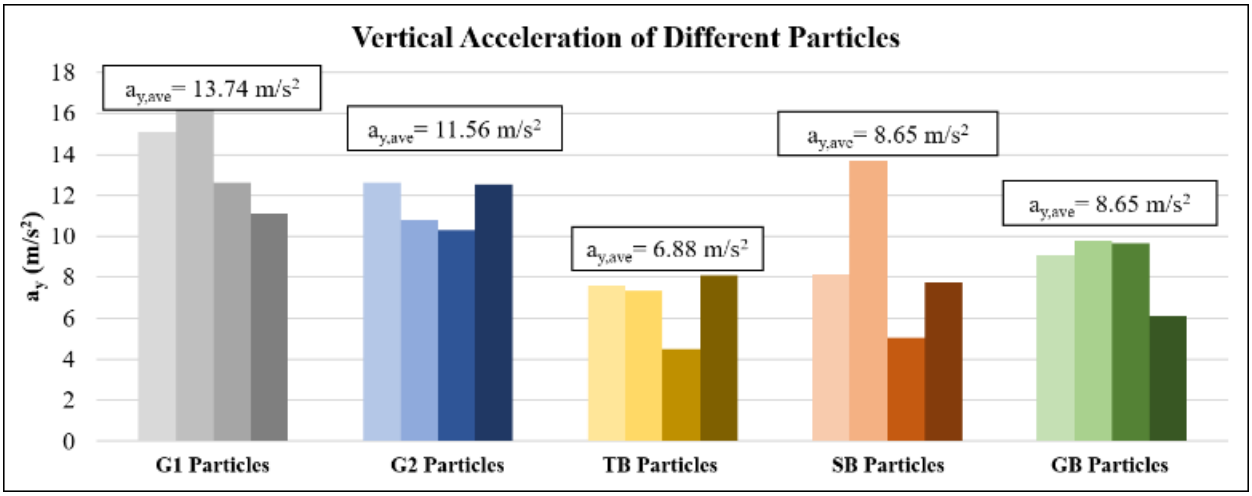

Figure 69. Vertical Acceleration for Different Particles

From Figure 68 and Figure 69, where different colors stand for different gravel particles, the following observations can be made:

1) By comparing the value of the horizontal and vertical accelerations of gravels with different D_{50}, it can be observed that when the particles are smaller, the acceleration tends to be smaller, too. This means that when the soil has smaller D_{50} or if it is more uniform, the amplitude of vibration before departure will be smaller.

2) By comparing the value of acceleration between the uncoated Teflon balls TB, and the sand coated Teflon balls SB which have particles with the same D_{50}, it is concluded that when the surface of the particles is smoother, the accelerations are smaller. The particles with rough surface show more vibration, which means the force acting on these particles are larger.

Another goal of the study was to compare the shear stress measurements with the shear stress values obtained from Moody Chart (Eq. 3). In order to calculate the drag force from the results of the video analysis described in the previous section, the horizontal acceleration was multiplied by the particle mass in the water flow for each flow velocity. Similarly, the product of the vertical acceleration and the particle mass in the water flow was calculated as the normal force for each flow velocity. Note that for non-symmetrical particles, two symmetric points on the particle needed to be tracked and the mean value of the displacement, velocity and acceleration were obtained to be more accurate. The equations that were used in the calculations are:

$F_{drag} = (m + m_a)a_x$, $F_{normal} = (m + m_a)a_y$, $m = \rho V$, $m_a = \rho_w \times \frac{1}{2}V$, $\tau = \frac{F_{drag}}{A_s}$, $\sigma = \frac{F_{normal}}{A_c}$. Where F_{drag}=drag force, m=mass of the particle, a_x=horizontal acceleration, F_{normal}=normal force, a_y=vertical acceleration, ρ=particle density, V=particle volume measured from Tracker, ρ_w=water density, τ=shear stress, σ=normal stress, A_s=surface area of the particle, A_c=cross-section area of the particle. Table 4 shows the results including the values of the drag force, normal force, shear and normal stress as well as some of the properties of the chosen particle and the erosion rates recorded in the EFA at different velocities (equal and/or larger than the critical velocity) for each sample.

Table 4. Calculated Values of the Gravel Particles

	ρ	A_s	A_c	V	F_{drag}	F_{normal}	v v>=v_c	$\dot{z}$	τ Eq.(3)	τ Video Analysis	τ_c	σ Video Analysis	σ_c
	g/cm^3	cm^2	cm^2	cm^3	mN	mN	m/s	mm/hr	Pa	Pa	Pa	Pa	Pa
G1	2.65	1.90	0.90	0.685	13.125	4.230	0.96	0.1	10.76	69.08	69.08	47	47
					17.269	8.899	1.18	21.93	15.75	90.89		98.88	
					23.039	10.418	1.76	1140	35.31	121.26		115.76	
G2	2.65	0.565	0.30	0.103	2.479	0.690	0.875	0.1	6.5	43.87	43.87	23	23
					3.201	1.512	1.17	15	11.71	56.66		50.41	
					3.625	1.804	1.53	758.9	19.85	64.16		60.13	
TB	2.20	0.39	0.195	0.065	2.95	0.741	0.5	0.1	1.94	75.59	75.59	38	38
					3.18	1.064	0.75	456	4.36	81.47		54.56	
SB	2.20	0.39	0.195	0.065	3.40	0.741	0.5	0.1	1.94	87.29	87.29	38	38
					3.82	1.064	0.75	309	4.36	97.99		54.56	
GB	2.65	0.39	0.195	0.065	2.48	0.624	0.65	0.1	3.33	63.63	63.63	32	32
					2.57	1.056	0.84	400	5.56	65.93		54.17	
					2.73	1.158	1.18	4722	10.97	69.88		59.37	

The critical normal stress (σ_c) is obtained after subtracting the weight of the water displaced water by the particle from the unsubmerged weight of the particle. As shown in Table 4, the measured shear stresses are much larger than the calculated shear stresses using Eq. (3). Table 4 shows that the normal stress and the shear stress values increase when the flow velocity increases. Figures 70 and 71 also show that the values of $\frac{\dot{z}}{0.1}$ and $\frac{\tau}{\tau_c}$, as well as the values of $\frac{\dot{z}}{0.1}$ and $\frac{\sigma}{\sigma_c}$ can be proportionally correlated to each other. The new model proposed in Eq. (2) incorporates the effects of both normal stress values and shear stress values as opposed to previous models where the erosion rate was only a function of shear stress.

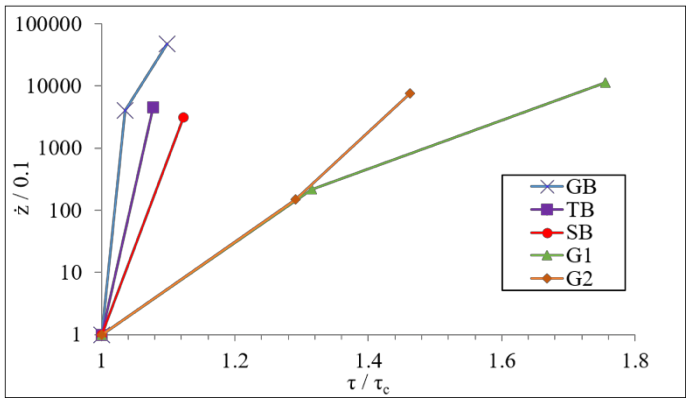

Figure 70. Plots of $\dot{z}/z$ Versus τ/τ_c for Tested Samples

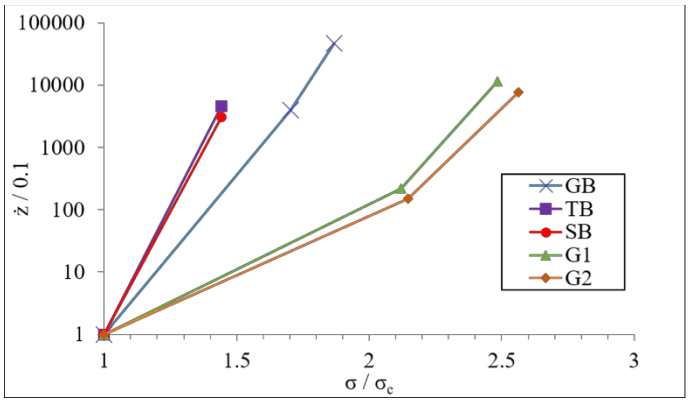

Figure 71. Plots of $\dot{z}/z$ Versus σ/σ_c for Tested Samples

Since the water velocity, D_{50} and some other conditions are different between tests, it's also important to normalize the values of horizontal velocity and acceleration, vertical velocity and acceleration, drag force and normal force, shear stress and normal stress so that they are comparable. Such results are shown in Table 5. The calculated values were normalized by water density ρ_w, water velocity v, and grain size D_{50} as $\frac{V_x}{v}$, $\frac{V_y}{v}$, $\frac{a_x D_{50}}{v^2}$, $\frac{a_y D_{50}}{v^2}$, $\frac{\tau}{\rho_w v^2}$, $\frac{\sigma}{\rho_w v^2}$, $\frac{F_{drag}}{\rho_w v^2 D_{50}^2}$, and $\frac{F_{normal}}{\rho_w v^2 D_{50}^2}$. Where V_x=horizontal velocity (m/s), V_y=vertical velocity (m/s), a_x=horizontal

acceleration (m/s^2), a_y=vertical acceleration (m/s^2), τ=shear stress (Pa), σ=normal stress (Pa), F_{drag}=drag force (mN), F_{normal}=normal force (mN).

Table 5. Normalized Values of the Gravel Particles

	G1 v=1.76 m/s, D_{50}=11mm	G2 v=1.53 m/s D_{50}=6mm	TB v=0.75 m/s D_{50}=5mm	SB v=0.75 m/s D_{50}=5mm	GB v=1.18 m/s D_{50}=5mm
V_x/v	0.0429	0.0792	0.0819	0.1189	0.0627
V_y/v	0.0623	0.0681	0.0602	0.0599	0.0340
$a_x D_{50}/v^2$	38.0682	36.1427	100.8596	143.9260	38.2402
$a_y D_{50}/v^2$	53.5221	32.3385	67.5785	72.3029	20.1670
$\tau/\rho_w v^2$	39.1464	27.4083	144.8356	174.2044	31.0578
$\sigma/\rho_w v^2$	37.3709	25.6867	96.9956	96.9956	26.3867
$\frac{F_{drag}}{\rho_w v^2 D_{50}^2}$	0.3381	0.1290	0.5653	0.6791	0.1213
$\frac{F_{normal}}{\rho_w v^2 D_{50}^2}$	0.0278	0.0214	0.0757	0.0757	0.0206

By comparing the normalized values fro the gravels G1, G2 and GB, it comes that when the particles are smaller, both the drag force and normal force tend to be smaller. The shear stress and normal stress also have a tendency to get smaller. By comparing the normalized values for the Teflon balls TB and SB, it comes that the normal force is basically the same, but when the skin friction gets bigger, the shear stress tends to get bigger, too. So is the drag force.

Table 6 shows the erosion model parameters (i.e. α, β) obtained after fitting Eq. (2) to the measured data for each sample. It can be concluded that normal stresses as well as shear stresses play a noticeable role in the detachment of gravel particles from the surface of a riverbed. Table 6 shows that the effect of the normal stresses is much more pronounced in TB, SB, and GB where

the particles are smaller and therefore lighter. On the other hand, shear stresses have a more prominent effect on the erosion of G1 and G2, where the soil particles are larger and heavier.

Table 6. Erosion model parameters based on Equation (2)

	α	β
G1	12.3	2.63
G2	19.59	1.62
TB	5.42	21.96
SB	6.87	19.9
GB	19.96	14.16

5. CONCLUSIONS AND CONTRIBUTION

5.1 Conclusions

It is concluded that shear stresses tend to be larger for rougher particles, while normal stresses are larger in samples with a bigger mean particle size (D_{50}). Also, it was observed that when the particles are more uniform in size, the displacement of the particles prior to detachment tends to be smaller. The vibration frequency of particle movement also tends to be smaller when the soil is composed of smaller particles.

Both normal and shear stresses were observed to be proportionally correlated with the erosion rate. The effect of normal stresses tends to be more prevalent on smaller gravel particles, while the effect of shear stresses seems to play a more prominent role in the erosion of larger gravel particles.

5.2 Contribution

The authors have implemented a novel and simple method to measure the normal and shear forces acting on gravel particles using video analysis. Five gravel samples were prepared in the erosion laboratory of Texas A&M University and tested in the Erosion Function Apparatus (EFA).

A new erosion model is proposed, and the effect of normal and shear stress components of the proposed model is studied for different samples.

REFERENCES

Briaud, J.L., Govindasamy, A.V., Shafii, I., 2017, "Erosion Charts for Slected Geomaterials". *Journal of Geotechnical and Geoenvironmental Engineering,* Vol. 143(10).

Ambuj Dwivedi, Bruce W. Melville, Asaad Y. Shamseldin, Tushar K. Guha, 2011, "Flow Structures and Hydrodynamic Force during Sediment Entrainment".*Water Resources Research*, Vol. 47. W01509.

Shan, H., Shen, J., Kilgore, R., Kerenyi, K., 2015, "Scour in Cohesive Soils". *US Department of Transportation, Federal Highway Administration*. Publication No. FHWA-HRT-15-033.

Hofland, B., Battjes, J.A., Booij, R., 2005, "Measurement of Fluctuating Pressures on Coarse Bed Material". *Journal of Hydraulic Engineering*, Vol. 131(9), pp.770-781.

Kudrolli, A., Scheff, D., Allen, B., 2016, "Critical Shear Rate and Torque Stability Condition for A Particle Resting on A Surface in A Fluid Flow". *J. Fluid Mech,* Vol. 808, pp. 397-409.

Maali, A., Pan, Y., Bhushan, B., Charlaix, E., 2012, "Hydrodynamic Drag-Force Measurement and Slip Length on Micro structured Surfaces". *Physical Review E 85*, 066310.

Shafii, I., Briaud, J. L., Chen, H. C., and Shidlovskaya, A., 2016, "Relationship between Soil Erodibility and Engineering Properties". *8th International Conference on Scour and Erosion*, Oxford, U.K.

Croad, R.N., 1981, "Physics of Erosion of Cohesive Soils". PhD Thesis, Department of Civil Engineering, University of Auckland, NZ.

Briaud, J.L., Chen, H.C., Cao, Y., Han, S.W., Kwak, K.W., 2011, "Erosion Function Apparatus for Scour Rate Predictions". *Journal of Geotechnical and Geoenvironmental Engineering,* Vol. 127(2).

Shan, H., Wagner, A., Kerenyi, K., Guo, J., Xie, Z., 2011, "An Ex-situ Scour Testing Device for erosion research of cohesive soils". *Engineering Mechanics Institute Conference*, Northeastern university, Boston, MA.

Tracker [Computer software], 2018. Retrieved from https://physlets.org/tracker/.